Technische Universität München
TUM School of Medicine and Health

Influence of early microbial colonisation and the IκB transcription co-factor Bcl3 on intestinal immune homeostasis

Amelie Christin Köhler

Vollständiger Abdruck der von der TUM School of Medicine and Health der Technischen Universität München zur Erlangung einer Doktorin der Naturwissenschaften (Dr. rer. nat.) genehmigten Dissertation.

Vorsitz: Prof. Dr. Markus Gerhard

Prüfende der Dissertation:

1. Priv.-Doz. Dr. Caspar Ohnmacht
2. Prof. Dr. Michael Schloter

Die Dissertation wurde am 01.02.2024 bei der Technischen Universität München eingereicht und durch die TUM School of Medicine and Health am 08.05.2024 angenommen.

CONTENTS

PUBLICATION STATEMENT

PARTS OF THIS THESIS HAVE BEEN PUBLISHED IN THE FOLLOWING ORIGINAL RESEARCH ARTICLE:

[1] The atypical IκB family member Bcl3 determines differentiation and fate of intestinal RORγt+ regulatory T cell subsets.

Amelie Köhler; Anna-Lena Geiselhöringer; Daphne Kolland; Luisa Kreft; Miriam Hils; Maria Pasztoi; Elena Zurkowski; Johannes Vogt; Tilo Biedermann; Ingo Schmitz; Wiebke Hansen; Matthias M. Gaida; Carsten B. Schmidt-Weber; Nadine Hövelmeyer and Caspar Ohnmacht

Mucosal Immunology (2024); doi: https://doi.org/10.1016/j.mucimm.2024.04.002

ABSTRACT

Due to the constant contact with a plenitude of foreign antigen, the gut is especially vulnerable towards unwanted immune responses. These reactions frequently manifest as food allergies or inflammatory bowel diseases when homeostasis is disturbed and dysbiosis arises. Peripherally induced regulatory T cells (pTregs) expressing the retinoic acid receptor related orphan-receptor gamma t (RORγt) develop predominantly as a response to bacterial colonisation in the gut where they are essential to uphold immune tolerance. Although microbiome-specific pTregs may be induced constantly during lifetime, their induction outside of a critical window of opportunity during weaning predestines for inflammatory diseases.

In this study mice raised under germfree conditions (GF) or receiving a broad spectrum of antibiotics early in life showed an altered composition of intestinal T cells and decreased Treg TCR diversity after colonisation. Furthermore, microbial complexity during weaning impacted the outcome of allergic sensitisation to dietary antigens. While co-housing aligned pTreg frequencies and the microbiome, ex-GF mice developed drastically less severe anaphylactic reactions. Other studies show that members of the NFκB family affect the formation of thymus derived Tregs (tTregs) and support their survival in peripheral organs. Nevertheless, the cell-intrinsic molecular mechanisms regulating the abundance of pTregs in the gut and its draining lymph nodes, have not been fully explored. In this thesis, transcriptional differences between intestinal pTregs and tTregs were analysed on a single cell level to gain insight into their divergent developmental paths. Specific gene signatures for tTregs and pTregs could be generated showing distinctly lower expression of NFκB signature genes in pTregs. This difference confirmed the importance of the NFκB pathway in controlling intestinal Treg survival and development.

Furthermore, direct evidence is presented to claim that the atypical IκB family member Bcl3 inhibits the differentiation of pTregs in a T cell-intrinsic system. Loss of Bcl3 enabled the development of an atypical intestinal Treg population expressing both usually exclusive transcription factors RORγt and Helios. In the absence of Bcl3, the inflated

RORγt^{+} Treg populations exhibited an overall activated phenotype and produced increased levels of the anti-inflammatory cytokines TGFβ and IL-10. In addition to the cytokine surplus, Bcl3-deficient Tregs were perfectly efficient at restraining effector T cells in a transfer colitis model regardless of an intrinsic bias to trans-differentiate in favour of a Th17-like cell type. Finally, a Bcl3-dependent gene signature was discovered in pTregs indicating modified sensitivity to the cytokines IL-2, IL-6, and TNFα.

In summary, these results illustrate the importance of healthy microbial colonisation early in life and that Bcl3 acts as a molecular set point to restrict the accumulation of intestinal Treg populations and could thereby appear as an innovative target for the treatment of inflammatory bowel disease by re-establishing intestinal immune tolerance.

ZUSAMMENFASSUNG

Durch den ständigen Kontakt mit einer Fülle von Fremdantigenen ist der Darm besonders anfällig für unerwünschte Immunreaktionen. Diese Reaktionen äußern sich häufig als Nahrungsmittelallergien oder entzündliche Darmerkrankungen, bei welchen die Homöostase gestört ist und eine Dysbiose auftritt. Peripher induzierte regulatorische T-Zellen (pTregs), die RORγt (retinoic acid receptor related orphan-receptor gamma t) exprimieren, entwickeln sich vor allem als Reaktion auf die bakterielle Besiedlung im Darm, wo sie für die Aufrechterhaltung der Immuntoleranz unerlässlich sind. Obwohl Mikrobiom-spezifische pTregs im Laufe des Lebens ständig induziert werden können, prädestiniert ihre Induktion außerhalb eines kritischen Zeitfensters während der Entwöhnung für entzündliche Erkrankungen.

In dieser Studie zeigten Mäuse, die unter keimfreien Bedingungen (GF) aufgezogen wurden oder früh im Leben ein breites Spektrum an Antibiotika erhielten, eine veränderte Zusammensetzung der intestinalen T-Zellen und eine geringere Treg-TCR Diversität nach der Kolonisierung. Darüber hinaus wirkte sich die mikrobielle Komplexität während der Entwöhnungsphase auf die Schwere von Nahrungsmittelallergien aus. Während die gemeinsame Unterbringung der Mäuse ihre pTreg-Frequenzen und ihre mikrobielle Besiedlung auf das gleiche Level bringt, entwickeln ex-GF-Mäuse eine deutlich mildere Anaphylaxis. Andere Studien zeigen, dass Mitglieder der NFκB-Familie die Bildung von Thymus Tregs (tTregs) beeinflussen und deren Überleben in peripheren Organen fördern. Dennoch sind die zellintrinsischen molekularen Mechanismen, die die Häufigkeit von pTregs im Darm und seinen drainierenden Lymphknoten regulieren, noch nicht vollständig erforscht. In dieser Dissertation wurden die transkriptionellen Unterschiede zwischen intestinalen pTregs und tTregs auf Einzelzellebene analysiert, um einen Einblick in ihre unterschiedlichen Entwicklungswege zu gewinnen. Es konnten spezifische Gensignaturen für tTregs und pTregs erstellt werden, die eine deutlich geringere Expression von NFκB Signaturgenen in pTregs zeigten. Dieser Unterschied bestätigte die Bedeutung des NFκB Signalwegs für die Kontrolle des Überlebens und der Entwicklung intestinaler Tregs.

Darüber hinaus wird gezeigt, dass das atypische IκB-Familienmitglied Bcl3 die Differenzierung von pTregs T-Zell-intrinsisch hemmt. Der Verlust von Bcl3 ermöglichte die Entwicklung einer atypischen intestinalen Treg-Population, die die Transkriptionsfaktoren RORγt und Helios exprimiert, welche sich üblicherweise gegenseitig ausschließen In Abwesenheit von Bcl3 wiesen die expandierten RORγt^{+} Treg-Populationen einen aktivierten Phänotyp auf und produzierten erhöhte Mengen der entzündungshemmenden Zytokine TGFβ und IL-10. Zusätzlich zu dem Zytokin-Überschuss waren Bcl3-defiziente Tregs vollkommen effizient bei der Hemmung von Effektor-T-Zellen in einem Transfer-Colitis-Modell, unabhängig von einer intrinsischen Tendenz zu Th17-ähnlichen Zellen zu transdifferenzieren. Schließlich wurde eine Bcl3-abhängige Gensignatur in pTregs gezeigt, die auf eine veränderte Empfindlichkeit gegenüber den Zytokinen IL-2, IL-6 und TNFα hinweist.

Zusammenfassend zeigen diese Ergebnisse, wie wichtig eine gesunde mikrobielle Besiedlung in den ersten Lebensjahren ist und, dass Bcl3 als molekularer Regulator die Anhäufung von intestinalen Treg-Populationen einschränkt. Somit kann Bcl3 einen neuen Angriffspunkt für die Behandlung entzündlicher Darmerkrankungen darstellen, indem die intestinale Immuntoleranz wiederhergestellt würde.

ABBREVIATIONS

Acronym	Meaning
ABX	Antibiotics
ACK	Ammonium-chloride-potassium buffer
AF	Alexa Fluor®
Aire	Autoimmune regulator
APC	Allophycocyanin
APCs	Antigen presenting cells
ASF	Altered Schaedler flora
Bcl3	B-cell lymphoma 3-encoded protein
BM	Bone marrow
bp	Base pairs
BSA	Bovine serum albumin
BV	BD Horizon BrilliantViolet™
CD	Cluster of differentiation
cDNA	Complementary DNA
CT	Cholera toxin
CTL	Cytotoxic T lymphocyte
Ctrl	Control
DAMP	Damage associated molecular pattern
DC	Dendritic cell
DEGs	Differentially expressed genes
DMSO	Dimethylsulfoxide
DN	Double negative
DNA	Desoxyribonucleic acid
DP	Double positive
DPTreg	Double positive Treg
EDTA	Ethylenediaminetetraacetic acid
eF	eFluor™
ELISA	Enzyme-Linked Immunosorbent Assay
ex-GF	Formerly germfree mice
FACS	Fluorescence activated cell sorting
FCS	Fetal calf serum
FITC	Fluorescein
Foxp3	Forkhead box p3
Fwd	forward
GATA3	GATA binding protein 3
GF	germfree
GFP	Green fluorescent protein
GSEA	Gene set enrichment analysis
h	hours
HEPES	N-2-hydroxyethylpiperazine-N-2-ethane sulfonic acid
i.g.	Intragastric gavage

i.p.	Intra peritoneal injection
i.v.	Intra venous injection
Ig	Immunoglobulin
IL	Interleukin
Int	Intermediate
IκB	Inhibitor of NFκB
IKK	IκB kinase
iTreg	Induced Treg
KLRG1	Killer cell lectin-like receptor g1
KO	Knockout
LP	Lamina propria
MACS	Magnetic assisted cell sorting
MHC-I / MHC-II	Major histocompatibility complex class I / class II
min	Minutes
mLN	Mesenteric lymph nodes
mTEC	Medullary thymic epithelial cell
NFκB	Nuclear factor κB
Nrp1	Neuropilin1
ns	Not significant
OE	Overexpression
OVA	Ovalbumin
PAMP	Pathogen-associated molecular pattern
PB	Pacific Blue
PBS	Phosphate buffered saline
PCA	Principal component analysis
PCR	Polymerase chain reaction
PD-1	Programmed cell death protein 1
PE	Phycoerythrin
PEC	Peritoneal cavity lavage
PerCP	Peridinin-chlorophyll-protein complex
PMA	Phorbol-12-myristate-13-acetate
PP	Peyer's patches
PRR	Pattern recognition receptor
pTreg	Peripherally induced Treg
Rag	Recombination activating gene
RAR	Retinoic acid receptor
Rel	V-rel avian reticuloendotheliosis viral oncogene homolog
Rev	Reverse
RFP	Red fluorescent protein
RM	Reduced microbiome
RNA	Ribonucleic acid
RORγt	RAR-related orphan receptor gamma t
rpm	Revolutions per minute
RPMI	Roswell Park Memorial Institute
RT	Room temperature

scRNAseq	Single cell RNA sequencing
SD	Standard deviation
sec	Seconds
seq	sequencing
SI	Small intestine
SP	Single positive
SPF	Specific pathogen free
STAT	Signal Transducer and Activator of Transcription
TAE	Tris-acetate-EDTA buffer
TCR	T cell receptor
TE	TRIS-EDTA buffer
Tfh	T follicular helper cell
TGF	Transforming growth factor
Th	T helper cell
TKF	Transcription factor
TLR	Toll-like receptor
TNF	Tumor necrosis factor
TNFRSF	TNF receptor superfamily
Treg	Regulatory T cell
tSNE	t-distributed stochastic neighbour embedding
tTreg	Thymically induced Treg
UV	Ultraviolet
VDJ / V(D)J	Variable, Diversity and Joining gene segment
WT	wildtype
xg	Relative centrifugal force

1 INTRODUCTION

1.1 INNATE AND ADAPTIVE IMMUNITY

The immune system is a complex arrangement of different mechanisms to protect the host organism from threats. Those potential harms can either be external pathogens such as bacteria, viruses, and parasites or internal threats in the form of malfunctioning or cancerous cells. Whereas the first line of defence against external intrusion is always anatomical structures in the form of epithelial barriers or mucosal tissues, the immune system is usually separated into two major compartments: the evolutionarily older innate and the more specific adaptive immunity [2], [3].

The innate immune system is built around the activation of specialized pattern recognition receptors (PRR) such as toll-like receptors (TLR) sensing potential harm. They recognize pathogen-associated molecular patterns (PAMPs) which are tightly conserved structures, expressed by a broad spectrum of microorganisms but not by host cells. Furthermore, PRR will also be activated by endogenous DAMPs (damage-associated molecular patterns) associated with stressed, damaged, or infected host cells. This reactivity towards conserved signals allows for an immediate reaction towards recognized threats by initiating the cellular and humoral components of innate immunity. Humoral immunity broadly consists of extracellular macromolecules. Its innate components involve the complement system, cytokines, and antimicrobial peptides. However, the cellular response of innate immunity involves the killing of infected body cells and the direct ingestion of pathogens by phagocytosis. Both branches of innate immunity additionally contribute to the activation and recruitment of adaptive immune cells by cytokine signalling on the one hand and antigen presentation in lymphoid organs on the other hand [2].

In addition to that, the adaptive immune system can be directly activated in the periphery by recognising foreign peptides presented on infected or malfunctioning cells. This detection is based on an extensive repertoire of specific receptors to run a very precise immune response against a defined antigen. There is again a humoral and a cellular

division to the adaptive immune response: differentiated B cells, called plasma cells, producing antigen-specific immunoglobulins (Ig) and T cells with a specialized antigen-specific receptor, respectively. In contrast to PRR in the innate system, the adaptive system does not recognise conserved structures but rather every foreign antigen that it was not educated to tolerate. This mechanism results in a slower reaction time, but an antigen-specific clearance of threats and long-lasting protection due to memory formation [2].

1.2 Antigen presentation

To achieve this precise immune reaction, the antigen must be presented in an accessible way for the adaptive immune system. Therefore, almost all host cells, except for erythrocytes, express the major histocompatibility complex class I (MHC-I). Cytosolic proteins are processed into small peptides in the endoplasmic reticulum, bound to MHC-I and presented on the cell surface. If viral peptides are present in infected cells, they are also displayed on MHC-I, recognised by cytotoxic $CD8^+$ T cells and then the host cell is killed. MHC class II (MHC-II), however, is only expressed on specialized antigen presenting cells (APCs) such as B cells, macrophages, and dendritic cells (DC). Some functions of these cells are to eliminate pathogens, debris, and dead cells via phagocytosis. Exogeneous peptides from the thereby formed vesicles are then sampled, processed, and presented to $CD4^+$ T cells on MHC-II [4]. In contrast to MHC-I, the APCs are not killed upon recognition of foreign peptides on MHC-II, but a targeted adaptive immune reaction is triggered against the antigen [2].

1.3 B cell and T cell development

The main actors of the cellular adaptive immune system are T cells and B cells with their broad repertoire of antigen recognition receptors. Both populations initially develop from the common lymphoid progenitor in the bone marrow and B cells only leave the bone marrow before their final maturation. To create a vast spectrum of antibodies and T cell receptors (TCR), a process called V(D)J-recombination is mediated by the recombination activating genes (Rag). The genetic immunoglobulin domain consists of several distinct versions of the variable (V), diversity (D) and joining (J) gene segments. During B cell and

T cell development these segments are randomly selected and rearranged to form a unique coding sequence for the resulting antibody or TCR. After a B cell progenitor successfully expresses light and heavy chains of a full immunoglobulin, central tolerance is ensured by eliminating self-reactive antibodies before the B cells leave the bone marrow for final maturation [2].

T cells, on the other hand, migrate to the thymus in the common lymphoid progenitor stadium where Notch signalling commits the precursor cell to the T cell lineage. As the two major subpopulations of $\alpha\beta$T cells are $CD4^+$ T helper cells and $CD8^+$ cytotoxic T cells, the developmental stages of T cells in the thymus are named after the expression of CD4 and CD8. While the TCR gene domain is still in germ line arrangement in the first double negative stage (DN1), V(D)J-recombination of the β-chain begins during DN2 and only cells with successful β-chain rearrangement reach DN4. The α-chain recombination is subsequently carried out during the double positive (DP) stage. Due to the unguided rearrangement of VDJ segments, a vast majority of the generated TCRs are non-functional or reactive towards autoantigen [2]. Hence, cortical epithelial cells in the thymus present self-peptide:self-MHC complexes to positively select DP thymocytes with an MHC binding TCR by supplying them with survival signals [5]. Non-binding T cells are thereby eliminated and, depending on which MHC class is bound, the CD4 or CD8 effector fate of the cell is determined, resulting in a single positive (SP) stage. However, this positive selection of self-binding TCRs shifts the TCR repertoire towards recognition of self-antigen and thereby an elevated risk of autoimmunity. Subsequent negative selection ensures the necessary elimination of self-reactive TCRs. To that end, specialized stromal cells called medullary thymic epithelial cells (mTECs) express the autoimmune regulator gene (Aire) enabling them to produce tissue-specific antigen, normally presented in peripheral organs, in the thymus [6], [7]. Thymocytes are then selected according to the binding strength of their TCR towards self-antigen presented on mTEC MHC. While SP cells with a low-affinity TCR can fully mature, strongly autoreactive TCRs are negatively selected and eliminated. Consequently, mutation of Aire in humans leads to a severe autoimmune disease called autoimmune polyendocrinopathy-candidiasis-ectodermal dystrophy due to ineffective negative selection and self-reactive T cells [8].

As mTEC-mediated negative selection in the thymus may not eliminate all self-reactive T cells and foreign antigen might also be harmless, other immune regulating mechanisms are additionally needed. One of these safety mechanisms is the necessity of co-stimulation to trigger a T cell response. The co-stimulatory molecule CD28 is expressed on the surface of naïve T cells to bind the co-stimulatory ligands CD80 and CD86 expressed along with MHC-II by professional APCs. Both the primary stimulatory signal via TCR – MHC:peptide binding and the secondary stimulatory signal via CD28 – CD80/CD86 are needed for a fully functional T cell response. If either signal is missing, the T cell does not induce an immune reaction or differentiation program but instead enters a state of anergy [2], [9].

1.4 $CD4^+$ T HELPER CELLS

As previously described, $CD8^+$ cytotoxic T cells are responsible for directly killing infected or malignant host cells via MHC-I recognition, while $CD4^+$ T helper cells coordinate and trigger a broad spectrum of immune responses while also contributing to maintaining immune tolerance in response to peptide:MHC-II complexes presented on APCs. To enable a specific immune reaction and thereby efficient clearance of pathogens, the subtypes of $CD4^+$ T helper cells have distinct characteristics. Infections with different pathogens create a unique environment that, in combination with TCR activation and co-stimulation, induces naïve T cells to differentiate. They receive cytokines produced by distressed host cells leading to the activation of distinct STAT proteins, causing the expression of master transcription factors (TKFs) and thereby determining the differentiation of naïve $CD4^+$ T cells [10]. The most prominent helper T cell subpopulations are Th1, Th2, Th17, follicular T helper cells (Tfh) and regulatory T cells (Tregs). However, Tregs will be addressed in a separate chapter.

Initially, only Th1 and Th2 cells were defined based on their different production of cytokines [11], [12]. During a viral infection, innate lymphoid cells produce the type I cytokine IFNγ (interferone gamma). Together with TCR and co-stimulatory signals, IFNγ binding leads to STAT1 (Signal Transducer and Activator of Transcription 1) activation in naïve $CD4^+$ T cells and hence the expression of the Th1 master transcription factor T-bet

[2], [10], [13]. Further IL-12 signalling from DCs and corresponding STAT4 activation, solidifies the Th1 fate of the cell by elevating T-bet expression [14]. Supporting the immune response against viruses and other intracellular pathogens is the main function of Th1 cells. They produce IFNγ to aid macrophages in killing ingested pathogens. Nonetheless, Th1 cells have the potential to become pathologic by reacting to commensal microbiota and thereby inducing colitis [15], [16].

If the naïve T helper cell is stimulated in the inflamed milieu of a parasitic infection, it receives IL-4 (interleukin 4) produced by basophils or other innate immune cells, instead of IFNγ [17], [18]. IL-4 signalling results in the activation of STAT6 and thereby the transcription factor GATA3 is expressed, which is sufficient and essential for the differentiation and function of Th2 cells [19], [20]. Th2 function can also be induced by IL-33 signalling from damaged epithelial cells binding ST2 [21]. Activated Th2 cells support the anti-parasitic immunity of mast cells and eosinophils by producing the type 2 cytokines IL-4, IL-5 and IL-13 [2]. In B cells, IL-4 signalling results in class switching and thereby the production of anti-parasitic IgE. However, aberrant type 2 immune response against harmless dietary antigen can result in IgE-mediated food allergy and severe anaphylaxis [22].

The third major type of $CD4^+$ T helper cells is the more recently described Th17 cells named according to their production of IL-17 [23], [24]. In mucosal areas with high bacterial load innate immune cells produce TGFβ and IL-6. Upon TCR binding and co-stimulation on naïve $CD4^+$ T cells, these cytokines activate STAT3 and thereby stimulate the expression of the orphan nuclear receptor RORγt [2], [10]. RORγt is the master transcription factor of the Th17 cell fate and is necessary for the production of IL-17 [25]. In contrast to Th1 and Th2 cells, Th17 cells do not produce the necessary cytokines for a positive feedback loop, as their defining cytokines are not TGFβ and IL-6 but IL-17 and IL-22. While IL-17 stimulates the release of chemokines from surrounding cells and thereby the recruitment of neutrophils, IL-22 triggers the production of antimicrobial peptides in the mucosal epithelial barrier [2]. Although Th17 cells were demonstrated to aid in viral infections, their key function is defence against extracellular bacteria and fungi [26]–[28]. Concordant with their role in antibacterial immunity, Th17 cells can be induced

by colonisation of the intestinal tract with SFB (Segmented filamentous bacteria) [29]. Their homeostatic importance in the intestine is highlighted by the role of aberrant Th17 cell response in autoimmune disease and chronic inflammation [25].

In the B cell follicle germinal centre, a distinct morphological area of secondary lymphoid organs, a fourth subpopulation of T helper cells can be found: T follicular helper (Tfh) cells. In contrast to the previously described T helper subsets, the differentiation of follicular T helper cells (Tfh) is not clarified beyond doubt. The predominant hypothesis states that DCs initially induce the differentiation of Tfh cells but constant stimulation by B cells is needed to maintain the Tfh cell status [30]. However, signalling of IL-6 and IL-21 via STAT3, either on B cells or directly on $CD4^+$ T cells, was also demonstrated to trigger expression of the Tfh defining transcription factor Bcl6 (B cell lymphoma 6) [31]–[33]. Instead of Bcl6, all other T helper subsets express Blimp-1. These two transcription factors have an antagonistic relationship and are mutually exclusive, thereby committing Tfh cells to their differentiation [32], [34]. Nevertheless, Tfh cells produce low amounts of the Th1, Th2 and Th17 cytokines IFNγ, IL-4 and IL-17, respectively. Tfh cells are required for B cell support in the germinal centre including affinity maturation, differentiation into antibody-producing plasma cells, memory B cell formation and class switching. Therefore, some data indicates that the production of effector T helper cytokines regulates class switching to ensure that the most effective type of immunoglobulin is produced for the infection at hand [30].

1.5 Regulatory T cells

To avoid overshooting immune reactions or responses against self-antigen or harmless foreign antigen, specialized suppressive $CD4^+$ T cells have evolved. Contrary to supporting an inflammatory reaction, like T helper cells, they regulate it and are therefore called regulatory T cells (Tregs). By utilizing various suppression mechanisms such as cell-cell interactions and cytokine secretion, they not only inhibit self-reactivity and induce tolerance but also support wound healing and tissue homeostasis, making them a promising tool in immunotherapy (Reviewed in [35]).

As previously mentioned in **1.3 B cell and T cell development**, T cells with a randomly generated TCR are selected in the thymus based on their reactivity towards self-antigen:MHC combinations. Cells which do not bind at all and highly self-reactive cells undergo apoptosis and TCRs with a low self-antigen binding allow the cell to leave the thymus as a naïve T cell. However, there is a third option: if the TCR displays intermediate affinity towards self-antigen presented on mTECs during the negative selection step, the respective $CD4^+$ T cell will differentiate into a Treg, providing this cell type with a diverse self-reactive TCR repertoire [36], [37]. Upon this selection in the thymus, Tregs upregulate the lineage master transcription factor Foxp3 (forkhead box protein 3), enabling the expression of suppression molecules [38], [39]. Consequently, loss of functional Foxp3 leads to loss of Tregs in mutant scurfy mice and hence, lethally severe inflammation and multi-pathology caused by overly proliferative lymphocytes [40]. A similar disease pattern is described for humans with a fatal point mutation in the FOXP3 gene, causing immune dysregulation, polyendocrinopathy, enteropathy, X-linked syndrome (IPEX) [41], [42]. Additionally, loss of Foxp3 in committed Tregs can lead to pathogenic conversion towards pro-inflammatory Th17 cells in autoimmune arthritis [43], emphasizing the requirement of epigenetic Foxp3 stabilization for long-term Treg functionality and lineage commitment [44]. Although there are different opinions on who came first, CD25 or Foxp3, it is undisputed that both are important for unimpaired Treg performance [45]–[47]. CD25 is a high affinity IL-2 receptor and is constitutively expressed on Tregs and crucial for their maintenance *in vivo* [48], [49]. The CD25 ligand IL-2 is produced by activated T cells in an inflammatory setting. As Tregs cannot produce IL-2 themselves, they are highly reliant on exogenous IL-2 from other cells and therefore colocalise with its producers, leading to a negative feedback loop of the ongoing immune reaction [35]. This negative feedback is achieved by the superior affinity of CD25 towards IL-2 leading to a consumption of the available cytokine by Tregs, depriving other responder T cells, especially $CD8^+$ T cells, of IL-2 and thereby causing impaired differentiation and proliferation [50], [51]. Next to CD25 to compete for cytokines, Tregs also express CTLA-4 (cytotoxic T lymphocyte antigen 4). CTLA-4 is used by Tregs for binding the co-stimulatory ligands CD80/CD86 presented on APCs and extracting them via trogocytosis [52], [53]. Thereby the APCs are impaired in their potential for co-stimulation, and self-reactive

T cells binding the APCs will undergo anergy. Furthermore, Tregs produce the anti-inflammatory cytokines TGFβ and IL-10 to directly suppress T cell dependent immunopathology (Reviewed in [54]).

In addition to its role in the suppressive function of Tregs, TGFβ together with IL-2 enables $CD4^+CD25^-$ T cells to differentiate into $Foxp3^+$ Tregs *in vitro* even after negative selection in the thymus [55], [56]. As they are artificially induced and not naturally occurring, those cells are called iTregs (induced Tregs) [57]. To differentiate Tregs generated in the thymus, according to their intermediate self-reactive TCR, from other subtypes, they are henceforth termed thymically derived Tregs (tTregs). Usually, tTregs are discriminated according to their expression of the Ikaros transcription factor family member Helios [58].

Specialized Tregs found in various peripheral tissues such as visceral adipose tissue, muscle, gut and skin have been named tissue Tregs (tisTreg) due to their role in tissue repair [59]–[63]. As tisTreg express Helios, they are assumed to derive from the thymus, however, they also express GATA3, associating them with Th2 immunity [64], [65]. Most importantly however, tisTregs are characterized by their expression of KLRG1 (Killer cell Lectin-like receptor G1), Areg (Amphiregulin) and ST2 [61], [63], [65]. ST2 is an IL-33 receptor encoded by the *Il1rl1* (Interleukin1 receptor-like 1) gene. It enables tisTregs to sensor IL-33 excreted from damaged epithelial cells leading to tisTreg recruitment and clonal expansion [66]–[68]. Thereby they can promote tissue repair during inflammation and reduce tissue damage during colitis [61], [62], [69].

Even in healthy individuals the intestinal tract is particularly susceptible to undesired T cell responses due to the constant proximity to a plenitude of innocuous antigen from commensal bacterial or dietary origin. Another specialized subtype of $Foxp3^+$ regulatory T cells, expressing the retinoic acid receptor-related orphan-receptor gamma t (RORγt), has been identified in the gut and is thought to control the activation of effector T cells in response to harmless microbial antigens. Contrary to tTregs they do not develop in the thymus but differentiate locally from naïve $CD4^+$ T cells to provide active immune tolerance towards commensal microbes [70]–[72]. Concomitant with their non-thymic origin, these Tregs neither express Helios nor a TCR with intermediate self-reactivity, ensuing distinct TCR repertoires [73]. Although, $ROR\gamma t^-$ Treg subtypes can also be induced

in the periphery of the intestine by the presence of dietary antigen [74], in this study, pTregs (peripherally induced Tregs) will be defined as microbiota-specific RORγt^{+}Helios^{-} Tregs. In line with their bacteria induced RORγt^{+} T helper counterpart, Th17 cells, pTregs are absent in germfree (GF) mice and can be induced by bacterial colonisation. However, not all bacteria are equally effective inducers but distinct bacterial species, especially *Clostridia* strains, are more potent than others [71], [72], [75]. The molecular and cellular pathways leading to their differentiation have yet to be fully elucidated, however corresponding to *in vitro* induced iTregs, pTregs need TGFβ and IL-2 to upregulate Foxp3 [76]. Surprisingly, although pTregs may thus be induced later in life, to avoid pathological imprinting, a critical window of opportunity must be adhered to. During the weaning of newborn mice, their microbiome changes drastically, leading to a spike in pTreg induction. Failure to induce an adequate pTreg population during this specific timeframe causes increased susceptibility towards allergic inflammation and colitis, highlighting their importance in gut homeostasis [77].

1.6 MICROBIAL TOLERANCE

The intestinal lumen is colonised by a multitude of different viral, bacterial and fungal strains, called the commensal microbiome, that are not pathogenic towards the host but have a symbiotic relationship [78]. Due to a co-dependence of host and microbiota, it is essential for the immune system to differentiate harmless from pathogenic strains and inhibit undesired immune reactions. Th17 cells, pTregs and also ILC3s (innate lymphoid cells type 3) are inducible by microbiota, show increased abundance in the intestines and they all express RORγt, highlighting the significance of RORγt for intestinal tolerance [79]. Because those potentially tolerogenic immune cells and the bacteria in the gut lumen are spatially separated by mucosal tissues, sophisticated pathways for their induction evolved. Macrophages can take up antigen from the intestinal content and transmit them to DCs migrating to the gut-draining lymph nodes: the mesenteric lymph nodes (mLN) [80]–[83]. In the mLN stromal cells produce tolerance inducing TGFβ as a response to bacterial derivates enabling the DCs to induce pTregs from naïve CD4^{+} T cells [82]–[85]. Concerning bacterial derivates, it was furthermore demonstrated that certain products from commensal bacterial strains such as surface polysaccharides [86], short-chain fatty

acids (SCFAs) - a metabolic byproduct [87] - or secondary bile acids also play a role in pTreg induction [88], [89]. As previously mentioned in **1.1 Innate and adaptive immunity** innate lymphoid cells possess specialized PRRs called TLR recognizing conserved bacterial structures to initiate a swift immune response. However, those receptors are also necessary for immune homeostasis and tolerance [90]. Ablating the TLR adaptor MyD88 specifically in Tregs led to a shifted Th17/pTreg balance towards more pathological Th17 cells and decreased levels of IgA [91].

The production of large amounts of microbiota-specific IgA supports tolerance of commensal microbiota and promotes bacterial diversity while also preventing the invasion of pathogens [92]. This is achieved by secreting IgA into the gut Lumen where it coats the bacteria [93]. Surprisingly, secretion of microbiome-specific IgA in the milk of nursing mothers inherits their homeostatic capabilities to their offspring, resulting in transmitted pTreg frequencies and intestinal tolerance [94]. Impaired secretion of IgA in the intestinal tract leads to disturbed microbial homeostasis, called dysbiosis, favouring pathological species and thereby promoting the development of autoimmune or inflammatory diseases [95], [96].

1.7 INFLAMMATORY BOWEL DISEASE

Aberrant immune responses against intestinal bacteria and thereby absent tolerance to commensal microbiota, accompanied by dysbiosis, play an essential role in inflammatory bowel diseases (IBD) [97], [98]. The term IBD encompasses two distinct conditions with chronically reoccurring intestinal inflammation: Ulcerative colitis and Crohn's disease. Although many genetic risk factors such as IL-10/IL-10RA deficiency, disturbed intestinal integrity or a defective mucosal layer have been described, they will only account for up to 30% of IBD cases, demanding for other disease contributors (Reviewed in [99]).

Due to increased levels of IL-17 and elevated Th17 cell abundances in IBD patients, it was assumed that disease progression was determined by rampant Th17 cell populations [100], [101]. But IL-23R expressing pathogenic Th1 cells have been demonstrated to be contributors to the development of colitis as well [15], [102]. Concomitant with a shift of Tregs towards pathogenic Th17/Th1 cells, distinct clonal TCR overlap between effector

cells and Tregs was found in patients with ulcerative colitis [103]. Furthermore, microbiome transplants from IBD patients shifted the intestinal balance of pTreg/Th17 cells towards more Th17 cells and increased the severity of colitis in murine recipients compared to the microbiome of healthy patients [104]. Together with impeded TLR-dependent transmission of microbial signals, these results illuminate the role of dysbiosis and tolerance in IBD progression [90]. As failing to induce pTregs leads to intestinal inflammation in DDX5-deficient mice and the intestinal microbiome of IBD patients displays a reduced abundance of pTreg-inducing *Clostridia* species, the importance of pTregs in intestinal homeostasis is verified once more [99], [105]. Hence, a potential application of Treg based immunotherapy for IBD patients has been frequently discussed (Reviewed in [106]–[108]).

1.8 MICROBIOTA IN FOOD ALLERGY

Dysregulated intestinal immunity does not only induce inflammatory diseases such as IBD but also hypersensitive reactions to harmless antigen: Allergy. In recent decades, incidences of allergic diseases escalated as climate change and pollution dramatically impacted air quality and increased pollen load [109], [110]. In addition to environmental factors, the development of allergic hypersensitivity is determined by the microbiome. Modern perturbations such as birth by caesarean section or frequent use of antibiotics, but also more sterile living conditions and thereby reduced occurrence of infections increase the risk of allergies by altering the microbiome [109], [111]. Consequently, with the advancing spread of the Western lifestyle accompanied by these microbial changes, food allergies are on the rise [112], [113]. Dietary allergies are an aberrant type 2 immune response due to loss of oral tolerance towards food antigen, which can lead to potentially fatal anaphylaxis [114], [115]. This acute immune reaction is caused by the degranulation of mast cells loaded with allergen specific IgE. Specialized Th2-like Tfh cells skew the class-switching in B cells to produce these allergy mediating IgE antibodies [116]. Thereby, IgE levels and specificity can be used as a diagnostic marker in allergic diseases [117].

In GF and antibiotic treated mice, food allergen drives the generation of Th2-biased Tfh cells and thereby elevates the levels of serum IgE [118], [119]. Furthermore, basophils

and Th2 cells are increased in abundance in those mice due to a lack of microbiota-induced pTregs regulating type 2 immunity [71], [118]. The importance of healthy commensal microbiota in food allergy is additionally supported by the exacerbation of allergic reactions in GF mice colonised with microbiota from allergic children [120]. Consequently, microbiome therapy by administering commensal bacterial strains such as *Clostridia* is able to reduce serum IgE levels, increase pTreg frequencies via MyD88 and thereby ameliorate the severity of allergic responses [71], [119], [121].

1.9 THE NFκB PATHWAY

MyD88 (myeloid differentiation primary response gene 88) is an adaptor protein, needed to transmit signals from activated TLR downstream to the NFκB (nuclear factor κB) pathway [122]. In general, after receptors recognise their cognate ligand, they recruit adaptor proteins activating IKK (IκB kinase) complexes and thereby enabling the NFκB pathway. Through this mechanism, a plethora of immune signals are processed towards the survival, proliferation or differentiation of a cell by regulating gene expression [123]. In more detail, the NFκB transcription factors are homo- or heterodimers of proteins with a Rel homology domain, enabling DNA binding and dimerization [123], [124]. This family consists of five proteins: RelA (encoded by *Rela*), RelB (*Relb*), c-Rel (*Rel*), p50 (*Nfkb1*), and p52 (*Nfkb2*). However, only RelA, RelB and c-Rel have a transactivation domain, allowing them to positively regulate gene expression after binding. Therefore, p50 and p52 dimers in the absence of a transactivation domain can bind κB sites but only suppress gene expression [125]. In their inactive form, NFκB dimers reside in the cytosol, either due to a bound IκB (Inhibitor of κB) or because they are dimerized to p100 or p105, the precursor proteins of p52 and p50, respectively [126], [127]. IκBα (*Nfkbia*), IκBβ (*Nfkbib*), and IκBε (*Nfkbie*) are classical IκB proteins retaining NFκB dimers in the cytosol. Upon receptor activation and signalling, IKK complexes initiate degradation of IκB proteins and thereby enable translocation to the nucleus, where the NFκB dimer binds κB binding sites in promoter or enhancer regions [125], [128]. Atypical IκB members in contrast are localised in the nucleus and inhibit or promote transcriptional regulation by stabilizing bound NFκB dimers [128].

Two alternate pathways of NFκB mediated gene regulation are activated by different receptors and target distinct genes. When the canonical pathway is activated, by diverse immune receptors such as TLRs, TCR/BCR or cytokine receptors, IKK complexes phosphorylate IκB proteins for degradation or p105 for cleavage. Thereby, preformed heterodimers, mainly RelA:p50 or c-Rel:p50, can pass into the nucleus [129]. On the other hand, the non-canonical or alternative pathway is activated by members of the TNFRSF (TNF receptor superfamily) leading to cleavage of p100 to p52, enabling translocation of RelB:p52 heterodimers [130]. Overall, the NFκB pathway is crucial for many fundamental functions of the immune system. For example, it is essential for proper Treg differentiation and maintenance as deficiency of c-Rel and RelA in T cells or Tregs decreases thymic Treg differentiation and function in the periphery [131]–[135]. Consequently, mutations or dysregulations of NFκB can lead to various diseases including immunodeficiency, chronic inflammation or cancer [136].

1.10 Role of Bcl3 in gut homeostasis

B cell lymphoma 3 (Bcl3), a nuclear transcription co-factor, was initially described as a proto-oncogene in patients suffering from chronic B cell lymphoblastic leukaemia [137], [138]. Chromosomal translocation upstream of the *BCL3* gene in these patients leads to Bcl3 overexpression and thereby altered lymphoproliferation [139]. However, Bcl3 deficient mice ($Bcl3^{KO/KO}$) displaying altered lymphoid organ microarchitecture and increased susceptibility towards infectious diseases soon revealed the relevance of Bcl3 in healthy immune responses [140], [141]. Thereby Bcl3 was the first described member of the atypical IκB family otherwise containing IκBζ (encoded by *Nfkbiz*), $IκB_{NS}$ (*Nfkbid*), IκBη (*Ankrd42*) and IκBL (*Nfkbil1*) [128], [142]. The transcription co-factor resides in the nucleus and contains two transactivation domains to enable positive regulation of gene expression [125], [143]. The bilateral role of Bcl3 in regulating gene expression is transmitted via different paths. Binding p50 or p52 in hetero- or homodimers can either suppress or activate the transcription, depending on the dimer and the signal on hand [144], [145]. As p50 does not possess a transactivation domain, binding of p50 homodimers to the DNA blocks IκB sites and thereby inhibits transcription [125]. Bcl3 can inhibit the binding of p50:p50 complexes to IκB sites or bind to DNA-bound p50 and

directly activate NFκB gene expression via transactivation domains [146], [147]. On the other hand, Bcl3 has also been demonstrated to delay p50 turnover by halting ubiquitination or recruiting co-repressors to inhibit transcription of NFκB target genes [148]–[150]. More recently *Pan et al.* described the essential aspect of Bcl3 in the formation of p52 homodimers promoting proliferation, migration and inflammation delivering a possible explanation for the course of Bcl3 in cancer [151]. Hence, as Bcl3 might stabilize or impair homodimer binding, recruit co-activators or co-repressors and even directly transactivate gene expression, it has versatile and two-sided immunorelevant functions. Consequently, Bcl3 expression is tightly regulated but can be modified by immune signals AP-1 or STAT3 [152], [153]. Next to blood cancer, dysregulation of Bcl3 can lead to inflammatory or autoimmune diseases through proinflammatory or anti-inflammatory regulation (Reviewed in [144]). More precisely, overexpression (OE) of Bcl3 impedes T cell proliferation and activation [154] but Bcl3 deficiency causes exacerbated severity of a Lupus-like phenotype [155], impaired Th2 differentiation through reduced GATA3 activation [156], and increased susceptibility towards infectious diseases [140], [141]. Furthermore, $Bcl3^{KO/KO}$ mice were protected from dextran-sodium sulphate (DSS) induced colitis, suggesting involvement of Bcl3 in intestinal homeostasis. This is moreover supported by an inability of Bcl3 deficient Th1-differentiated cells to induce colitis in an IBD model called T cell transfer colitis [157]. In IBD patients, Bcl3 expression was indeed found to be upregulated, and a corresponding overexpression of Bcl3 exclusively in T cells resulted in the development of spontaneous colitis in these animals, underlining the importance of Bcl3 in intestinal T cells [158]. However, it remains to be determined if Bcl3 impacts gut homeostasis by regulating intestinal regulators such as pTregs.

1.11 AIMS OF THIS STUDY

The importance of the NFκB pathway in intact immune responses is well described as well as its importance for proper Treg development and thereby immune homeostasis [125], [135]. Given the vast surface area of the intestinal tract in close proximity to an excessive load of non-self-antigens, defining molecular nodules governing the induction and maintenance of microbiota dependent Tregs presents the possibility of establishing more targeted concepts to influence pTreg populations. This understanding might be utilized to either treat IBD which is known to be often associated with dysfunctional Tregs or reinforce effector T cell responses in case of infectious diseases.

The first aim of this study is to determine transcriptional differences between tTregs and pTregs to gain insight into their divergent developmental paths and to assess the influence of disturbed intestinal colonisation on TCR diversity and the outcome of allergic sensitisation to dietary antigens. To this end, the transcriptome and TCR repertoire of intestinal Tregs will be analysed on a single cell level in undisturbed mice and after maturing with an altered intestinal microbiome. Mice raised under either germfree conditions or while receiving a broad spectrum of antibiotics are intended to be utilized for this purpose. To further analyse the influence of altered microbial diversity on the severity of food allergy, it is proposed to assess allergic sensitisation on mice with different microbial colonisation early in life. Thereby, distinct pathways of pTreg induction and the impact of microbial diversity on the TCR repertoire and food allergy will be pinpointed.

The second aim of this thesis is to elucidate the involvement of the atypical IκB family member Bcl3 in the differentiation and function of RORγt^{+}Helios^{-} Tregs and how it affects intestinal homeostasis. Hence, intestinal T cell populations of Bcl3 deficient animals will be analysed in detail at steady state. To evaluate possible bystander influences or a T cell intrinsic effect, mixed bone marrow chimeras and mice specifically lacking Bcl3 in Tregs will be assessed. It is additionally aimed to determine the functionality of Bcl3 deficient Tregs by detecting their potential for cytokine production and analysing their suppressive capacity *in vivo* in a T cell transfer based model of colitis. To gain further insight into the effect of Bcl3 deficiency on the Treg transcriptome, mice with fluorescent reporters for

Foxp3 and RORγt will be cross-bred with a Bcl3 deficient mouse line enabling in -depth characterization of different WT and $Bcl3^{KO/KO}$ Treg subpopulations via bulk RNA sequencing. Thereby, the implementation of Bcl3 in the generation of intestinal T cells is addressed to gain further understanding of the underlying mechanisms leading to altered homeostasis in Bcl3 deficient animals. These results will be confirmed on protein level and investigated for *in vivo* relevance by assessing mice with relevant deficiencies for their intestinal Treg landscape.

2 MATERIALS AND METHODS

2.1 MATERIALS

2.1.1 Instruments

Table 1: List of instruments used in this thesis.

Instrument	Manufacturer
Analytic scales	Mettler (Columbus, OH, USA), Scaltec
Autoclave	HP Labortechnik (Oberschleißheim, Germany)
Bioanalyzer 2100	Agilent (Waldbronn, Deutschland)
Cell culture CO^2 incubator	Eppendorf (Hamburg, Germany)
Centrifuges	Eppendorf
Chromium Controller	10X Genomics (Pleasanton, CA, USA)
Dissecting tools	Fine Science Tools (Foster City, CA, USA)
FACS Aria III™ Cell Sorter	BD (Franklin Lakes, NJ, USA)
Flow cytometer BD Accuri™ C6	BD
Flow cytometer BD LSRFortessa™	BD
Fluorescence microscope Leica DM4B	Leica (Wetzlar, Germany)
Freezer -20 °C	Liebherr (Bulle, Germany)
Freezer -80 °C	New Brunswick, Eppendorf
Gel Imaging System	Intas (Göttingen, Germany)
Heating block Thermomixer	Eppendorf
HiSeq 2500	Illumina (San Diego, CA, USA)
Ice machine	Manitowoc Ice (Manitowoc, WI, USA)
Infrared lamp	Philips (Amsterdam, the Netherlands)
Magnetic stirrer RCT basic	IKA (Staufen im Breisgau, Germany)
Mouse restrainer	LabArt (Waldbüttelbrunn, Germany)
NanoDrop™ Spectrophotometer	Peqlab (Erlangen, Germany)
Nexus Gradient PCR cycler	Eppendorf
NovaSeq 6000	Illumina
PerfectBlue Agarose gel chamber	Peqlab
PH-Meter	VWR (Radnor, PA, USA)
Pipettes	Eppendorf
Pipettor accu-jet pro	BrandTech (Wertheim, Germany)
QuadroMACS Separator	Miltenyi Biotec (Bergisch Gladbach, Germany)
Qubit™ 4	Invitrogen (Waltham, MA, USA)
Rectal probe	World Precision Instruments Germany GmbH, (Friedberg, Germany)
Refrigerator	Liebherr
Shaking Incubator Innova 42	New Brunswick
Thermometer for rectal probe	World Precision Instruments Germany GmbH
Tissue Processor for dehydration	Leica

Ultrapure water system Milli-Q®	Merck (Darmstadt, Germany)
Vacuum collecting bottle	Carl Roth (Karlsruhe, Germany)
Vacuum pump	Gilson Inc. (Middleton, WI, USA)
Vortex Genie 2	Scientific industries (Bohemia, NY, USA)

2.1.2 Kits and Reagents

Table 2: Kits and Reagents used in this thesis.

Kit / Reagent	**Manufacturer**
Agarose	Sigma Aldrich (St. Louis, MO, USA)
AMPure XP beads	Beckman Coulter
Bioanalyzer High Sensitivity DNA Assay	Agilent
Bioanalyzer RNA 6000 pico Kit	Agilent
Brefeldin A	Sigma Aldrich
CD4+CD25+ Regulatory T cell Isolation Kit, mouse	Miltenyi
CD4+CD62L+ T cell Isolation Kit, mouse	Miltenyi
Chromium Next GEM Single Cell 3' Kit v3.1	10X Genomics
Chromium™ Single Cell 5' Library Kit	10X Genomics
Chromium™ Single Cell V(D)J Enrichment Kit, Mouse T cell	10X Genomics
CollagenaseD	Sigma Aldrich
DNA stain clear G	Serva (Heidelberg, Germany)
DNase I	Sigma Aldrich
EconoTaq® PLUS GREEN 2x Mastermix	Lucigen (Middleton, USA)
EDTA ultrapure	Gibco, Life Technologies by Thermo Fisher
ERCC ExFold RNA Spike-In Mixes	Invitrogen
Formaldehyde solution 37%	Merck
Foxp3 / Transcription Factor Staining Buffer Set	eBioscience (Thermo Fisher Scientific)
Gel Bead Kit	10X Genomics
GeneRuler DNA Ladder Mix	Thermo Fisher Scientific
Hematoxylin + Eosin Y alcoholic	Labor + Technik (Salzburg, Austria)
IDT DNA/RNA index Plate B	Illumina
Ionomycin	Cayman
L-glutamine	Gibco
LEGEND MAX™ Mouse OVA Specific IgE ELISA Kit	BioLegend (San Diego, CA, USA)
Murine CD4 T cell enrichment kit	Miltenyi
Nextera XT DNA Library Prep Kit	Illumina
Paraffin	Thermo Fisher Scientific
Penicillin/Streptomycin	Gibco
Percoll	GE Healthcare

PMA (Phorbol 12-myristate 13-acetate)	Biomol
Proteinase K	Sigma Aldrich
Qubit™ dsDNA HS assay kit	Invitrogen
RNeasy® Plus micro Kit	Quiagen
SMART-Seq v4 ultra-low input RNA kit	Takara
TotalSeq™-B0157 anti-CD45.2	BioLegend
TotalSeq™-B0178 anti-CD45.1	BioLegend

2.1.3 *In vivo* reagents

Table 3: List of substances used in in vivo experiments.

Reagent	**Manufacturer**
Ampicillin sodium salt	Cayman
Choleratoxin	List Biological Laboratories (Campbell, CA, USA)
Glucose	Sigma Alrdich
Isofluorane	Baxter
Metronidazole	Actavis
OVA EndoFit,	InvivoGen
OVA III chicken egg albumin grade III	Sigma Aldrich
Streptomycin sulfate	Sigma Aldrich
Vancomycin hydrochloride	Cayman

2.1.4 Consumables

Table 4: Consumables used in this thesis.

Consumable	**Company**
0.5 ml, 1.5 ml, 2 ml, 5 ml reaction tubes	Sarstedt (Nümbrecht, Germany)
100 µm cell strainer	Corning Inc. (Corning, NY, USA)
15 ml, 50 ml Tubes	Sarstedt
2 ml, 5 ml, 10 ml, 25 ml, 50 ml serological pipettes	Sarstedt
200 µl PCR tubes	Starlab GmbH (Hamburg, Germany)
40 µm cell strainer	Sarstedt
6-, 12-, 24-, 48-well plate	Thermo Fisher Scientific (Waltham, MC, USA)
96 well plate U-bottom	Greiner
96 well plate V-shaped bottom	Greiner (Kremsmünster, Austria)
Capillary tubes Na-Heparin, disposable	Hirschmann Laborgeräte (Eberstadt, Germany)
FACS tubes	Thermo Fisher Scientific
FACS tubes small	Greiner
Filtropur Bottle top filter 0.2 µm	Sarstedt
MACS columns	Miltenyi Biotec
Millex-GV syringe 0.22 µm Filter	Merck

Pasteur pipettes	Carl Roth
Petri dishes	Sarstedt
Pipette tips	Sarstedt
Serum tubes with EDTA, Monovette®	Sarstedt
Serum tubes with gel, Microvette®	Sarstedt
Sterican Canula	B. Braun (Melsungen, Germany)
SuperFrost Plus, Slides + Coverslide	Thermo Fisher Scientific
Syringes	B. Braun

2.1.5 Buffers

Table 5: Preparation of buffers used in this thesis.

Buffer	**Preparation**
1.5 % Agarose Gel	1X TAE buffer, 1.5 % (m/v) agarose, 4 x 10^{-3}% DNA stain clear G
100 % Percoll	Percoll stock, 10% 10X PBS
50X TAE buffer	2 M Tris, 50 mM EDTA disodium salt, 1M acetic acid, ddH2O, pH 8
ACK Lysis buffer	155 mM NH_4Cl, 10 mM $KHCO_3$, 1 mM Na_2EDTA, ddH2O, pH 7.4
Bcl3 ear clip lysis buffer	100 mM Tris HCl pH=8, 5 mM EDTA, 0.2% SDS, 200 mM NaCl, ddH2O
Digestion medium	RPMI1640 (Gibco), 25 mM HEPES (Gibco), 0.5 mg/ml CollagenaseD, 10 µg/ml DNAse I
Ear clip lysis buffer	10 mM Tris HCl pH 8.0, 50 mM KCl, 0.5 % NP-40, 0.5 % Tween® 20
FACS buffer	PBS, 1% Fetal calf serum (FCS; Sigma Aldrich), 2.5 mM EDTA
MACS buffer	PBS, 0.5% FCS, 2 mM EDTA
PBS	Dilute 1:10 (v/v) from 10X DPBS (Gibco)
RNA lysis buffer	RLT buffer from RNeasy® Plus micro Kit, 1% β-mercaptoethanol
RPMI complete	RPMI1640, 10% FCS, 1% glutamine, 1% Penicillin/Streptomycin, 50 µM β-mercaptoethanol (Sigma)
TE buffer	10 mM Tris HCl, 1 mM EDTA, ddH2O

2.1.6 Flow cytometry

Table 6: Reagents and antibodies used in flow cytometry.

Reagent / antigen	Fluorochrome	Clone	Dilution	Manufacturer
CD3	APC	145-2C11	400	BioLegend
CD3	eF450	145-2C11	100	eBioscience

Extracellular stains/antibodies	CD3e	a700	17A2	100	BioLegend
	CD3e	FITC	145-2C11	200	BD
	CD4	APC-e780	RM-4.5	500	eBioscience
	CD4	BV785	GK1.5	400	BioLegend
	CD4	BV711	RM-4.5	300	BioLegend
	CD45	APC-e780	30-F11	100	eBioscience
	CD45	BV605	30-F11	600	BioLegend
	CD45.1	BV605	A20	100	BioLegend
	CD45.1	AF700	A20	100	Southern Biotech (Birmingham, AL, USA)
	CD45.2	APC-CY7	104	100	BioLegend
	CD8	APC-a780	5H10	800	eBioscience
	CD83	BV650	Michel-19	50	BioLegend
	CD8a	e450	53-6.7	400	eBioscience
	Fc-block™	-	2.4G2	10	BD
	Lineage Cocktail	Biotin	CD5, CD11b, CD45R, Anti-7-4, Anti-Gr-1 (Ly6G/C), and Anti-Terr-119	30	Miltenyi
	Streptavidin	BV785		250	BioLegend
Live/Dead	Live/dead	Aqua		800	BioLegend
	7-Amino-actinomycin D (7AAD)			5 µg/ml	Enzo Life Sciences (Farmingdale, NY, USA)
Intracellular antibodies	Foxp3	PerCP-Cy5.5	FJK-16s	100	eBioscience
	Gata-3	eF660	TWAJ	20	eBioscience
	Helios	PacificBlue	22F6	33	BioLegend
	IL-10	BV711	JES5-16E3	50	BD
	IL-17A	PE-Cy7	TC11-18H10.1	400	BioLegend
	Ki-67	PE-Cy7	B56	200	BD
	RORyt	PE	AFKJS-9	50	eBioscience
	T-bet	PE-CY7	4B10	40	BioLegend
	TGF-b1	APC	TW7-16B4	50	BioLegend

2.1.7 Software and Websites

Table 7: List of software and websites used for data analysis and interpretation.

Software / Website	**Publisher**
BD FACS Diva	BD
BioRender	https://app.biorender.com
CellRanger v6.1.1 or 3.0.2	10X Genomics (Pleasanton, CA, USA)
FlowJo V10	Tree Star (Ashland, USA)
GraphPad Prism 10	GraphPad software Inc. (La Jolla, USA)
Inkscape V 1.2	https://inkscape.org/; GNU General Public License

Las X imaging software	Leica
Loupe Browser 6	10X Genomics
Loupe VDJ Browser v3	10X Genomics
Mendeley Desktop V 1.19.8	Mendeley Ltd., Elsevier
NanoDrop 100 V3.7.0	Peqlab (Erlangen, Germany)
Nextflow nf-core/rnaseq	https://zenodo.org/record/7998767 [159]
Pubmed Literature Database	https://pubmed.ncbi.nlm.nih.gov/
R V 4.0.3	https://cran.r-project.org/
RStudio V1.4.1103	https://posit.co/download/rstudio-desktop/; GNU General Public License

2.1.8 R packages

Table 8: List of R packages used for RNA sequencing data analysis.

R Package	Source
biomaRt	https://bioconductor.org/packages/release/bioc/html/biomaRt.html [160]
DeSeq2	https://bioconductor.org/packages/release/bioc/html/DESeq2.html [161]
EnhancedVolcano	https://bioconductor.org/packages/release/bioc/html/EnhancedVolcano.html [162]
eulerr	https://cran.r-project.org/web/packages/eulerr/index.html [163]
fgsea	https://bioconductor.org/packages/release/bioc/html/fgsea.html [164]
ggplot2	https://ggplot2.tidyverse.org/ [165]
org.Mm.eg.db	http://bioconductor.org/packages/release/data/annotation/html/org.Mm.eg.db.html
pheatmap	https://cran.r-project.org/web/packages/pheatmap/index.html
RcolorBrewer	https://cran.r-project.org/web/packages/RColorBrewer/index.html
Rhea	https://lagkouvardos.github.io/Rhea/ [166]
Seurat	https://satijalab.org/seurat/ [167]
tximport	https://bioconductor.org/packages/release/bioc/html/tximport.html [168]

2.1.9 Mouse lines

Table 9: Mouse lines used in this thesis. If not stated otherwise, all mice were bred on a C57Bl/6 background.

Mouse line	Description	Source
BALB/c; CD83 $^{\Delta Tcell}$ (CD4-Cre, CD83$^{fl/fl}$)	CD4-Cre mediated loss of floxed *Cd83* [169]	W. Hansen, University Hospital Essen

Bcl3-flox (*Bcl3*$^{fl/fl}$)	Insertion of loxP sites in exon 1 of the *Bcl3* gene [157]	P. M. Murphy, National Institute of Health
Bcl3-KO (*Bcl3* ^{tm1Ver})	Genetic targeting of the Bcl3 gene resulting in the lack of functional BCL3 protein [140]	E. Glasmacher, Helmholtz Center Munich
Bcl3OE^{Tcell} / Bcl3OE^{Treg} (*Rosa26*^{flox}*STOP*^{flox} *Bcl3-eGFP*; *Cd4*-Cre / Foxp3-Cre)	T cell specific (Tcell) or Treg specific (Treg) Bcl3 overexpression by insertion of a *Bcl3* transgene into the *Rosa26* locus downstream of *loxP* flanked STOP cassette, crossed with *Cd4*-Cre or Foxp3-Cre mice respectively [158]	N. Hoevelmeyer, University Mainz
Bcl3$^{\Delta Treg}$ (Bcl3-flox, Foxp3-Cre)	*Foxp3*-Cre mediated deletion of *Bcl3*-floxed alleles	Generated in the lab
CD45.1 (*Ptprc*^{a})	Congenic leukocyte marker [170]	N. Hoevelmeyer, University Mainz
Double reporter Bcl3-KO (*Bcl3* ^{tm1Ve}, *Foxp3*^{RFP}x*Rorc*^{GFP})	Mice with loss of functional Bcl3 protein intercrossed with Foxp3-RFPxROR(γt)-GFP double reporter line	Generated in the lab
Foxp3-Cre (Tg(*Foxp3*-EGFP/cre)	Foxp3 promotor-driven BAC transgenic Cre mice [171]	The Jackson Laboratory
Foxp3^{RFP}x*Rorc*^{GFP}	*Foxp3*-RFP knock in and *Rorc*-GFP BAC transgenic double reporter mice [71]	G. Eberl, Institute Pasteur Paris
Germfree mice (GF)	Wildtype mice bred and housed under fully microbiota-free conditions	Hannover Medical School
Rag1-KO (Rag1^{tm1Mom}/J)	Targeted loss of function mutation of the *Rag1* gene resulting in loss of all mature lymphocytes [172]	N. Hoevelmeyer, University Mainz
Reduced Microbiome Bcl3-KO (RM-Bcl3)	*Bcl3* ^{tm1Ver} mice initially colonised with a reduced microbiome based on the altered Schaedler flora [173] held under specific pathogen free conditions	I. Schmitz, University Braunschweig

2.1.10 Primers

Table 10: Genotyping primers used in this thesis.

Primer	**Sequence**
Bcl3 WT rev.	CCACAGAGCAACCTGGAAGCA
Bcl3 fwd.	GGCTCCCAAGCTTGAAAAGGC
Bcl3 KO rev.	GCATCGCCTTCTATCGCCTTC
Foxp3 Cre int. fwd.	CAAATGTTGCTTGTCTGGTG
Foxp3 Cre int. rev.	GTCAGTCGAGTGCACAGTTT
Foxp3 Cre fwd.	CGGGTCAGAAAGAATGGTGT

Foxp3 Cre rev.	CAGTTTCAGTCCCCATCCTC
Bcl3 flox fwd.	GGGCCTCTCAACCTCTTTCCTA
Bcl3 flox int rev.	GCGCCGCCCCGACTGAC
Bcl3 flox neo rev.	CGTCCCCAGAGCCCGCAACCAC

2.2 METHODS

2.2.1 Animal maintenance

All mice were housed in individually ventilated cages with food and water *ad libitum*. In all experiments, either littermate controls or age and sex-matched controls were used. All interventions were performed following the European Convention for Animal Care and Use of Laboratory Animals and were approved by the local ethics committee and appropriate government authorities.

2.2.1.1 Animal husbandry

If not stated otherwise in **Table 9** all mice were bred on a C57Bl6/J background and kept under specific pathogen free (SPF) conditions. All interventions were performed according to the European Convention for Animal Care and Use of Laboratory Animals and were approved by the local ethics committee and appropriate government authorities. Rag1-KO, CD45.1, Bcl3OE^{Treg} and Bcl3OE^{Tcell} mice were bred and housed at the Molecular Medicine department of the University Mainz under the supervision of Dr. Nadine Hoevelmeyer. CD83$^{\Delta Tcell}$ animals were bred on a BALB/c background and provided by Prof. Dr. Wiebke Hansen from the Molecular Infection Immunology of the University Hospital Essen. RM-Bcl3 mice hosting a reduced microbiome (RM) compared to unrestricted SPF mice were originally colonised with bacterial strains defined as Altered Schaedler flora (ASF) [173]. After initial colonisation the animals were kept under SPF conditions, therefore it was assumed that they displayed a reduced microbiome rather than ASF. RM-Bcl3 mice were maintained and provided by Prof. Dr. Ingo Schmitz at the University of Braunschweig. Germfree (GF) mice were housed in isolator cages to maintain their germfree status. They were provided by the Hannover Medical School. For food allergy experiments commercially available wildtype mice were used as an additional control.

All other mice including wildtype controls (WT) were bred and housed at Helmholtz Munich Core Facility for Laboratory Animal Services Area E.

2.2.1.2 Genotyping

2.2.1.2.1 Ear clip lysis

Genotyping was performed via PCR on genetic material from ear biopsies. Ear clips were collected at weaning of 3 - 4 week old mice. As the genotyping of the Bcl3-KO line was more fragile, DNA from those ear clips had to be isolated more elaborately. Therefore, clips were incubated at 56°C overnight in 500 µl Bcl3 ear clip lysis buffer containing 0.2 mg/ml Proteinase K. Afterwards samples were vortexed and centrifuged at 12,000 xg for 8 min to sediment any residue. The supernatant was transferred to a new 1.5 ml reaction tube and DNA was precipitated by adding 500 µl isopropanol. After spinning down the DNA at 12,000 xg for 5 min, the supernatant was discarded, and the DNA was washed in 1 ml 70% ethanol (v/v ddH2O). Samples were again centrifuged at 12,000 xg for 5 min, the supernatant was discarded, and the pellet was air dried for approximately 20 min. Finally, the DNA was resuspended in 100 µl TE buffer and incubated at 56°C for one hour.

For all other mouse lines fresh or frozen ear clips were added to 50 µl ear clip lysis buffer and heated to 95°C for 10 min to inactivate endogenous enzymes. After cooling the samples down another 50 µl ear clip lysis buffer and Proteinase K with a final concentration of 0.2 mg/ml was added. Ear clips were then digested overnight at 56°C, vortexed and heat inactivated at 95°C for 15 min. Before preparing the PCR reactions, the lysed ear clip samples were centrifuged at 10,000 xg for 10 min to remove undigested material.

2.2.1.2.2 PCR protocols

Lysed ear clip supernatants, and primers (10 µM) according to **Table 10** and EconoTaq® PLUS GREEN 2x Mastermix were used to prepare genotyping PCR mixes according to **Table 11**. The reactions were then carried out according to programs listed in **Table 12** in a PCR cycler.

Table 11: Pipetting schemes for genotyping PCR mixes

Volumes in µl	*Bcl3*-WT	*Bcl3*-KO	*Foxp3*-Cre	*Bcl3*-flox
EconoTaq Mix	12.5	12.5	12.5	12.5
Water	8.5	8.5	2.5	6.5

Primer fwd.	1	1	2.5	2
Primer rev.	1	1	2.5	1
Primer int fwd.	-	-	1	-
Primer int rev.	-	-	1	1
DNA template	2	2	3	2
Total volume	25	25	25	25

Table 12: Genotyping PCR programs

	Bcl3-WT		*Bcl3*-KO		*Foxp3*-Cre		*Bcl3*-flox	
Unit	T (°C)	t (s)	T (°C)	t (s)	T (°C)	t (s)	T (°C)	t (s)
Initial denaturation	95	60	95	60	94	180	94	180
denaturation	94	30	94	30	94	30	94	30
annealing	58	30	58	30	92	30	60	45
elongation	72	105	72	105	72	30	72	60
Cycles	30		30		30		32	
Final elongation	72	600	72	600	72	120	72	300

2.2.1.2.3 PCR product detection

After the reaction, the PCR products were visualized and assessed according to their length using agarose gel electrophoresis. 1x TAE buffer diluted from 50x TAE buffer in H2O was boiled for 3 min in a microwave with 1.5% agarose powder (v/w). After letting the mixture cool down, 0.08 µl/ml DNA Stain was added before pouring the gel into the mould containing the required combs. The gel was then allowed to polymerize for at least 30 min. Then the gel was moved into a gel electrophoresis chamber containing 1x TAE buffer, the combs were removed, and the PCR products were loaded into the pockets. The GeneRuler Mix was additionally loaded as a size reference. Gel electrophoresis was then run at 100 mA for 45 min and finally, DNA bands were visualized and digitalized by excitation with UV light in a Gel Imaging system.

2.2.1.2.4 Genotyping via flow cytometry

For cross-breeding of the *Bcl3*-KO and the *Foxp3*^{RFP}x*Rorc*^{GFP} line to achieve a Bcl3 deficient line expressing both reporters, it was necessary to genotype the offspring for their reporter expression. This was achieved by flow cytometric analysis of the blood lymphocytes that were isolated as described in **2.2.8.1 Blood lymphocytes**. Cells were then stained with Live/Dead Aqua, anti-CD3 APC, anti-CD4 BV785, and anti-CD45 APC-eF780 for 30 min on ice, washed and analysed using the BD LRSFortessa™. RFP was

excited by the yellow laser at 561 nm and detected by the 585/15 PE channel and GFP was excited by the blue laser at 488 nm and detected by the 530/30 FITC channel. Signal intensity and the percentage of positive cells were used to determine the genotype.

2.2.2 Antibiotic treatment

Several double breedings containing one male and two females were set up on day 0. On day 18, approximately one week before birth one pregnant dam from the double breedings received drinking water containing 2% glucose, 1 mg/ml Vancomycin, 1 mg/ml Ampicilin, 5 mg/ml Streptomycin and 0.5 mg/ml Metronidazole. The second dam from the breeding received unsupplemented drinking water. The bottles containing the mixture of antibiotics (ABX) were exchanged and all adult animals were weighed twice a week. On day 45 the pups were weaned and continued to receive their respective drinking water. Germfree mice were added to the cages of control mice at day 62 to allow for colonisation with their healthy microbiome and ABX treatment was stopped. The bedding was exchanged between the groups to create a more equal cage microbiome. On day 63 one part of the GF mice and some of the control mice were sacrificed to check their initial immunological profile. On day 81 three mice from each group were sacrificed, their SI were harvested and the two samples with the best quality from each group were sorted for single cell RNA sequencing. On day 82 the remaining animals were sacrificed, and their organs were analysed via flow cytometry.

2.2.3 Food allergy model

Two weeks before the start of the experiment 6-10 week old germfree (GF) mice were co-housed with age-matched SPF mice from either our in-house animal facility (AF) or commercially acquired from Charles River (CR). This ensured colonisation of the mice with their cagemate microbiome, resulting in a no longer germfree status, hence, ex-GF. Except for unsensitised controls, all mice were then sensitised for five weeks with 5 mg OVA grade III and 10 µg choleratoxin in 300 µl PBS via intragastric gavage (*i.g.*). Unsensitised animals received *i.g.* 300 µl PBS and 10 µg choleratoxin. Sensitization was performed on days 0, 2, 7, 14, 21, and 28 of the experiment and on day 35 mice were challenged to an anaphylactic reaction against OVA. Before the challenge, the basic body temperature of each mouse was determined by carefully measuring it with a rectal probe.

Then anaphylaxis was triggered via *i.v.* application of 12.5 µg OVA EndoFit in 200 µl warm PBS to the tail vein. Afterwards, the body temperature was measured every 5 min and the overall condition of the mice was tightly monitored for one hour or until the initial body temperature was reached again. On day 36 of the experiment, mice were sacrificed, and organs were harvested for analysis.

2.2.4 Bone marrow chimeras

For bone marrow chimeras recipient Rag1-KO mice were lethally irradiated with 9.5 Gy. After a five-hour gap to allow for repair processes, the irradiation was repeated. The mice were then injected *i.v.* with $1x10^7$ purified bone marrow cells from either $CD45.1^+$ congenically labelled mice, $CD45.2^+$ Bcl3-KO mice or with a 50:50 mixture of both bone marrow cells. From five days before irradiation until three weeks afterwards, the mice were maintained on Borgal antibiotics to reduce the risk of infection. Lymphoid organs and intestines of the animals were sacrificed and analysed 16 weeks after bone marrow transplantation. Irradiation and cell transfer were performed by Elena Zurkowski of the University of Mainz.

2.2.5 T cell transfer colitis

To induce T cell transfer mediated colitis, naïve $CD4^+CD62L^+$ T cells were isolated via MACS enrichment from spleens of $CD45.1^+$ mice according to the manufacturer's instructions. Rag1-KO mice aged 6-25 weeks (age equally distributed to groups) received $5x10^5$ purified naïve T cells via *i.p.* injection. Furthermore, splenic regulatory T cells were isolated from WT and Bcl3-KO mice using a $CD4^+CD25^+$ regulatory T cell MACS kit. In addition to the naïve T cells, one group received $5x10^5$ WT Tregs and one group received $5x10^5$ $Bcl3^{KO/KO}$ Tregs. A third group remained with only naïve $CD4^+$ T cells and no Tregs to allow for undisturbed colitis development. All recipients were then weighed and monitored for 5-6 weeks. Cell transfer and monitoring were performed by Elena Zurkowski of the University of Mainz.

2.2.6 Histology

Cross sections of the proximal colon and Swiss rolls of the most distal third of the small intestine were fixed in 4% formaldehyde (v/v in PBS) for 24 hours at room temperature. After samples were thoroughly fixed, they were watered in tap water for 90 min and then

transferred into the first step of the dehydration process containing 70% ethanol. Next followed a series of graded ethanol baths and finally perfusion with paraffin mediated by an automatic tissue processor. Samples were then embedded, cut into 4 µm sections, deparaffinized with heat and xylene and rehydrated using alcoholic dilutions. To determine the grade of inflammation, samples were then stained with hematoxylin and eosin in accordance with standard protocols. Histopathological scoring regarding lymphocyte infiltration, gobleT cell loss and epithelial hyperplasia was performed by a blinded pathologist.

2.2.7 Enzyme-Linked Immunosorbent Assay (ELISA)

To assess blood concentrations of OVA specific IgE of mice in a food allergy model, blood was drawn at day 0 and day 35 of the experimental workflow. The withdrawal was performed as described in **2.2.8.1 Blood lymphocytes** but blood was collected in serum tubes with gel instead of EDTA tubes. Then serum was separated by centrifugation for 10 min at 10,000 rpm at 4°C. Then OVA-specific IgE was measured using the Legend MAX™ Mouse OVA Specific IgE ELISA Kit according to the manufacturer's instructions. The concentration was calculated using the standard solutions contained in the kit as a reference.

2.2.8 Cell isolation from murine organs

Immediately before organ withdrawal mice were sacrificed via cervical dislocation. For organ analysis, mice were between 5 and 25 weeks old.

If not indicated otherwise, all centrifugation steps were performed at 450 xg and 4°C and all digestion steps were performed at 37°C while shaking with 80 rpm.

2.2.8.1 Blood lymphocytes

For blood lymphocytes mice were anaesthetized via inhalation of 2% isoflurane and retrobulbar blood was drawn by applying a glass capillary behind the eye using a rotating movement. The blood was collected in Li-Heparin tubes and inverted. For erythrocyte lysis 100 µl blood was transferred into a 15 ml tube and 2 ml ACK lysis buffer was added. After incubating for 2 min at room temperature, 10 ml PBS was added to dilute the lysis buffer. Cells were then centrifuged for 5 min and the colour of the pellet was assessed. If

erythrocytes were sufficiently lysed the pellet was white and proceeded to washing once with PBS. If the pellet was still red, ACK lysis was repeated.

2.2.8.2 Peritoneal cavity lavage (PEC)

For peritoneal exudate cells, the abdominal skin of sacrificed mice was opened while leaving the peritoneum intact. Then the peritoneal cavity was flushed with 10 ml cold PBS and the abdomen was gently agitated to release cells. Afterwards, cells were carefully retrieved as thoroughly as possible and kept on ice.

2.2.8.3 Isolation of single cells from mesenteric lymph nodes and thymus

Thymi and all mesenteric lymph nodes of mice were excised, thoroughly freed from fat, and meshed through a 70 µm filter in a 6-well containing PBS. Afterwards, the single cell suspension was collected into 15 ml tubes, centrifuged for 5 min, and then resuspended in PBS and stored on ice.

2.2.8.4 Isolation of lymphocytes from Peyer's patches and intestinal lamina propria

Small intestine and colon were excised from mice as a whole and remaining fat was thoroughly cleaned off. Peyer's patches were cut out and placed in a 48-well plate containing 2 ml RPMI 1640 on ice until further steps. The intestines were opened longitudinally and remaining faecal contents were washed out with PBS. To remove any mucus, the gut was then cut into 1 cm long pieces and incubated in 50 ml Falcons with PBS and 30 mM EDTA for 30 min on ice. Afterwards, the tubes were vigorously shaken for 30 sec before being poured into Petri dishes. The tissue pieces were collected back into the tube and ice-cold PBS was added for washing. The washing steps were repeated at least six times or until the PBS was completely clear. Next, tissue pieces were collected in a 6-well plate and minced into 1 mm pieces using scissors. Then 5 ml room temperature digestion medium was added, and the intestines were digested for 10 min. Afterwards, the tissue pieces were pipetted up and down for 45 sec using a 1000 µl pipette tip with a cut-off tip to disintegrate the tissue. The supernatant was strained through a 100 µm filter placed on a 50 ml tube containing 10 ml RPMI with 10% FCS on ice. The filter was then flushed with 5 ml cold RPMI with 10% FCS to halt the digestion. With the remaining tissue pieces, this digestion procedure was repeated two more times with 20 min and 30 min digestion times. The collected cell suspensions were then centrifuged at 550 xg, 4°C for

10 min. Afterwards, the cell pellet was resuspended in 5 ml room temperature 40% Percoll (v/v, 100% Percoll/RPMI), transferred to a 15 ml tube and a glass Pasteur pipette was used to underlay 5 ml 80% Percoll (v/v, 100% Percoll/RPMI). Samples were then centrifuged at 1600 xg for 15 min at room temperature with the brakes turned off. This achieved density gradient centrifugation of the contained lymphocytes into the interphase of both liquids. The interphase was collected in a fresh 15 ml tube containing 10 ml cold PBS, and centrifuged for 5 min.

For Peyer's patches, the RPMI1640 was removed, they were also minced with scissors and 2 ml digestion medium was added. After 30 min of digestion, the cells were released from the remaining tissue by pipetting up and down as described above. The suspension was then strained through a 100 µm filter and digestion was halted by adding 10 ml cold RPMI with 10% FCS. Finally, cells were centrifuged for 5 min and washed in PBS.

2.2.8.5 Preparation of splenocytes

The spleen was extracted and placed in a 70 µm filter placed in a 6-well plate containing PBS. The organ was then meshed through the filter and afterwards, the cell suspension was collected in a 15 ml tube. After centrifugation for 5 min, the pellet was resuspended in 2 ml ACK lysis buffer and incubated at room temperature for 2 min to lyse erythrocytes. Then 10 ml PBS was added to abort the lysis and cells were centrifuged for 5 min. The pellet was then washed once in PBS and resuspended in 1 ml PBS on ice. For flow cytometry approximately one third of splenocytes was used. Cells for single colour controls originated from the spleen.

2.2.9 Cell counting

For accurate determination of total cell numbers, samples were counted using either of two methods. For limited sample numbers, cells were manually counted by adding 10 µl cell suspension to 90 µl pre-diluted trypan blue (final concentration 0.2%) as a viability dye. Cells were then loaded into a Neubauer hemocytometer chamber and manually counted under a microscope. Alternatively, all cells from one organ were seeded into a 96-well plate, centrifuged at 450 xg for 2 min at 4°C and the supernatant was thoroughly decanted. Then the cells were resuspended in 100 µl PBS. Exactly 10 µl of the cell suspension were transferred into a small FACS tube containing 90 µl PBS and 1 µl anti-

CD45-FITC and 1 µl 1:10 diluted Propidium Iodide (PI) solution. Cells were then analysed via flow cytometry on BD Accuri™ C6.

2.2.10 Intracellular staining of cytokines

To stain for cytokine production, cells were isolated as previously described and up to $5x10^6$ cells were seeded in a 96-well U-bottom plate in 50 µl RPMI complete. To stimulate the cells, 50 µl RPMI complete with PMA (200 ng/ml final concentration) and ionomycin (1 µg/ml final concentration) was added. Unstimulated controls received only 50 µl RPMI complete. Cells were then incubated at 37°C, 5% CO_2 for 5 hours. After the first 3 hours of incubation, 5 µg/ml Brefeldin A was added to all samples and the remaining incubation time proceeded. Afterwards, cells proceeded to preparation as described in **2.2.11 Flow cytometry**.

2.2.11 Flow cytometry

All steps were carried out on ice, incubation steps were done in the dark. Staining reagents and antibodies can be found in **Table 6**. Cells from murine organs or *ex vivo* stimulation were collected in a 96-well V-bottom plate. They were then washed twice by centrifugation at 450 xg and 4°C for 2 min and adding 150 µl PBS. Cell numbers were then reduced to a maximum of approximately $1x10^7$ cells. Then 5 µl Fc-block™ in PBS were added to the cell pellets and incubated for 5 min. Next, cells were incubated for 30 min in 50 µl of the proper mixture of extracellular antibodies and Live/Dead Aqua in PBS. Cells were again washed twice and if one of the antibodies was conjugated to Biotin, Streptavidin was stained in 50 µl for 10 min and washed off again. If only extracellular staining was needed, cells would then be filtered and proceeded to flow cytometry analysis. However, to stain intracellular markers, cells were fixed overnight at 4°C using the Foxp3/Transcription Factor Staining Buffer Set according to the manufacturer's instructions. Afterwards, cells were washed twice in 150 µl of the Permeabilization buffer (Perm Buffer) contained in the kit and centrifuged at 550 xg for 2 min. Then 50 µl of the intracellular antibodies in Perm Buffer were added, resuspended, and incubated for 1 h at room temperature. Finally, cells were washed in 150 µl Perm buffer and centrifuged at 550 xg for 2 min twice and then resuspended in 50 – 150 µl of PBS, depending on pellet

size. Before acquisition with a BD LSRFortessa™, cells were filtered. FACS data was analysed with FlowJo software.

2.2.12 Fluorescence activated cell sorting

Murine single cell suspensions from the small intestine, mesenteric lymph nodes and spleen were created as described in **2.2.8 Cell isolation from murine organs**. To achieve faster sorting speed and therefore reduce the processing times of the sorted cells, cells from the spleen and mLN were enriched for CD4 T cells prior to staining using a CD4 T cell enrichment Kit according to the manufacturer's instructions. All samples were then stained extracellularly for 30 min on ice with anti-CD45, anti-CD3 and anti-CD4 antibodies in FACS buffer. Directly before sorting, 7AAD was added to the samples and they were filtered. Then using a FACSAria™ III cell sorter, cells were analysed for their marker expression and sorted into 1.5 ml tubes accordingly. For the first bulk RNAseq experiment of Bcl3-KO, WT and Bcl3OE^{Treg} mice all animals expressed a reporter for Foxp3. *Foxp3*^{RFP} for Bcl3-KO and WT mice and *Foxp3*^{GFP} for Bcl3OE^{Treg} mice. Two populations were sorted from each sample: Th (7AAD$^-$, CD45$^+$, CD3$^+$, CD4$^+$, Foxp3$^-$) and Treg (7AAD$^-$, CD45$^+$, CD3$^+$, CD4$^+$, Foxp3$^+$). For the second experiment Bcl3 deficient and WT controls from the double reporter line were used, expressing *Foxp3*^{RFP}x*Rorc*^{GFP}. Again, two populations were sorted: RORγt$^-$ Tregs (7AAD$^-$, CD45$^+$, CD3$^+$, CD4$^+$, Foxp3$^+$, RORγt$^+$) and (7AAD$^-$, CD45$^+$, CD3$^+$, CD4$^+$, Foxp3$^+$, RORγt$^-$). For single cell RNA sequencing experiments approximately 25.000 7AAD$^-$, CD45$^+$, CD3$^+$, and CD4$^+$ cells were sorted.

Selected cells were sorted either into RNA lysis buffer for Bulk RNA sequencing experiments or into PBS with 0.04% BSA for scRNAseq. Sort purity was checked individually after every sample.

2.2.13 RNA sequencing preparation

2.2.13.1 Bulk RNA sequencing

After cells were directly sorted into RNA lysis buffer, they were vortexed and immediately frozen on dry ice. To isolate the RNA from the samples the RNeasy Micro Plus kit was used according to manufacturer's protocol. To reduce sample degradation at room temperature only ten samples were isolated at once. Prior to RNA extraction, all

equipment and the workplace were cleaned using UV-light for 60 min and RNAse away. In short, the total volume of the sample was evaluated and filled up to 350 µl using RNA lysis buffer. After vortexing the samples, genomic DNA was excluded via elimination columns. Next 350 µl 70% ethanol was added to the flowthrough, mixed, added to a spin column and centrifuged to bind the RNA to the column. After washing with two different wash buffers contained in the kit and 80% ethanol, the spin column was dried. Finally, the RNA was eluded in 15 µl RNase free water. Subsequently, RNA quantity and quality were evaluated using the Bioanalyzer Kit RNA 6000 pico according to the manufacturer's instructions.

For cDNA synthesis, the SMART-Seq® v4 Ultra low Input RNA Kit was used. To achieve equal outcomes, the concentrations of some samples had to be adapted. Therefore 8 µl of RNA solution was used containing a maximum of 2 ng RNA, otherwise, RNase-free water was substituted. Afterwards, the RNA content of the samples varied approximately between 400 pg and 2 ng RNA, a trial run using different dilutions of one sample was performed to determine the required number of PCR cycles. Subsequently, cDNA synthesis was done with 12 cycles. ERCC RNA Spike-Ins were used with a final dilution of 1:100,000 and AmPure XP Bead Cleanup was only performed with eight samples simultaneously. Quality and quantity of cDNA were evaluated using the Bioanalyzer High sensitivity DNA Kit and Qubit dsDNA HS Kit. Concentration ranked between 0.25 and 4.75 ng/µl.

For tagmentation and library preparation, the Nextera XT DNA Library Prep Kit was used according to the manufacturer's instructions. To achieve a library with approximately 450 bp in size but at least 300 bp, a trial run was performed by using different input concentrations of cDNA. Afterwards, it was decided to dilute all samples to a concentration of 0.2 ng/µl and then use 3 µl of cDNA for tagmentation and amplification. For indexing the IDT DNA/RNA UD indexes plate B was used. Again, the quality and quantity of the samples were assessed using the aforementioned Bioanalyzer and Qubit kits, respectively and the average size was 547 bp. To properly pool the library, molarity was calculated for each sample via this formula:

$$molarity\ [nM] = \frac{concentration\ [ng/\mu l]}{(660 * average\ size\ [bp]} * 10^6$$

All samples in one pool need to have equal concentration. Hence, the required sample volumes were calculated with the following formula and added to the library pool:

$$Sample\ volume\ in\ pool\ [\mu l] = \frac{Volume\ pool\ (300\ \mu l) * Molarity\ pool\ (12nM)}{\#\ of\ indexes\ (72) * Sample\ molarity}$$

The final concentration of each sample in the pool was 0.05 ng/µl.

Finally, the library was sequenced on an Illumina® NovaSeq 6000 using a NovaSeq 6000 S2 150 paired-end reads flow cell.

2.2.13.2 Single cell RNA sequencing

The 10X Genomics droplet based Chromium system was used to create the single cell library for scRNAseq. For the analysis of mixed bone marrow chimera cells, the samples were labelled with TotalSeq™-B0178 anti-CD45.1 and TotalSeq™-B0157 anti-CD45.2 feature barcoding antibodies in addition to extracellular antibodies. Staining was carried out according to the manufacturer's protocol.

For each separate scRNAseq experimenT cells from four individual mice were sorted into four separate wells. All sorted cells were used to prepare the sequencing library, as cell loss during washing and cell counting inaccuracy determined a final cell number of approximately 9.500 if 25.000 cells were sorted. Library construction was carried out according to the manufacturer's instructions and quality was ensured using a Bioanalyzer high sensitivity DNA Assay. For the analysis of mixed bone marrow chimera cells, the Chromium Next GEM Single Cell 3' Kit v3.1. and for the other experiments, the Chromium™ Single Cell 5' Library & Gel Bead Kit were used. The libraries were then sequenced on an Illumina® HiSeq 2500. To additionally sequence T cell receptor sequences, one part of the samples was prepared using the Chromium™ Single Cell V(D)J Enrichment Kit according to the manufacturer's instructions.

2.2.13.3 Analysis of bacterial diversity

Fresh faeces of individual mice were collected with minimal cross-contamination and stored in properly labelled sterile 1.5 ml tubes. They were then immediately frozen in

liquid nitrogen. Until the experiment was over, all collected samples were stored at -80°C to be prepared simultaneously. 16S rRNA sequencing library preparation and amplicon sequencing were then performed by the microbiome core facility of the Technical University Munich in Freising according to scientific standards. In short, genomic material was isolated using automated extraction via Maxwell Instruments (Promega). This was followed by a single 16S amplicon PCR. Libraries were then sequenced using an Illumina® MiSeq.

2.2.14 Bioinformatic data analysis

Illumina® sequencing output was directly converted from base-call files to text-based .fastq files by the sequencing facility to facilitate easier downstream analysis and data transfer.

2.2.14.1 Bulk RNA sequencing data analysis

Nextflow's nf-core/rnaseq pipeline was used to perform alignment and quantification of bulk RNA sequencing samples with Singularity as the container engine and standard parameters [159]. Alignment against the Illumina® reference genome GRCm38 was done using the STAR aligner and RSEM was used as a quantification method. Downstream analysis of the data and visualization was done in R. R/Bioconductor packages were used: *tximport* to import the data, *DeSeq2* for differential gene expression analysis and *biomaRt* for annotations [160], [161], [168]. Differentially expressed genes (DEGs) were then filtered with a log2 fold change of at least 2 and adjusted p-value below 0.05. Before the generation of heatmaps using *pheatmap* raw count data was log transformed using the R package *rlog*. From there volcano plots were generated using *EnhancedVolcano, tidyR* was used to calculate overlapping genes, *eulerr* produced the Venn diagrams and *ggplot2* was used to elevate visualizations. For every step the respective author documentation was followed. Gene set enrichment analysis (GSEA) was carried out using the R/Bioconductor packages *fgsea* and *org.Mm.eg.db*. The DEGs of Bcl3 deficient RORγt^{+} Tregs compared to their Bcl3 sufficient counterpart were analysed referring to the murine orthology-mapped hallmark gene set from MSigDB (mh.all.v2022.1.Mm.symbols.gmt) [174].

2.2.14.2 scRNAseq data analysis

The 10X Genomics Cell Ranger Software was used for scRNAseq data alignment and quantification using standard parameters. Downstream analysis was either performed using the Loupe Cell Browser software or further in depth using the R package *Seurat* [167]. Nevertheless, empty droplets and doublets were always excluded by setting nFeature between 300 and 4000. Cells with a percentage of mitochondrial genes over 5% were presumed dead and therefore also excluded. In the Loupe Cell Browser, filtered or Foxp3$^+$ cells were then reclustered using the Recluster function with default parameters and the built-in differential expression analysis was used to calculate marker genes.

To analyse VDJ sequencing results, the data was first aligned and quantified using the cellranger pipeline and then assessed in the Loupe VDJ browser. Hence, the number of different TCRs in one cluster and the reoccurrence of those TCRs within the cluster could be used to calculate Simpson's diversity index using the following formula.

$$Simpson's diversity\ index = \frac{\sum_{i=1}^{R} ni(ni-1)}{N(N-1)}$$

Cells from mixed bone marrow chimeras were analysed more in depth using *Seurat*. Normalization and scaling of the data according to variable features was carried out using the ScaleData function. Additionally, the influence of different cell cycle stages was regressed out. As one of the samples displayed insufficient quality, it was excluded from further analysis steps. To achieve dimensionality reduction RunTSNE and RunPCA were run to calculate and plot tSNE and PCA visualization, respectively. The FindAllMarkers function was then run to determine cluster defining genes and afterwards, the subset function was used to create a dataset containing only Foxp3 expressing cells. To investigate regulatory T cells (Tregs) more thoroughly, the previously described steps for cluster definition and finding marker genes were repeated on this subset. As cells were labelled with feature barcoding antibodies prior to sorting, their genotype could be determined by the expression profile of those features. Only cells clearly expressing one of both markers exclusively were used for downstream analysis. Genotype and Treg subcluster definitions were then combined to identify genotype dependent regulation of DEGs within one subcluster by running differential gene expression analysis of CD45.2$^+$

cells against CD45.1$^+$ cells within each subcluster. Visualizations were created using the *Seurat* DoHeatmap function for heatmaps, *eulerr* for Venn Diagrams and *ggplot2* and *RcolorBrewer* for general aesthetics.

2.2.14.3 16S sequencing data analysis

For the analysis of microbial taxa data, first, *qiime2* was used together with the Silva reference database to create OTU tables. Then downstream analysis was performed using the *Rhea* protocol. This protocol consisted of several distinct R scripts to facilitate the analysis of 16S data via OTU tables. Visualizations were prepared using *ggplot2* and *RColorBrewer*.

2.2.15 Statistical analysis

Except for RNA sequencing data, GraphPad Prism software was used for statistical analysis. If not indicated otherwise in Figure Legends, mean and SD are shown and each dot represents an individual mouse. To determine the significance of differences, either a two-tailed student t-test with Holm-Sidak correction was used or ANOVA corrected for multiple comparisons using the Sidak method. An adjusted p-value below 0.05 was considered significant and indicated using: * = $p < 0.05$, ** = $p < 0.01$, *** = $p < 0.001$, **** = $p < 0.0001$, ns = not significant.

3 RESULTS

3.1 MICROBIAL COLONISATION EARLY IN LIFE PERSISTENTLY IMPACTS IMMUNE HOMEOSTASIS

Colonisation of the intestinal tract by commensal microbes imposes a particular challenge to the adaptive immune system by the need to tolerate dietary antigens and antigens derived from commensal microbes while simultaneously maintaining responsiveness to infectious agents. Therefore, microbiome specific pTregs expressing RORγt and not Helios are especially abundant in organs with a high bacterial load such as the intestines [71], [72]. They are absent in germfree mice but can be induced by colonisation with different bacterial strains at varying degrees [71], [72]. Although induction at a later time point is possible, the generation of pTregs at the physiological time point of weaning was demonstrated to be essential to reduce the incidence of immunopathologies [77]. Additionally, it has been shown that pTreg mediated suppression of Th2 cells plays an important role in pathologic type 2 responses [71]. Hence, germfree mice display altered responses in models of food allergy, however, the exact direction of the effect remains disputed [175], [176].

The aims of this chapter were to better understand the differences between the subsets of intestinal Tregs and define specific transcriptomic signatures, to determine if the timepoint of colonisation influences the cellular composition and TCR diversity of intestinal $CD4^+$ T cells, and if microbial status during maturing influences tolerance to food allergens later in life.

3.1.1 Transcriptomic analysis of intestinal $CD4^+$ T cells on a single cell level

To further understand how specialised regulatory T cell subsets contribute to the maintenance of tolerance, $CD4^+$ T cells were isolated from the small intestine lamina propria of wildtype mice and profiled via single cell RNA sequencing (scRNAseq). Besides various $CD4^+$ effector T cells and a small population of naïve $CD4^+$ T cells, a distinct cluster similar to regulatory T cells (*Foxp3, Il2ra, Stat5*) (**Figure 1A**) was detected. Reclustering of the Foxp3 expressing cluster to further analyse its subpopulations revealed five distinct

Treg subclusters (**Figure 1B**). Two of these clusters transcriptionally resembled thymic-derived Tregs (tTreg) additionally expressing either repair features (tTreg repair, e.g., *Klrg1*, *Il1rl1*, and *Pdcd1*) or effector features (tTreg effector, e.g., *Itgae, Gzmb*). Two other clusters showed transcriptional similarities with peripherally induced Tregs (pTregs, e.g., *Rorc, Maf*), differing only in their expression of activation markers, while Cluster4 was scattered across all other clusters, possibly due to its distinct cell cycling stage (**Figure 1C**). This proposed cluster assignment was supported by the proportional distribution of Treg subclusters fitting the population distribution usually found in small intestine lamina propria via flow cytometry analysis (**Figure 1D**). Next, the differentially expressed genes (DEGs) acquired from this comparison (**Figure 1E**) were used to create and calculate scores for the different Treg subsets that could then be used in further experiments (**Figure 1F**).

While searching for overarching transcriptional differences between tTregs and pTregs, it was noted that an NFκB-associated gene signature was particularly abundant among tTregs (especially repair tTregs, **Figure 1G**). Although the expression of the atypical IκB family member Bcl3 seemed to be particularly high in Tregs (**Figure 1H**) there was no Treg subset dependent difference in Bcl3 expression (**Figure 1I**).

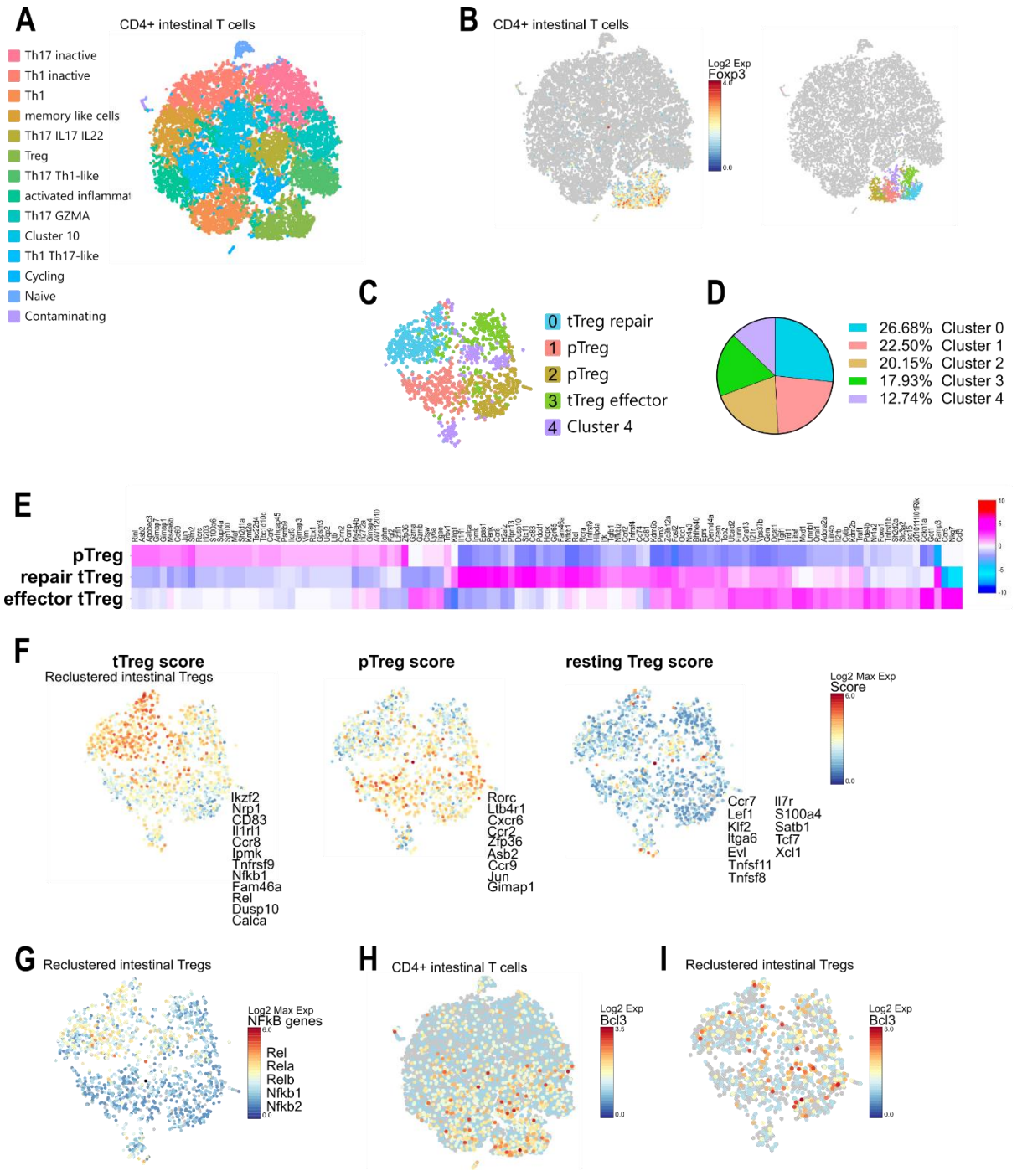

Figure 1: ***Single cell transcriptomic analysis reveals signature genes of intestinal Treg subpopulations. (A)*** *tSNE dimensionality reduction of filtered scRNAseq data of CD4⁺ T cells from small intestine lamina propria (SI). Including labels based on differentially expressed marker genes.* ***(B)*** *Feature plot depicting Foxp3 expression on cells from (A) (left) and tSNE plot showing the reclustered Foxp3⁺ cluster from (A) (right).* ***(C)*** *tSNE dimensionality reduction of Foxp3⁺ T cells reclustered from the dataset with sorted CD4⁺ T cells from small intestine lamina propria as shown in (A).* ***(D)*** *Proportional distribution of Foxp3⁺ subclusters among reclustered cells as shown in (C).* ***(E)*** *Mean expression levels of differentially expressed genes in clusters shown in (C) labelled as peripherally induced RORγt expressing Tregs (pTregs) compared to clusters defined as thymically derived repair or effector Tregs (repair/effector tTregs).* ***(F)*** *Transcriptional scores defining Treg subclusters in tTreg score (left, defined by Nrp1, Ikzf2, Cd83, Il1rl1, Calca, Ccr8, Tnfrsf9, Ipmk, Nfkb1, Fam46a, Rel and Dusp10); pTreg score (middle, defined by Rorc, Ltb4r1, Ccr2, Cxcr6, Zfp36, Asb2, Ccr9, Jun and Gimap1); restingTreg score (right, defined by Ccr7, Satb1, Lef1, Tcf7, Evl, Klf2,*

Tnfsf11, Tnfsf8 and Xcl1). ***(G)*** *Feature plot showing expression of selected NF-κB genes for cells from (D)* ***(H)*** *Feature plot depicting Bcl3 expression levels among intestinal CD4⁺ T cells as shown in (A).* ***(I)*** *Feature plot depicting Bcl3 expression levels for cells from (D). Each dot represents an individual cell, and each heatmap square represents the average over all selected cells and n=4 mice. Statistical analysis was performed using the 10X Genomics Loupe cell Browser.*

3.1.2 Early microbial diversity influences the composition and TCR diversity of intestinal T cells

The difference in the transcriptomic profile of tTregs and pTregs described above is consistent with the dissimilar development of both populations. Based on low to intermediate reactivity of their TCR towards self-antigen, tTregs originate in the thymus while pTregs differentiate as a response to foreign antigen in the periphery [37], [177]. Consequently, distinct TCR repertoires can be found in both populations [73]. Considering that pTregs may be induced late in life by microbial colonisation, it can be hypothesised that this altered induction influences the TCR diversity of Tregs.

To investigate the influence, the timepoint of microbial colonisation has on the TCR repertoire, double breedings with two dams and one male were established, minimizing ontogenetic or environmental differences in the analysed offspring, as littermates could not be used due to the experimental setup. The following treatment timeline is documented in **Figure 2A**. When the females were pregnant, they were separated into two groups. One group received antibiotic treatment (ABX) containing ampicillin, vancomycin, metronidazole, and streptomycin via drinking water to eradicate their microbiome and hence inhibit the microbial colonisation of their offspring. The other group received regular drinking water. The ABX offspring continued the antibiotic treatment after weaning until they were approximately six weeks old. Then the treatment was stopped, and they were co-housed with offspring from the control group to enable microbial colonisation (ex-ABX). Simultaneously age-matched germfree (GF) mice were introduced and co-housed with the other groups again allowing for microbial colonisation of the mice (ex-GF). After two weeks of co-housing, animals were sacrificed and analysed, resulting in three groups with distinct microbial status at the age of weaning but more aligned microbiomes at the time point of analysis.

Initially, the impact of co-housing on microbiota induced populations was investigated by sacrificing control and germfree mice before and after two weeks of co-housing and analysing their microbiome induced Th17 cell and pTreg populations in small intestine lamina propria (SI) and mesenteric lymph nodes (mLN) via flow cytometry. As expected, both Th17 cells and pTregs were absent in GF mice but were greatly induced in ex-GF mice after colonisation, to equal or even greater levels as compared to control (CTRL) animals (**Figure 2B**).

To monitor the microbiome, faeces samples were collected frequently from all animals throughout the experiment. Analysis of faecal 16S rRNA revealed a drastic decrease in bacterial Alpha Diversity of the ABX group after the antibiotic treatment was started, while the CTRL group stayed constant. However, as soon as the treatment was discontinued and the mice were co-housed at day 63, the bacterial diversity increased quickly, approaching CTRL levels. However, although the Alpha Diversity of faecal 16S rRNA in GF mice increased during co-housing, CTRL levels remained unreached (**Figure 2C**). Final flow cytometry analysis showed increased percentages of Th17 cells in ex-ABX and ex-GF SI as compared to CTRL mice and comparable abundances of pTregs, indicating successful induction of both cell types during colonisation (**Figure 2D**).

To assess the cellular composition of intestinal T cells within the three groups and their TCR diversity, scRNAseq of $CD4^+$ T cells from small intestine lamina propria was performed including VDJ characterization of the TCR repertoire. Surprisingly, when comparing the distribution of the main clusters among the three groups the biggest cluster in ex-GF mice is Th1 cells expressing high levels of granzyme A, granzyme B and granzyme K (**Figure 2E**). This cluster is only sparsely present in the other groups. On the other hand, Th17 cells are visually more abundant in ex-ABX mice and naïve $CD4^+$ T cells seem to be less frequent. The TCR repertoire analysis emphasises the extent of the TCR diversity present in naïve T cells with almost no reoccurring sequences. Subsequently, to their reduced abundance the TCR diversity of naïve T cells is marginally reduced in ex-ABX and ex-GF mice as compared to CTRL animals, when calculating Simpson's diversity index (**Figure 2F**). Although less drastic than naïve T cells, the TCR repertoire of Tregs is still obviously much more diverse than that of T effector populations. Furthermore, the TCR

diversity in Tregs seems to be changed in the manipulated groups. Reclustering of Foxp3 expressing clusters once more resulted in Treg subclusters as previously described in **Figure 1** (**Figure 2G** and **Figure 2H**). No drastic differences in TCR diversity can be noted between the Treg subsets, except increased complexity in resting Tregs presumably resulting from absent proliferation. Comparing Simpson's diversity index of TCRs within each Treg subpopulation confirms a trend towards decreased diversity in ex-ABX and ex-GF pTregs. However, the impact appears more visible in resting/naïve Tregs (**Figure 2I**).

Although it can be concluded that this data indicates an impact of the weaning microbiome on Treg TCR diversity, more work is needed to achieve significant results.

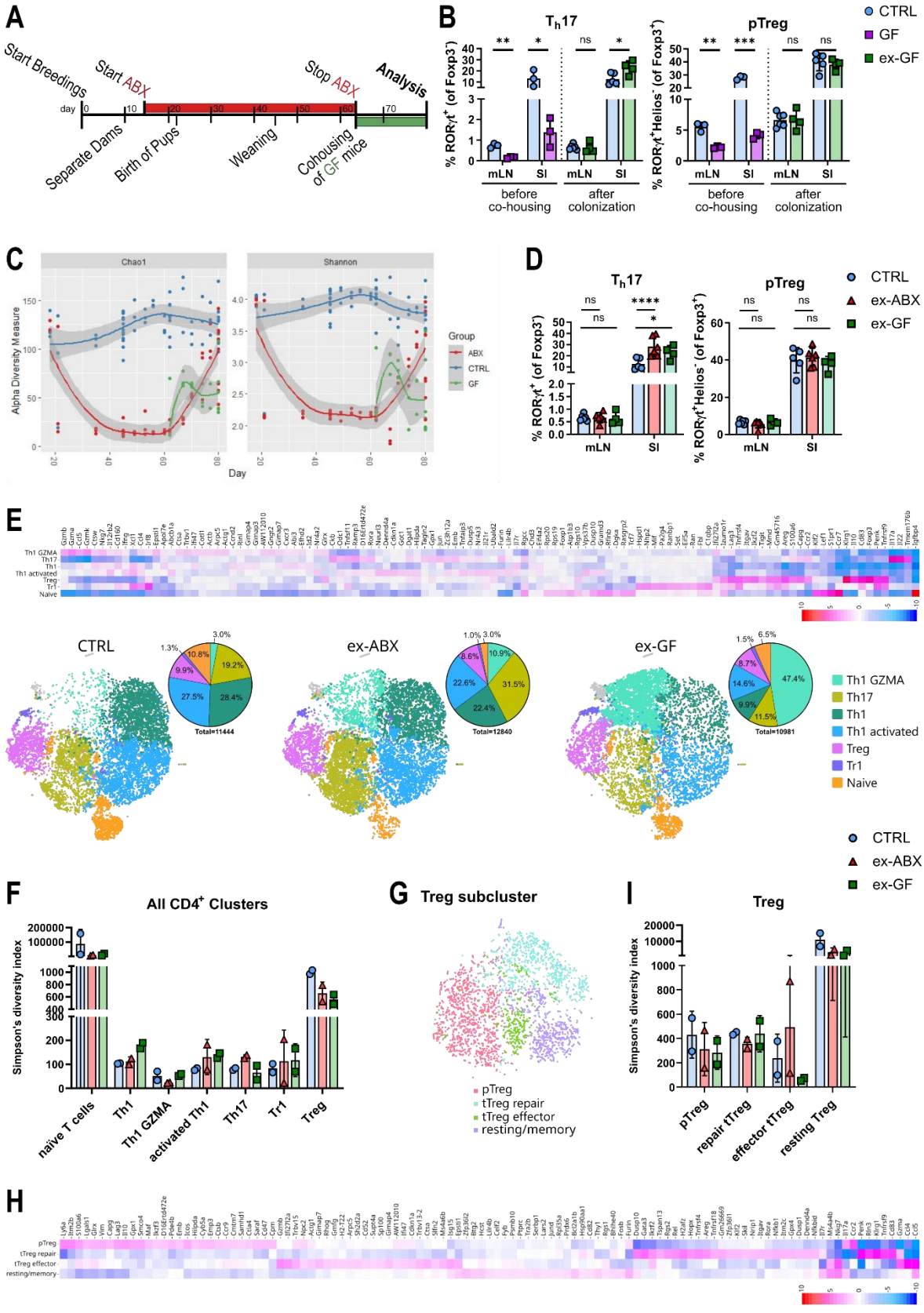

Figure 2: ***Reduced microbial diversity in maturing mice leads to decreased TCR diversity in intestinal regulatory T cells. (A)*** *Scheme of experimental setup to generate newly colonised animals by co-housing either antibiotics treated mice (ABX) or germfree mice (GF) with control (CTRL) animals.* ***(B)*** *Analysis of microbiota induced cell types before (GF) and after (ex-GF) colonisation of germfree mice via co-housing. Percentages of RORγt*

expressing Th17 cells pregated for Foxp3 (left) and RORγt⁺ Helios pTregs pregated on Foxp3+ (right) from mesenteric lymph nodes (mLN) small intestine lamina propria (SI). ***(C)*** *Alpha diversity of faeces microbiome over the duration of the experiment was calculated using either the Chao1 index or Shannon diversity.* ***(D)*** *Percentage of RORγt expressing Th17 cells pregated for Foxp3 (left) and RORγt⁺ Helios pTregs pregated on Foxp3+ (right) from mLN and SI after colonisation of ABX treated (ex-ABX) germfree mice (ex-GF).* ***(E)*** *Heatmap of top DEGs and tSNE dimensionality reduction of scRNAseq data from small intestine lamina propria CD4+ T cells. tSNE projection split up according to the experimental group: Control (left), ex-antibiotics treated (middle) and ex-germfree (right). Clusters were labelled according to signature gene expression. Pie charts depicting the distribution of labelled clusters within each group.* ***(F)*** *Simpson's diversity index of TCR clonotypes expressed by the CD4+ cells within one cluster of each sample as shown in (E).* ***(G)*** *tSNE dimensionality reduction of reclustered cells from Treg cluster as shown in (E). Clusters are labelled according to marker gene expression.* ***(H)*** *Heatmap of top differentially expressed genes in Treg subclusters as shown in (E).* ***(I)*** *Simpson's diversity index of TCR clonotypes expressed by the Tregs within one subcluster of each sample as shown in (G). Each dot represents an individual mouse. Mean ± SD is shown. CRLT n≥3 mice, GF n=3 mice, ex-GF n=4 mice and ex-ABX n=6 mice. Statistical analysis was performed using either a two-tailed student t-test corrected for multiple comparisons using the Holm-Sidak method (B) or two-way ANOVA corrected via Sidak (D). P value of <0.05 was considered statistically significant with * p <0.05, ** p < 0.01, *** p < 0.001, **** p < 0.0001, ns = not significant.*

3.1.3 Disparate immune tolerance in mice with distinct early microbial colonisation

The previous results showed that delayed induction of intestinal pTregs influences their TCR repertoire which could contribute to pathological imprinting as described by *Nabhani et al* [77]. On the other hand, pTregs have been indicated to suppress the functionality of Th2 cells in helminth defence and Th2 driven pathology [71]. Additionally, the incidence of food allergy in children has been linked to alterations in their microbiome and GF mice demonstrate an altered response to food allergen sensitisation than SPF mice [120], [175], [176], [178]. These data suggest a possible role of early microbial complexity and pTreg induction on allergic sensitisation.

To investigate if early colonisation before the age of weaning influences the outcome of oral sensitisation, an OVA specific food allergy model was set up with co-housed mice. The mice originated from three different breeding backgrounds: germfree mice (ex-GF), SPF mice bought from Charles River (SPF-CR) and SPF mice bred in an in-house animal facility (SPF-AF). Consequently, the mice in those groups harboured three different microbiomes early in life. Two weeks before the start of the sensitisation, the animals were co-housed to allow for an exchange in the microbiome and induction of equal pTreg levels as previously demonstrated in **Figure 2B**. Afterwards, the mice were sensitised for

four weeks using choleratoxin (CT) and ovalbumin (OVA) as a model allergen by oral gavage. Unsensitised control mice (Ctrl) received only CT. One week after the last sensitisation the mice were challenged with OVA *i.v.* and their core body temperature was monitored to assess the anaphylactic reaction. On the next day, animals were sacrificed, and their organs were harvested for flow cytometry analysis (**Figure 3A**).

All sensitised groups displayed distinct loss of body temperature after the challenge, however, ex-GF mice lost significantly less temperature than the SPF groups and recovered quickly after approximately 25 min indicating only mild anaphylaxis (**Figure 3B**). Anaphylaxis was worst in SPF-AF mice with loss of body temperature even exceeding SPF-CR levels and only slowly recovering circa 40 min after the challenge. To confirm sensitisation severity as observed in the challenge, OVA-specific IgE in serum was measured via ELISA and calculated according to the reference dilutions. As expected, sensitisation towards OVA significantly increased OVA-specific IgE in all groups and, in line with their challenge reaction, SPF-AF mice produced slightly higher OVA-IgE concentrations than SPF-CR mice. Interestingly, the level of OVA-specific IgE was highest in ex-GF mice although they only reacted modestly towards the OVA challenge (**Figure 3C**).

Furthermore, flow cytometry analysis of SI and mLN showed no significant differences in the Th2 populations of sensitised animals, but a higher abundance of Th17 cells in SI of SPF-CR mice (**Figure 3D**). Other studies have described that elevated levels of microbiota induced pTregs correspond to decreased severity in food allergen sensitisation [121]. In accordance with that, the SI of SPF-CR mice in tendency had increased abundances of pTregs as compared to SPF-AF SI, but ex-GF mice displayed the highest percentage of pTregs in their SI reflecting the ranking of groups during anaphylaxis (**Figure 3E**).

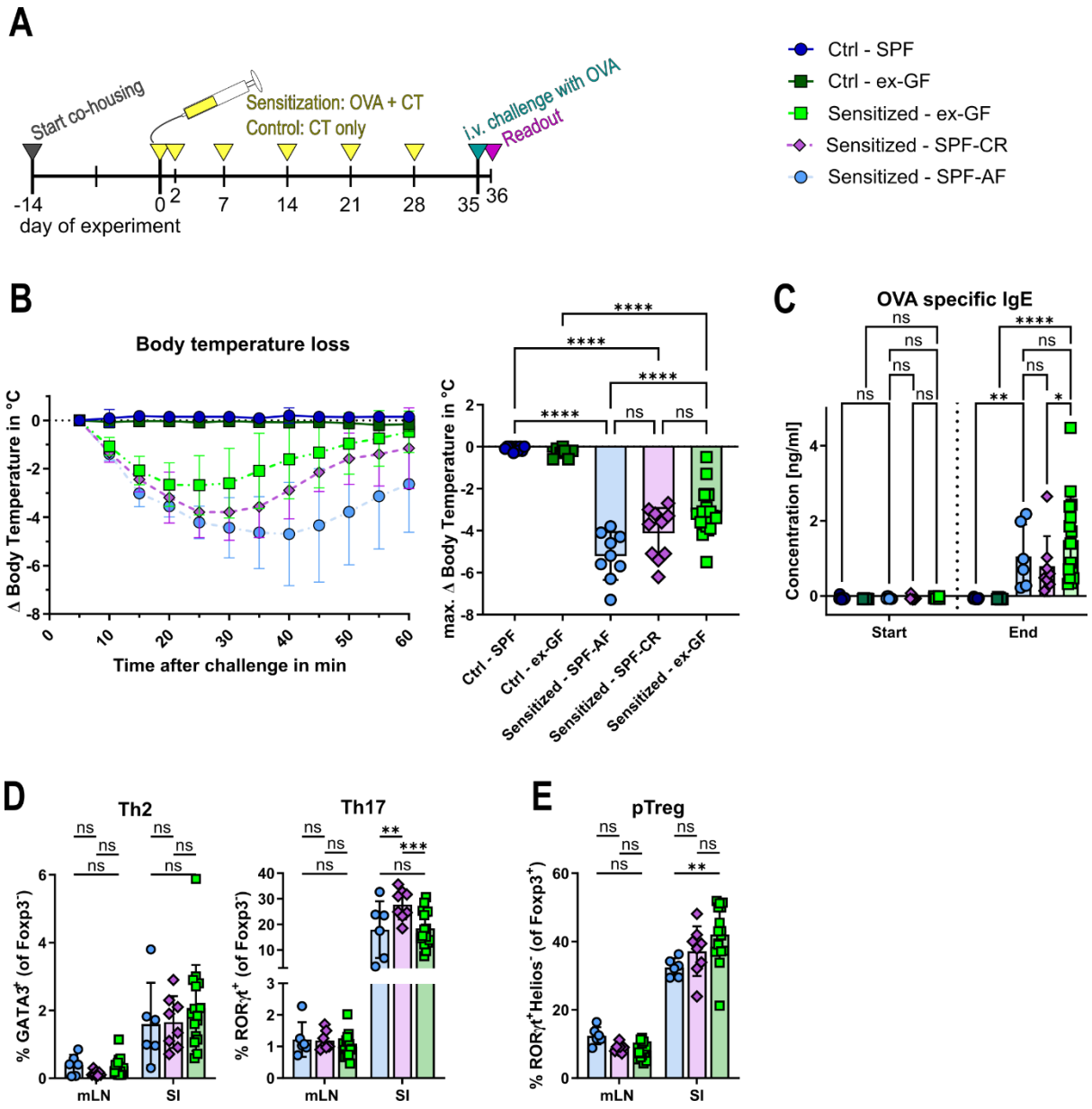

Figure 3: ***Composition of intestinal microbiome influences the severity of food allergen sensitisation. (A)*** *Scheme showing the experimental setup of the food allergy model. Germfree mice (ex-GF), wildtype SPF mice from Charles River (SPF-CR) and wildtype SPF mice from in-house husbandry (SPF-AF) were co-housed for two weeks prior to sensitisation. Then sensitisation was performed orally with OVA and CT, or only CT for control animals and mice were challenged i.v. with OVA. For specifics see the Material and Methods section.* ***(B)*** *Body temperature loss and recovery over time (left) and maximum body temperature loss (right) after challenge.* ***(C)*** *Serum concentration of OVA specific IgE in blood drawn on day -1 (start) and day 35 (end) and measured via ELISA.* ***(D)*** *Percentage of GATA3$^+$ Th2 cells (left) and RORγt$^+$ Th17 cells (right) pre-gated on Foxp3$^-$ T helper cells.* ***(E)*** *Percentage of RORγt$^+$ Helios$^-$ (pTreg) cells pre-gated on Foxp3$^+$ regulatory T cells. Each dot represents an individual mouse. Mean ± SD of at least two independent experiments is shown. Ctrl-SPF n=10 mice, Ctrl-ex-GF n=7 mice, Sensitized-SPF-AF n=9 mice, Sensitized-SPF-CR n=10 mice and Sensitized ex-GF n=17 mice. Statistical analysis was performed using either one-way ANOVA corrected via Sidak (B), or two-way ANOVA corrected via Sidak (C - E). P value of <0.05 was considered statistically significant with * p <0.05, ** p < 0.01, *** p < 0.001, **** p < 0.0001, ns = not significant.*

3.1.4 Summary

The data shown in this chapter underlines the effect early colonisation of the intestine has on intestinal immunity later in life. In short, it was demonstrated that within two weeks of co-housing late in life, the bacterial complexity of mice with formally suppressed microbiome could be drastically increased. Along with microbial colonisation, pTregs and Th17 cells were induced, but late induction led to altered cellular distribution within $CD4^+$ T cell compartments and decreased TCR diversity in Tregs.

Furthermore, food allergen sensitisation was decreased in mice with delayed microbial colonisation and increased pTreg frequencies. The transcriptional differences of pTregs and tTregs were introduced on a single cell level, resulting in gene signatures to be used for further research and underlining the importance of the NFκB pathway in Treg differentiation.

3.2 Bcl3 determines differentiation and fate of intestinal RORγt$^+$ regulatory T cells

Analysis of single cell transcriptomic differences between pTregs and tTregs showed NFκB associated genes preferentially expressed in tTregs (**Figure 1G**). Additionally, the NFκB transcription factor RelA is necessary to maintain pTregs and atypical IκB family members are thought to control NFκB activity in various cell types including $CD4^+$ T cells [134]. For instance, it was recently published that IBD patients show high expression of the atypical NFκB member Bcl3 (B-cell lymphoma 3) in colonic T cells and overexpression of Bcl3 in T cells results in defective Treg differentiation and exacerbated intestinal inflammation in a T cell transfer colitis model [158]. In contrast, Bcl3 deficient T cells were unable to induce intestinal inflammation, possibly due to enhanced trans-differentiation of Th1 cells to less-pathogenic Th17 cells [179]. Although there was no clear subset specific difference in Bcl3 expression (**Figure 1I**) it was hypothesized that altered Bcl3 expression could influence pTreg levels, due to its role in gut homeostasis. This chapter aimed to investigate if altered Bcl3 expression regulates different Treg subsets, how Bcl3

is relevant for intestinal homeostasis, and to pinpoint a possible mechanism of Bcl3 dependent intestinal Treg regulation.

3.2.1 Bcl3 deficiency quantitatively and qualitatively alters Foxp3$^+$ regulatory T cell subsets

In mice with a complete knockout of Bcl3, systemic inflation in overall Foxp3$^+$ Treg frequencies was found in lamina propria of the small intestine, mesenteric lymph nodes, Peyer's Patches, peritoneal cavity and to a decreased grade even in the thymus, although these effects were less obvious in total cell numbers (**Figure 4A** and **B**). As the most striking difference was observed in the small intestine lamina propria which is also one of the organs where most pTregs can be found [71], [180], cells were next stained for the transcription factors RORγt and Helios, a combination that enables the differentiation between pTregs and tTregs [71], [72]. Indeed, a reliable increase of RORγt$^+$Helios$^-$ Tregs (pTregs) was observed in the small intestine lamina propria, mesenteric lymph nodes, and even in the spleen (**Figure 4C** and **D**). Surprisingly, an additional Treg population that is typically absent in wildtype animals appeared in Bcl3 deficient animals co-expressing RORγt and Helios (DPTreg) (**Figure 4C** and **E**). Consistent with these results elevated total cell numbers of pTregs and DPTregs were found in SI, mLN and spleen (**Figure 4D** and **E**).

Considering that Bcl3 strongly affects intestinal Treg populations it was next investigated whether these inflated Bcl3 deficient Treg populations retain their ability to perform effector functions such as anti-inflammatory cytokine production. Interestingly, *ex vivo*-isolated Tregs lacking Bcl3 were even greater producers of IL-10 and TGFβ than their Bcl3 sufficient counterparts, indicating either a direct regulation by Bcl3 or an elevated activation status of Tregs devoid of Bcl3 (**Figure 4F** and **G**). Notably, superior cytokine production was observed in all previously mentioned Treg subsets (tTreg, pTreg) including the newly labelled DPTregs, while IL-17 secretion stayed unchanged (**Figure 4G**). Overall, these results propose that Bcl3 is a key regulator influencing RORγt$^+$ Treg subsets and their ability for anti-inflammatory cytokine secretion in particular.

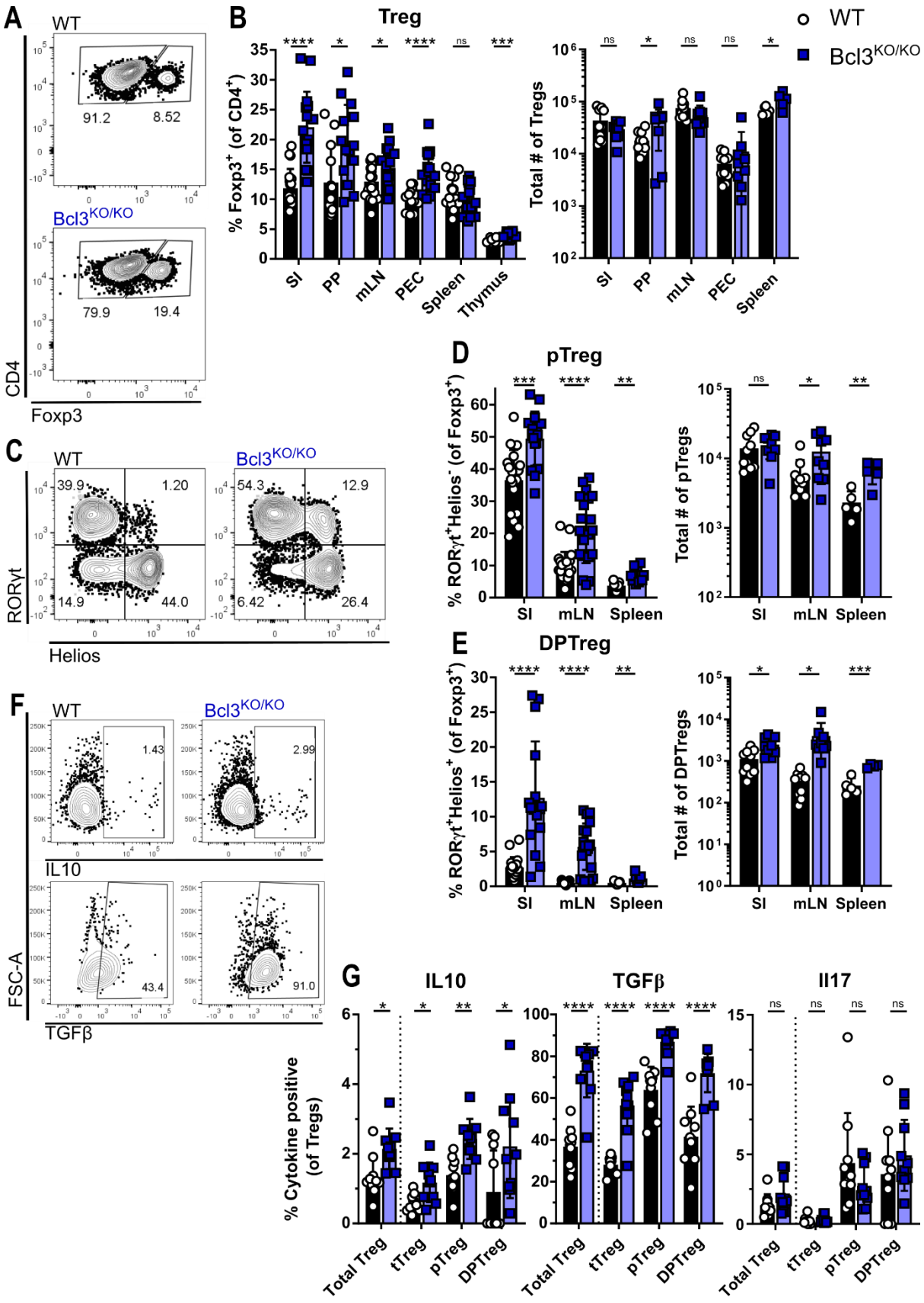

Figure 4: ***Bcl3 deficiency quantitively and qualitatively alters Foxp3⁺ regulatory T cell subsets.*** ***(A)*** *Representative flow cytometry plot for Foxp3 expression in CD4⁺ T cells from the lamina propria of the small intestine of WT and Bcl3$^{KO/KO}$ mice.* ***(B)*** *Summary of flow cytometry analysis from (A) showing Treg percentage (left)*

and absolute cell numbers (right) for small intestine lamina propria (SI), Peyer's patches (PP), mesenteric lymph nodes (mLN), peritoneal cavity (PEC), spleen and thymus. ***(C)*** *Representative flow cytometric analysis of RORγt and Helios expression in Foxp3$^+$ regulatory T cells from the small intestine of WT and Bcl3$^{KO/KO}$ animals.* ***(D*** *and* ***E)*** *Percentage and absolute cell numbers of RORγt$^+$Helios$^-$ (pTreg)* ***(D)*** *or RORγt$^+$Helios$^+$ (DPTreg)* ***(E)*** *pre-gated on Foxp3$^+$ regulatory T cells.* ***(F)*** *Representative flow cytometry plot for IL-10 (top) and TGFβ (bottom) cytokine$^+$ regulatory T cells from WT and Bcl3$^{KO/KO}$ after ex vivo restimulation of lymphocytes from mLN with PMA/Ionomycin.* ***(G)*** *Relative quantification of IL-10 (left), TGFβ (middle) and IL-17 (right) expression in different subpopulations of restimulated regulatory T cells as in (F). Each dot represents an individual mouse and mean ± SD from at least two independent experiments is shown. Control n ≥9 mice, Bcl3KO/KO n≥9 mice. Statistical analysis was performed using a two-tailed student t-test and corrected for multiple comparisons using the Holm-Sidak method. P value of <0.05 was considered statistically significant with * p <0.05, ** p < 0.01, *** p < 0.001, **** p < 0.0001, ns = not significant.*

3.2.2 RORγt expressing Tregs are influenced by Bcl3 in a cell-intrinsic manner.

The previous results show an elevated frequency of Tregs and particularly RORγt$^+$ Tregs in Bcl3 deficient mice with a simultaneous boost of their cytokine secretion potential. Nonetheless, the spontaneous inflation and the unusual phenotype of DPTregs in Bcl3$^{KO/KO}$ animals could hypothetically also be originating from cell-extrinsic effects of Bcl3 in other cell types as documented for B cells or dendritic cells [157], [181]. Thus, it was next analysed whether Bcl3 exerts this vast impact on the phenotype of Tregs in a cell-intrinsic manner by creating a Foxp3 specific conditional knockout of Bcl3 through cross-breeding of Foxp3$^{Cre/WT}$ x Bcl3$^{fl/fl}$ mice. In contrast to a complete loss of Bcl3, steady state analysis of spleen, mesenteric lymph nodes, and small intestine lamina propria from Foxp3$^{Cre/WT}$ x Bcl3$^{fl/fl}$ mice revealed a reduced total Foxp3$^+$ Treg frequency and Treg numbers in mesenteric lymph nodes (**Figure 5A** and **B**). However, sustained changes in the percentages of both pTregs and DPTregs among Foxp3$^+$ Tregs as well as an increase in total numbers of pTregs and DPTregs in mesenteric lymph node and small intestine were confirmed in conditional KO of Bcl3 (**Figure 5C** - **E**). This indicates a significant cell-intrinsic effect of Bcl3 on RORγt$^+$ Tregs.

It was furthermore hypothesized that the expression levels of Bcl3 may act as a regulator for the size of the RORγt expressing Treg population. Therefore, mice conditionally overexpressing Bcl3 in CD4$^+$ T cells (Bcl3^{TOE} [158]) were investigated.

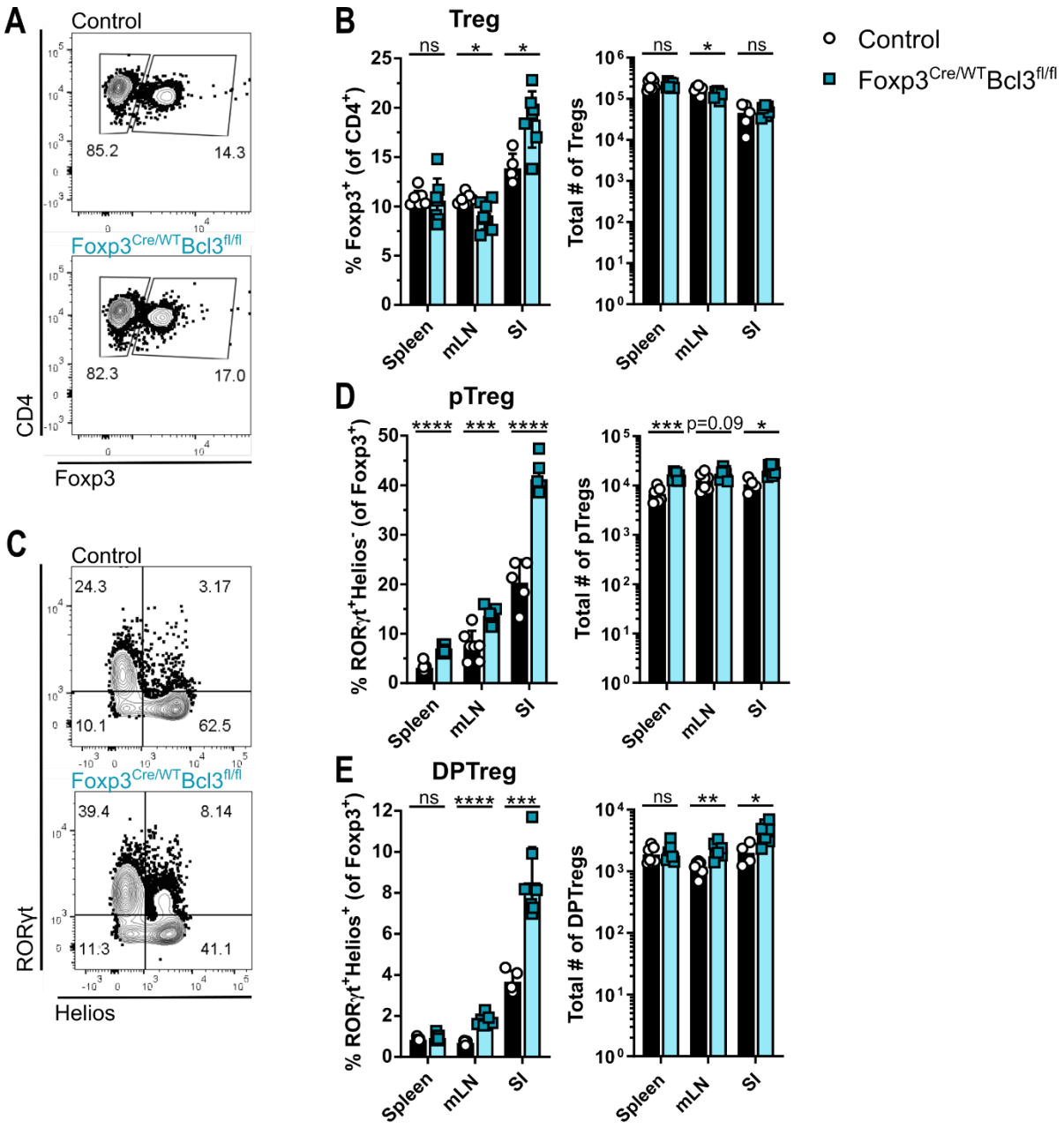

Figure 5: ***Increased numbers of RORyt expressing Tregs in mice with Foxp3 specific knockout of Bcl3. (A)*** *Representative flow cytometry plots of Foxp3 expression among CD4⁺ T cells from the lamina propria of the small intestine of Foxp3 specific conditional Bcl3 knockout (Foxp3$^{Cre/WT}$Bcl3$^{fl/fl}$) and littermate control animals.* ***(B)*** *Percentages (left) and absolute cell number (right) of analysis shown in (A) in the spleen, mesenteric lymph nodes (mLN) and small intestine (SI).* ***(C)*** *Representative flow cytometry plots for Helios and RORyt expression in pregated for Foxp3⁺ T cells of small intestine lamina propria cells from Foxp3$^{Cre/WT}$Bcl3$^{fl/fl}$ and control animals.* ***(D and E)*** *Percentages (left) and absolute cell numbers (right) of RORyt⁺Helios⁻ pTregs* ***(D)*** *and RORyt⁺Helios⁺ Tregs (DPTregs)* ***(E)*** *among Foxp3⁺ Tregs from spleen, mesenteric lymph nodes and small intestine as shown in (C).). Each dot represents an individual mouse and mean ± SD from at least two independent experiments is shown. Control n ≥5 mice and Foxp3$^{Cre/WT}$Bcl3$^{fl/fl}$ n=7 mice. Statistical analysis was performed using a two-tailed student t-test and corrected for multiple comparisons using the Holm-Sidak method. P value of <0.05 was considered statistically significant with * p <0.05, ** p < 0.01, *** p < 0.001, **** p < 0.0001, ns = not significant.*

Indeed, steady state analysis of spleen and mesenteric lymph nodes confirmed that specifically overexpressing Bcl3 led to significantly reduced Foxp3^{+} Treg frequency and diminished absolute Treg numbers (**Figure 6A** and **B**). Furthermore, the abundance and absolute cell number of RORγt^{+} pTregs in Bcl3^{TOE} mice were reduced accordingly (**Figure 6C** and **D**). However, while frequency and absolute number of DPTregs were reduced in the spleens of Bcl3^{TOE} mice as expected, there was an unforeseen increase in DPTreg abundance in mesenteric lymph nodes of Bcl3^{TOE} animals, presumably due to the low Treg numbers in Bcl3^{TOE} as this was not observed in total cell counts (**Figure 6C** and **E**). In conclusion, these results indicate that Bcl3 expression in regulatory T cells is sufficient to restrain RORγt^{+} Treg development in a cell-intrinsic manner.

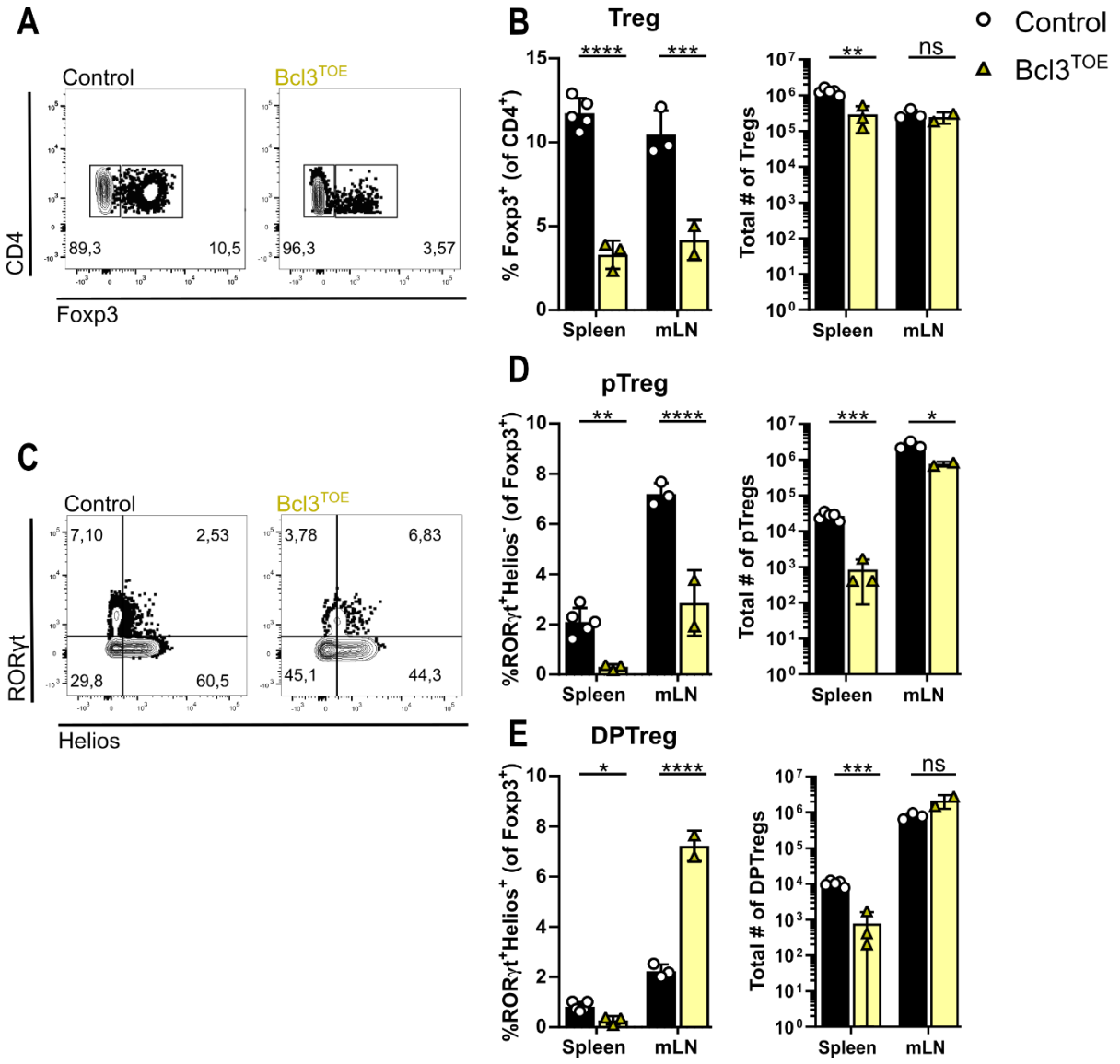

Figure 6: ***Decreased abundance of Tregs in mice with CD4 specific overexpression of Bcl3.*** *Representative flow cytometry plots of Foxp3 expression among splenic CD4$^+$ T cells from mice overexpressing Bcl3 in T cells (Bcl3^{TOE}) and control animals.* ***(B)*** *Summary of Foxp3$^+$ regulatory T cell percentages (left) and absolute cell numbers (right) as shown in (A) in spleen and mLN. (**C**) Representative flow cytometry plot from mLN showing RORγt and Helios in pre-gated Foxp3$^+$ T cells from Bcl3^{TOE} and control mice.* ***(D** and **E)** Percentages (left) and absolute cell numbers (right) of RORγt$^+$Helios$^-$ pTregs **(D)** and RORγt$^+$Helios$^+$ DPTregs **(E)** among Foxp3$^+$ Tregs in spleen and mLN from the animals in (C). Each dot represents an individual mouse and mean ± SD from at least two independent experiments is shown. Control n ≥3 mice and Bcl3OE^{Tcell} n ≥2 mice. Statistical analysis was performed using a two-tailed student t-test and corrected for multiple comparisons using the Holm-Sidak method. P value of <0.05 was considered statistically significant with * p <0.05, ** p < 0.01, *** p < 0.001, **** p < 0.0001, ns = not significant.*

3.2.3 Microbiome independent RORγt$^+$ Treg expansion by suppression of Bcl3

The population size of pTregs can vary between different animal facilities due to a varying microbiome as pTregs are very dependent on the intestinal microenvironment. Therefore, it was necessary to eliminate any influence of a possibly dissimilar microenvironment in Bcl3 deficient or Foxp3$^{Cre/WT}$ x Bcl3$^{fl/fl}$ animals bred in different mouse husbandries. Hence, Treg populations of Bcl3 deficient and wildtype mice that were initially colonised with a reduced microbiome (RM) based on the Altered Schaedler flora were analysed, to determine if the impact of Bcl3 on pTregs can be reproduced. Indeed, the overall increase of Tregs in Bcl3 deficient mice was not impacted by altering the bacterial colonisation of the mice (**Figure 7A**). Although the inflating effect of Bcl3 deficiency on pTregs and DPTregs could be reproduced in mice with reduced microbial complexity, it was overall attenuated (**Figure 7B** - **D**). This again highlights the general microbiome dependency of RORγt$^+$ Treg induction.

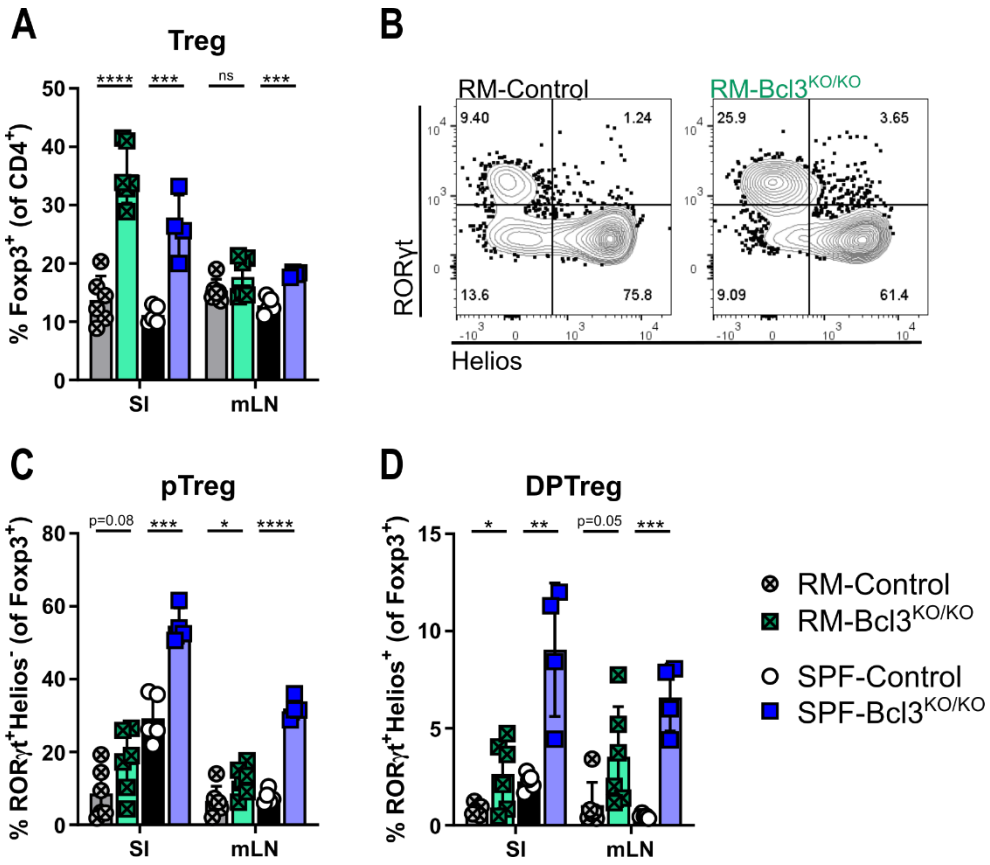

*Figure 7: **Increased abundance of RORyt⁺ Treg due to loss of Bcl3 does not depend on a specific microbiome**. Bcl3$^{KO/KO}$ and wildtype mice that were originally colonised with a reduced microbiome (RM) based on Altered Schaedler Flora (ASF) were analysed in parallel with Bcl3$^{KO/KO}$ and control mice with a more diverse specific pathogen free (SPF) microbiome. **(A)** Percentage of total Foxp3⁺ regulatory T cells among CD4⁺ T cells from the small intestine lamina propria (SI) and mesenteric lymph nodes (mLN) of reduced microbiome control (RM-Control), reduced microbiome Bcl3$^{KO/KO}$ (RM-Bcl3$^{KO/KO}$), specific pathogen free control (SPF-Control) and specific pathogen free Bcl3$^{KO/KO}$ (SPF-Bcl3$^{KO/KO}$) mice. **(B)** Representative flow cytometry plots for Helios and RORyt expression in pre-gated Foxp3⁺ T cells from mLNs of reduced microbiome control (RM-Control), reduced microbiome Bcl3$^{KO/KO}$ (RM-Bcl3$^{KO/KO}$) animals. **(C** and **D)** Percentage of RORyt⁺Helios⁻ (pTreg) **(C)** or RORyt⁺Helios⁺ (DPTreg) **(D)** Foxp3⁺ regulatory T cells as shown in (B). Each dot represents an individual mouse and mean ± SD from at least two independent experiments is shown. RM-Control n=6 mice, RM-Bcl3$^{KO/KO}$ n=6 mice; SPF-Control n=5 mice and SPF-Bcl3$^{KO/KO}$ n=4. Statistical analysis was performed using a two-tailed student t-test and corrected for multiple comparisons using the Holm-Sidak method. P value of <0.05 was considered statistically significant with * p <0.05, ** p < 0.01, *** p < 0.001, **** p < 0.0001, ns = not significant.*

3.2.4 Unabated suppressive capacity of Bcl3 deficient Tregs in a T cell transfer model of colitis.

The previously presented data suggested that increased Bcl3 deficient Foxp3⁺ Treg populations were functionally superior in terms of cytokine secretion (**Figure 4G**). Moreover, Bcl3 deficient Th1-differentiated cells were incapable of causing intestinal inflammation in a transfer colitis model [179]. Additionally, it was previously published that conditionally overexpressing Bcl3 in regulatory T cells weakened their *in vivo*

suppressive capacity [158]. Therefore, it was hypothesized that Bcl3 deficiency in Tregs would not impair the suppression of gut inflammation *in vivo*.

Thus, a T cell transfer model of colitis was set up to analyse whether Bcl3 sufficient and Bcl3 deficient Tregs were equally capable of suppressing effector T cells. As expected, the transfer of naïve CD45.1^{+} CD4^{+} T cells into Rag1$^{KO/KO}$ mice induced weight loss beginning around four weeks after transfer (**Figure 8A**). Notably, the co-transfer of Bcl3 deficient Tregs was at least as effective as the co-transfer of control Tregs in protecting mice from weight loss and impairing CD45.1^{+} effector T cell proliferation in various organs (**Figure 8A** and **B**). Furthermore, histological H&E staining of the colon and distal small intestine sections showed a drastic reduction of cellular infiltration in the colon, epithelial hyperplasia, and goblet cell loss by both Bcl3 sufficient and Bcl3 deficient Tregs (**Figure 8C** and **D**). Finally, the fate of transferred CD45.2^{+} Tregs originating from the spleens of control or Bcl3 deficient mice was analysed. Surprisingly, the overall abundance of Foxp3^{+} cells among transferred Bcl3 deficient Tregs was reduced in this inflammatory environment, indicating that Bcl3 is essential to sustain general Treg stability (**Figure 8E**). These ex-Tregs originating from Bcl3 deficient spleens primarily assumed a Th17-like cell fate (**Figure 8F**), a phenomenon previously described in autoimmune arthritis as a pathogenic conversion or trans-differentiation of Tregs towards Th17 cells [43]. These results provoked an investigation into whether Bcl3 deficiency might also result in inflated Th17 cell numbers in the other aforementioned mouse lines. Indeed, elevated RORγt^{+}Foxp3^{-} Th17 cell frequencies were observed in global Bcl3$^{KO/KO}$ mice and surprisingly also in Foxp3$^{Cre/WT}$ x Bcl3$^{fl/fl}$ animals (**Figure 9**).

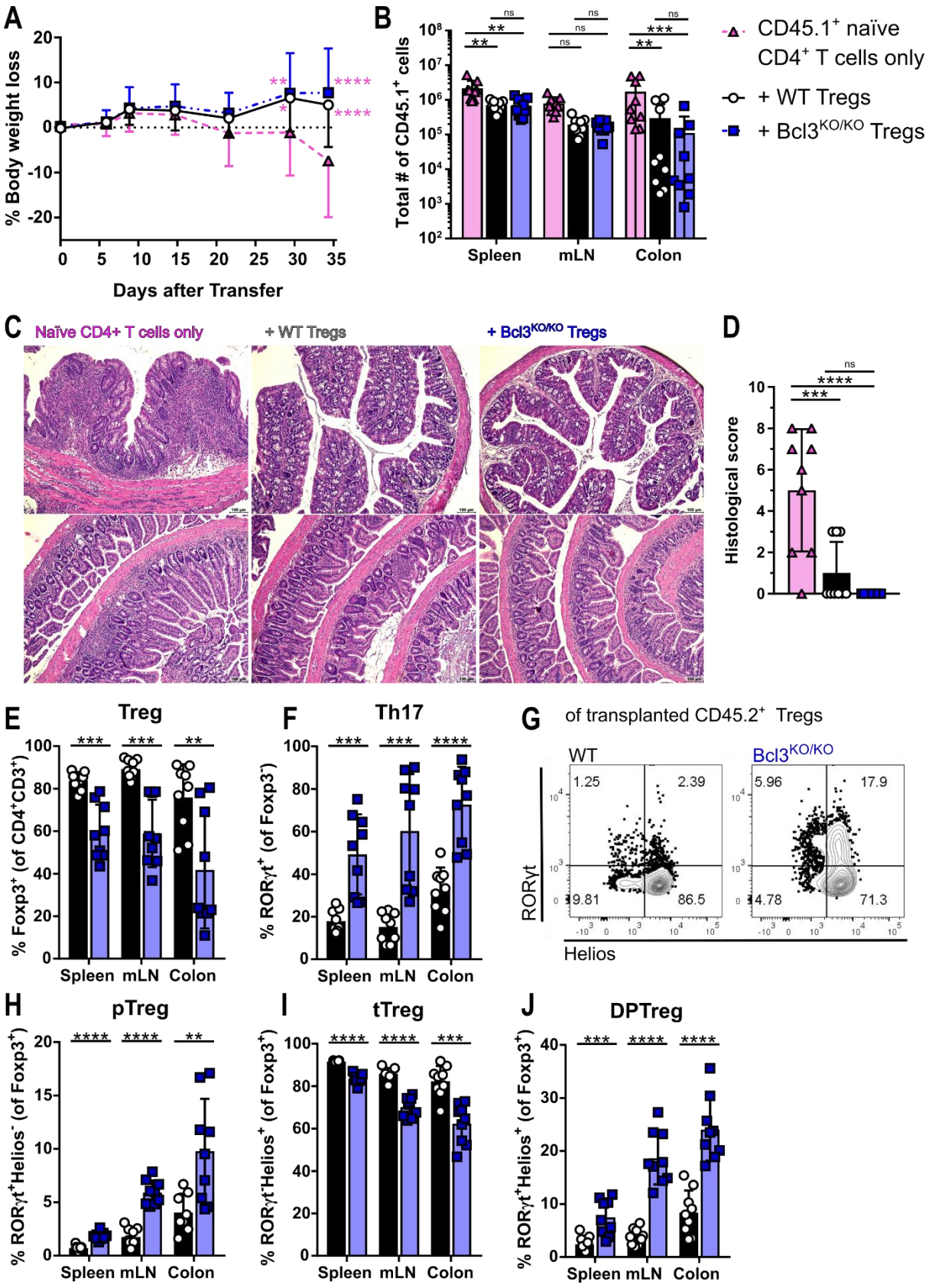

Figure 8: ***Bcl3$^{KO/KO}$ Tregs have unabated suppressive capacity and are protective in T cell transfer colitis.*** *T cell transfer colitis was performed as described in the material and methods section.* ***(A)*** *Kinetic of body weight loss at indicated time points after cell transfer.* ***(B)*** *Total number of recovered CD45.1$^+$ T cells isolated from each organ.* ***(C)*** *Representative H&E staining of histological cross sections from the proximal colon (upper row) and Swiss rolls from*

the distal small intestine (lower row) from each group. Scale bars = 100 µm ***(D)*** *Quantification of histological scores from (C) concerning inflammatory cell infiltrate, loss of goblet cells and epithelial hyperplasia.* ***(E)*** *Percentage of Foxp3^{+} regulatory T cells among transplanted CD45.2^{+} CD4^{+} T cells isolated from spleen, mesenteric lymph nodes (mLN) and proximal colon at the end of the experiment in (A).* ***(F)*** *Percentage of RORyt expressing cells among Foxp3^{-} cells (Th17) in the transferred CD45.2^{+} T cell compartment.* ***(G)*** *Representative flow cytometry plot depicting RORyt and Helios expression among Foxp3^{+} regulatory T cells in mLN of WT or Bcl3$^{KO/KO}$ Treg recipients.* ***(H-J)*** *Quantification of the data in (G) depicting percentages of RORyt^{+}Helios^{-} pTregs* ***(H)****, RORyt^{-}Helios^{+} tTregs* ***(I)*** *and RORyt^{+}Helios^{+} DPTregs* ***(J)*** *among transferred CD45.2^{+} Wildtype or Bcl3$^{KO/KO}$ Tregs. Each dot represents an individual mouse. Mean ± SD from at least two independent experiments is shown. CD45.1^{+} naïve CD4 T cells only n=9 mice, naïve T cells + WT Tregs n=9, naïve T cells + Bcl3$^{KO/KO}$ Tregs n=9 mice. Statistical analysis was performed using either two-way ANOVA corrected via Sidak (A + B), one-way ANOVA corrected via Sidak (D), or two-tailed students t-test corrected for multiple comparisons using the Holm-Sidak method (E - J). P value of <0.05 was considered statistically significant with * p <0.05, ** p < 0.01, *** p < 0.001, **** p < 0.0001, ns = not significant.*

Coherent with previously described results, higher percentages of pTregs were observed in animals co-transplanted with Bcl3 deficient Tregs and correspondingly decreased abundances of RORyt^{-}Helios^{+} Tregs (tTregs) (**Figure 8G** - **I**). Furthermore, the appearance of the RORyt^{+}Helios^{+} DPTreg population was again confirmed exclusively in Tregs originating from Bcl3 deficient mice (**Figure 8G** and **J**). Considering that the spleen usually harbours only very few pTregs (based on RORyt and Helios expression, see **Figure 4**), these observations indicate that the DPTreg population may be stemming from Helios^{+} tTregs and is not a result of *de novo* Treg cell differentiation.

In summary, these results show that Bcl3 deficient Tregs are completely unabated in their functionality and ability to suppress effector T cell proliferation and intestinal inflammation in comparison to their Bcl3 sufficient counterpart.

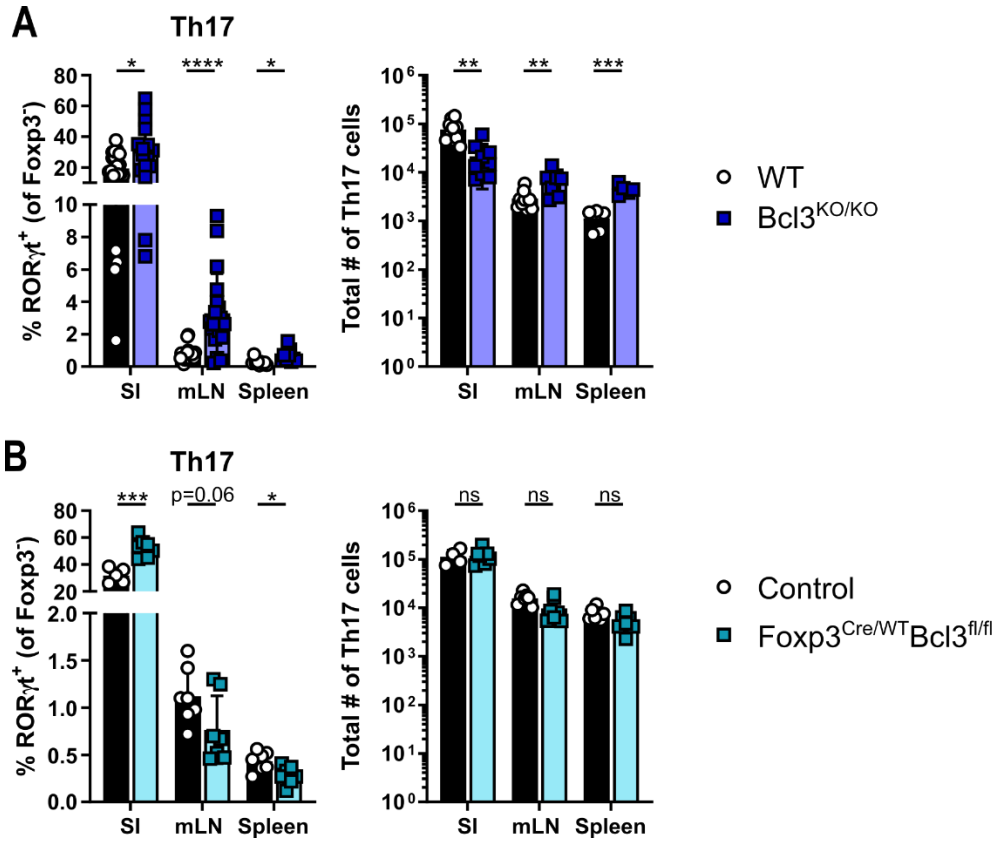

Figure 9: ***Increased abundance of Th17 cells in mice with Bcl3 deficient Tregs. (A)*** *Percentage and absolute number of RORγt⁺ cells among Foxp3⁻ CD4⁺ T helper cells from small intestine lamina propria (SI), mesenteric lymph nodes (mLN), and spleen of WT and Bcl3$^{KO/KO}$ mice.* ***(B)*** *Percentage and absolute number of RORγt⁺ cells among Foxp3⁻ CD4⁺ T helper cells from indicated organs of mice with Treg specific Bcl3 knockout (Foxp3$^{Cre/WT}$Bcl3$^{fl/fl}$) and control mice. Each dot represents an individual mouse. Mean ± SD from at least two independent experiments is shown. WT n≥5 mice and Bcl3$^{KO/KO}$ n≥5 mice; Control n≥5 mice and Foxp3$^{Cre/WT}$Bcl3$^{fl/fl}$ n=7 mice. Statistical analysis was performed using a two-tailed student t-test and corrected for multiple comparisons using the Holm-Sidak method. P value of <0.05 was considered statistically significant with * p <0.05, ** p < 0.01, *** p < 0.001, **** p < 0.0001, ns = not significant.*

3.2.5 Bcl3 deficiency produces a transcriptional profile supporting RORγt⁺ Tregs

To enable in depth transcriptional analysis of the effect Bcl3 has on Tregs, the Bcl3 deficient mouse line was backcrossed to a double reporter mouse line for Foxp3 and RORγt (*Foxp3*^{RFP}x*Rorc(γt)*^{GFP} x Bcl3$^{KO/KO}$). This new mouse line facilitated the identification and isolation of living total Foxp3⁺ Tregs, RORγt⁺ Tregs, and RORγt⁻ Tregs from Bcl3 deficient and respective control reporter mice (**Figure 10**) to perform bulk RNA sequencing (bulkRNAseq) of FACS sorted populations.

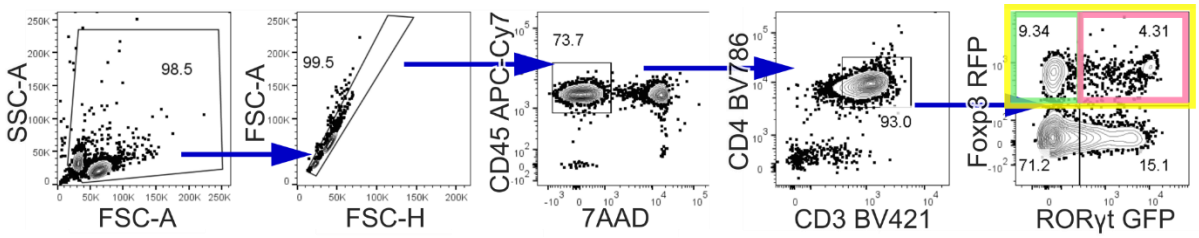

Figure 10: ***Gating strategy for sorting of different intestinal Treg subsets to perform RNA sequencing.*** *Representative gating strategy for cell isolation from mLN of Bcl3$^{KO/KO}$ x Foxp3^{RFP}xRorc(γt)^{GFP} mice. Coloured squares indicating sorted population: Total Treg – yellow, RORγt^{-} Treg – green and RORγt^{+} Treg – pink.*

First, total Foxp3^{+} Tregs from mLN and spleens of Bcl3$^{KO/KO}$, wildtype (WT), and Bcl3OE^{Treg} mice were sequenced (**Figure 11A**). Bcl3OE^{Treg} mice could be included because they expressed a Foxp3 reporter as well. As anticipated, overexpression or the absence of *Bcl3* in Bcl3OE^{Treg} and Bcl3$^{KO/KO}$ Tregs on the RNA level related to the respective genotype (**Figure 11A,** blue arrow). Furthermore, Bcl3 deficient Tregs displayed elevated expression of genes that were previously published to be involved in T cell and Treg activation and differentiation such as *Ctla2a, Tnfrsf8, and Cd86*. However, decreased expression of Treg marker genes *Foxp3* and *Il2ra* were measured in Tregs overexpressing Bcl3 matching with their reduced appearance (**Figure 6A** and **B**, yellow arrows**,** and [158]). Concomitant with the phenotype documented in flow cytometric analysis (**Figure 4D**), increased expression of genes associated with a pTreg transcriptional profile (as shown in **Figure 1F**) such as *Rorc, Cxcr6,* and *Asb2* was found in Tregs of Bcl3 deficient mice compared to Tregs of WT or Bcl3OE^{Treg} mice (**Figure 6A**, pink arrows). Because this effect likely originated from a different cellular composition of sorted total Foxp3^{+} Tregs, the subsequent analysis focused on pTregs by sorting only RORγt^{+} Tregs for bulk RNAseq from Bcl3 deficient and WT reporter mice. Confirming this suspicion, an increase in pTreg signature genes in Bcl3 deficient Tregs was no longer observed but an elevated expression of numerous tTreg signature genes such as *Ikzf2* (Helios), *Ccr8,* and *Cd83* was measured instead (**Figure 11B,** green arrows).

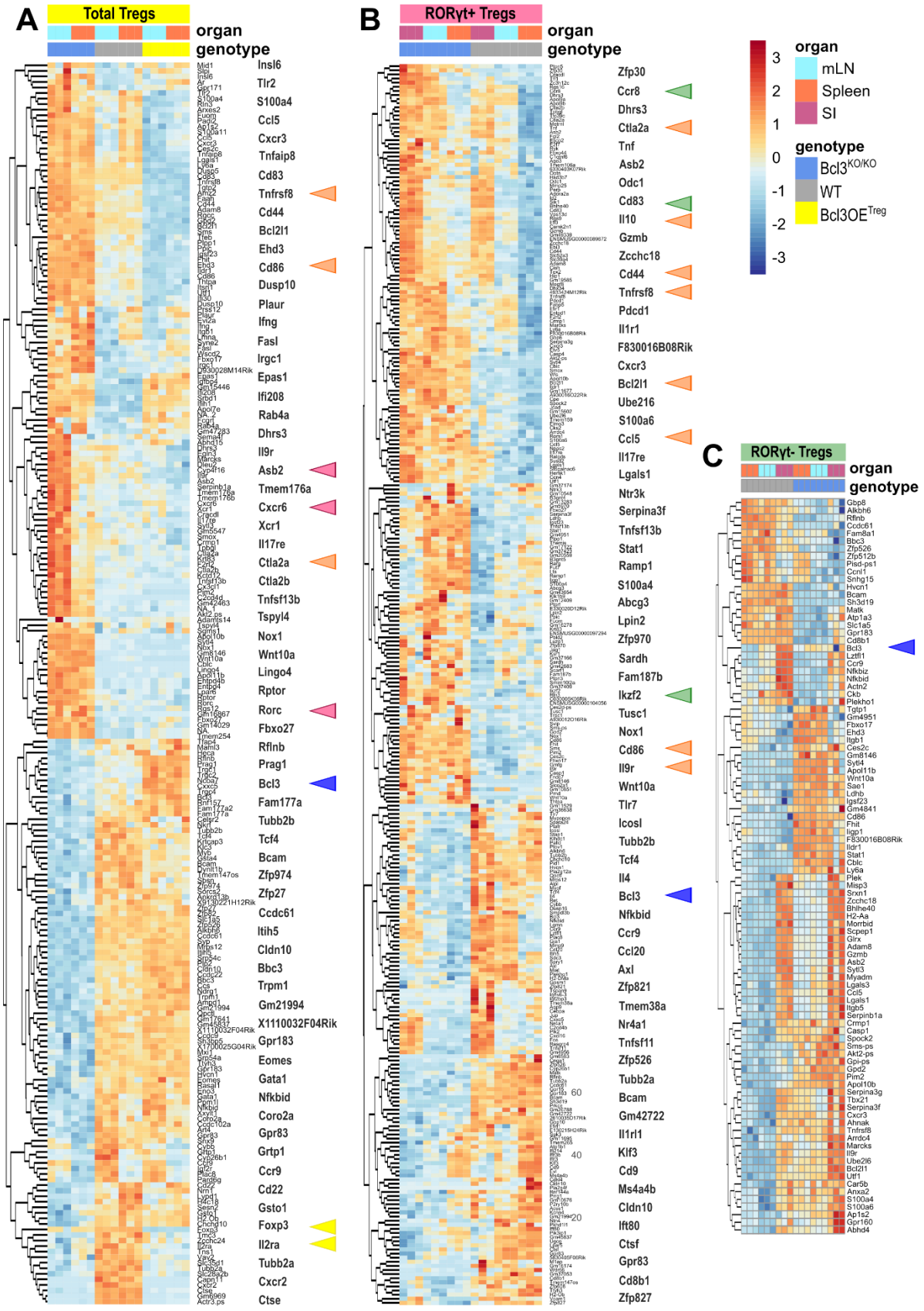

Figure 11: ***Differential gene expression in Bcl3 deficient total Tregs, RORγt⁺ Tregs and RORγt⁻ Tregs.*** *Bulk RNA sequencing data of Treg subsets from mesenteric lymph nodes (mLN), spleen or small intestine lamina propria (SI) of Bcl3$^{KO/KO}$ x Foxp3^{RFP}xRorc(γt)^{GFP} (Bcl3$^{KO/KO}$), Bcl3OE^{Treg} or Foxp3^{RFP}xRorc(γt)^{GFP} wildtype littermates (WT) purified via*

fluorescence activated cells sorting (FACS). ***(A)*** *Fully annotated heatmap showing differentially expressed genes (DEG; log2 fold change > 2, adjusted p-value < 0.05) in $Bcl3^{KO/KO}$ Tregs compared to WT and $Bcl3OE^{Tcell}$ Total Tregs additionally labelled with selected gene names.* ***(B)*** *Fully annotated heatmap of selected DEGs (log2 fold change > 2, adjusted p-value < 0.05) in RORyt expressing Tregs from $Bcl3^{KO/KO}$ mice compared to WT RORyt expressing Tregs additionally labelled with selected gene names.* ***(C)*** *Fully annotated heatmap of DEGs (log2 fold change > 2, adjusted p-value < 0.05) in $RORyt^-$ Tregs from $Bcl3^{KO/KO}$ mice compared to WT $RORyt^-$ Tregs. Each column represents an individual mouse and n=3 mice per group. Statistical analysis was performed using the R package DESeq2.*

Once more, these observations presumably echo a different composition of subpopulations among $RORyt^+$ Tregs within the sorted fraction, in particular the occurrence of $RORyt^+Helios^+$ DPTregs exclusively in Bcl3 deficient Tregs causing the increase in tTreg genes in Bcl3 deficient $RORyt^+$ Tregs. Nevertheless, consistent with previous results Bcl3 deficient $RORyt^+$ Tregs expressed elevated levels of genes involved in Treg activation such as *CD44, Bcl2l1, Tnfrsf8, Il9r, CD86, Ctla2, Ccl5,* and *Il10* (**Figure 11A** and **B**, orange arrows).

The varying impact of Bcl3 deficiency on the analysed Treg populations can be visualized by calculating Volcano plots depicting the log2 fold change and significance of DEGs (**Figure 12A**). These plots demonstrate that more genes are significantly changed and to a greater extent in $RORyt^+$ Tregs than in $RORyt^-$ Tregs. To further narrow down the influence of Bcl3 on Treg gene transcription the overlap of differentially expressed genes (DEGs) from Bcl3 deficient compared to wildtype and $Bcl3OE^{Treg}$ total Tregs (**Figure 11A**) with the DEGs of Bcl3 deficient $RORyt^+$ Tregs relative to their wildtype counterpart (**Figure 11B**) was calculated. The effect of Bcl3 on gene expression in $RORyt^-$ Tregs again was substantially weaker according to the number of DEGs of Bcl3 deficient and sufficient $RORyt^-$ Tregs (**Figure 11C** and **Figure 12A**). Thus, the focus was further fixed on the comparison of total Treg and $RORyt^+$ Treg DEGs (**Figure 12B**). It was evaluated that both RNAseq experiments displayed a substantial overlap in up- and downregulated DEGs implying that up to one third of DEGs could be accounted for differences in $RORyt^+$ Tregs. The shared upregulated genes included *Furin, Il9r, Cd86,* and *Cd83* which are associated with Treg function, activation, and differentiation. Finally, the aim was to determine potential biological pathways that could therefore cause the transcriptional profile of Bcl3-manipulated Tregs. Gene set enrichment analysis (GSEA) was performed against a published hallmark gene list reference representing various biological processes [174].

This GSEA discovered a significant reduction in TNFα target genes/signalling via NFκB such as *Bcl3*, *Nfkbia,* and *Ccl20* whereas the analysis also showed a significant increase in genes correlated with IL-2/STAT5 signalling (*Bcl2l1*, *Cd83,* and *Icos*) and IL-6/JAK/STAT3 signalling (*Cd44, Stat1,* and *Il9r*) (**Figure 12C**). In conclusion, these results indicate a transcriptional influence of Bcl3 on T cell activation and the sensitivity towards IL-2, IL-6, and TNFα signalling in Tregs.

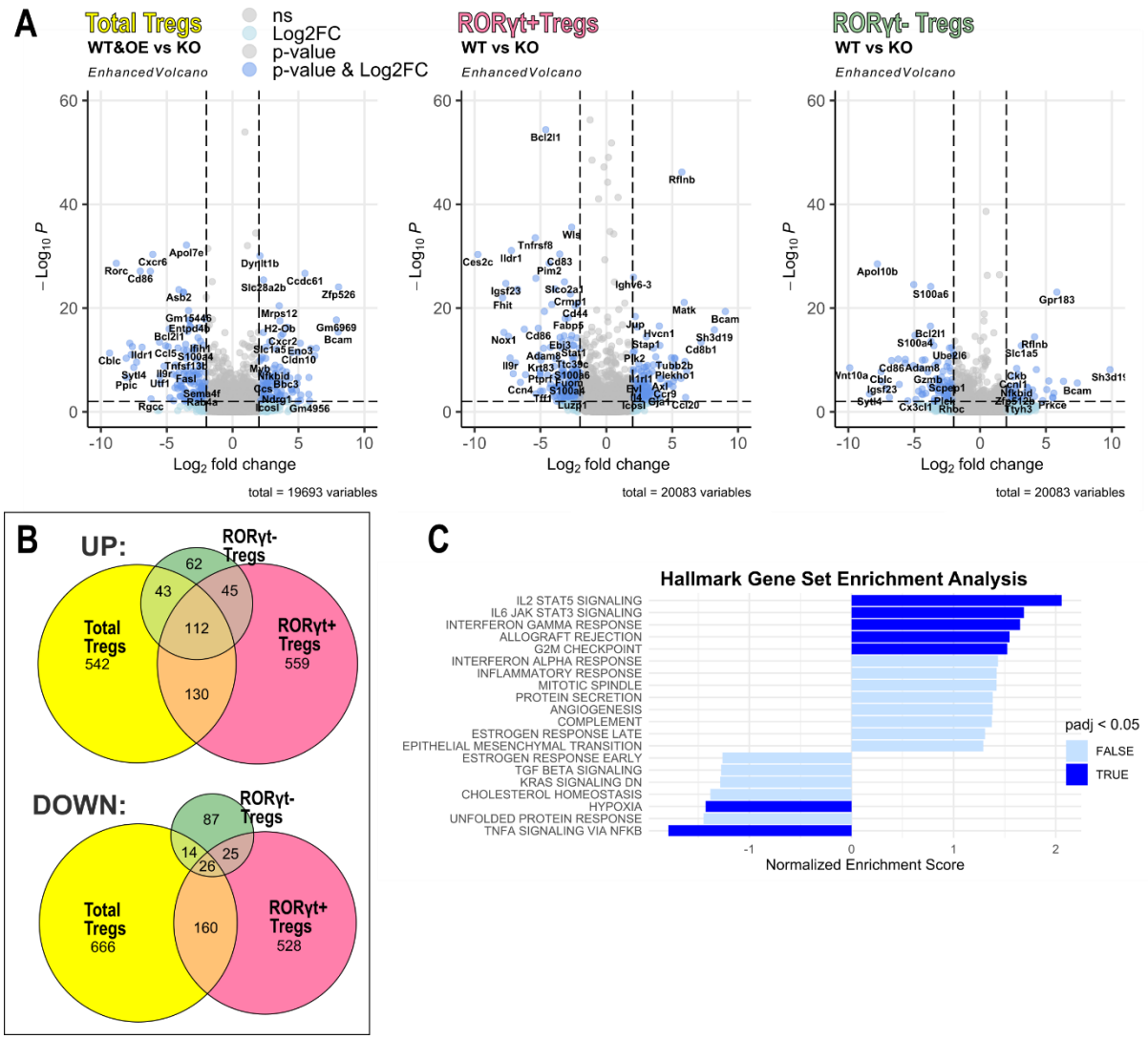

Figure 12: ***Bcl3 expression influences cytokine responsiveness in Tregs. (A)*** *Volcano plots illustrating the significance and fold change of DEGs in all Tregs (left), RORγt⁺ Tregs (middle) and RORγt⁻ Tregs (right) comparing WT and Bcl3OE^{Treg} (OE) versus Bcl3$^{KO/KO}$ (KO) cells or WT versus KO cells as indicated above plot.* ***(B)*** *Overlapping DEG from RNA sequencing analysis of total Tregs (yellow), RORγt expressing Tregs (pink) and RORγt negative Tregs (green). Shared upregulated genes – top, shared downregulated genes – bottom.* ***(C)*** *Gene Set Enrichment Analysis (GSEA) of DEG in RORγt expressing Tregs from Bcl3$^{KO/KO}$ mice compared to WT RORγt expressing Tregs. Each column represents an individual mouse and n=3 mice per group. Statistical analysis was performed using either R package fgsea or R package DESeq2.*

3.2.6 Biased development of Bcl3 deficient T cells in a competitive environment

Next, to analyse RORγt^{+} Treg differentiation from Bcl3 deficient and sufficient cells within the same microenvironmental setting, mixed bone marrow chimeras were created by transferring 50% congenically labelled (CD45.1) control and 50% of Bcl3 deficient (CD45.2) bone marrow cells into lethally irradiated, T and B cell deficient Rag1$^{KO/KO}$ animals.

Indeed, Bcl3 deficient bone marrow cells induced a greater percentage of Tregs in the small intestine lamina propria and spleen compared to Bcl3 sufficient cells (**Figure 13B**). Once more, this effect was especially prominent among RORγt^{+}Helios^{-} pTregs (**Figure 13A** and **C**) and the atypical RORγt^{+}Helios^{+} DPTreg population was also found solely among Tregs lacking Bcl3 (**Figure 13A** and **D**). While equal cell counts of Bcl3 deficient and competent bone marrow cells were injected into the recipients, the total numbers in the Treg compartment appeared remarkably different (**Figure 13F**). Moreover, the extensive surplus in pTreg and DPTreg cell numbers suggested a developmental bias in Bcl3 deficient cells towards RORγt^{+} Tregs (**Figure 13G** and **H**). Additionally, the increase of Th17 cells seen in Bcl3$^{KO/KO}$ mice and mice with a Treg specific loss of Bcl3 could again be reproduced exclusively in the Bcl3 deficient compartment of mixed bone marrow chimeras, supporting a hypothesis of Treg trans-differentiation (**Figure 13E** and **I**).

To investigate if loss of Bcl3 influenced the capability of cells to compete with Bcl3 competent cells, the distribution of both compartments was analysed in different organs. Surprisingly, there were significant differences in the distribution of WT and KO cells (**Figure 13J** and **K**). While there was only a sparse population of Bcl3$^{KO/KO}$ cells in the thymus and almost all CD45^{+} were of WT origin, the relation shifted towards the periphery with the colon harbouring distinctly more Bcl3 deficient than competent cells. This distributional bias was even more drastic when comparing distinct cell populations instead of organs. Approximately 60% of all CD45^{+} cells in the spleen were of WT origin, but among CD4^{+} T cells it was reduced to 50% and gating on Tregs revealed only about 25% of Bcl3 competent cells (**Figure 13L** and **M**). The most drastic difference, however, was seen in splenic RORγt^{+} Tregs only consisting of less than 20% WT cells. In the small intestine, the effect was even more pronounced.

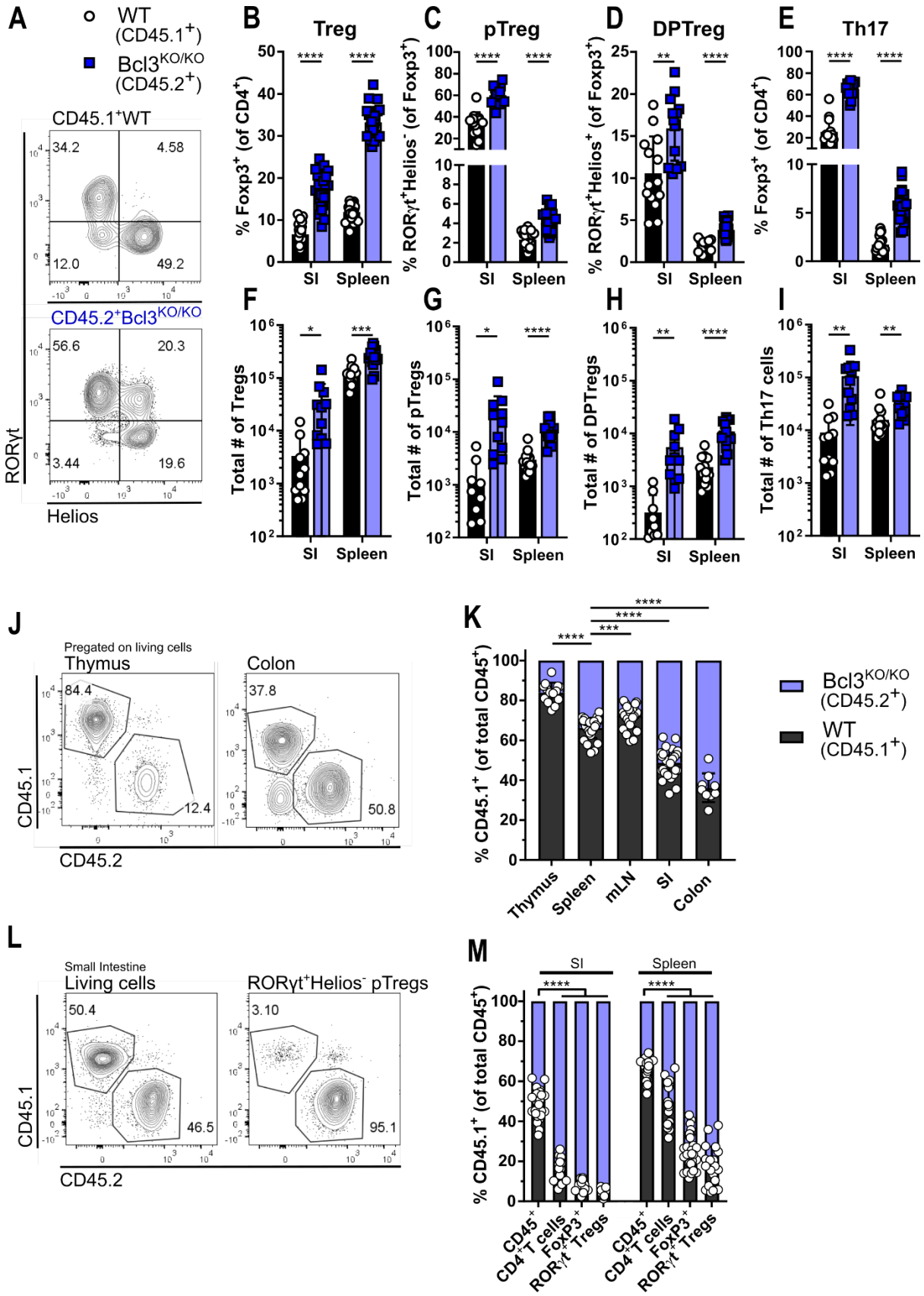

*Figure 13**: Increase of RORyt expressing Treg numbers in the Bcl3 deficient T cell compartment of mixed bone marrow chimeras.** Irradiated Rag1$^{KO/KO}$ animals were transplanted with an equal amount of CD45.2^{+} Bcl3$^{KO/KO}$ and CD45.1^{+} WT bone marrow cells and analysed 16 weeks after transfer. **(A)** Representative flow cytometry plot showing*

RORyt and Helios expression among pre-gated wildtype cells (CD45.1$^+$, top) or Bcl3$^{KO/KO}$ cells (CD45.2$^+$, bottom) Foxp3$^+$ T cells from small intestine lamina propria of mixed bone marrow recipients. ***(B)*** *Percentage of total Foxp3$^+$ regulatory T cells of CD45.1$^+$ or CD45.2$^+$ CD4$^+$ T cells from the small intestine lamina propria (SI) and spleen of mixed bone marrow chimeras.* ***(C*** *and* ***D)*** *Percentages of RORyt$^+$Helios$^-$ pTregs* ***(C)*** *and RORyt$^+$Helios$^+$ Tregs (DPTregs)* ***(D)*** *among pre-gated wildtype cells (CD45.1$^+$, top) or Bcl3$^{KO/KO}$ cells (CD45.2$^+$, bottom) Foxp3$^+$ Tregs from SI and spleen as shown in (A).* ***(E)*** *Percentage of Th17 cells in SI and spleen pre-gated on Foxp3$^-$ CD4$^+$ T cells from mixed bone marrow chimeras* ***(F-I)*** *Absolute cell number quantification of data shown in (B-E).* ***(J)*** *Representative flow cytometry analysis showing the different distribution of CD45.1$^+$ WT and CD45.2$^+$ Bcl3$^{KO/KO}$ cells among all living cells isolated from the thymus (left) or colon lamina propria (right).* ***(K)*** *Quantification of analysis as shown in (J) showing the percentage of CD45.1$^+$ WT cells out of all living CD45$^+$ cells isolated from the indicated organs.* ***(L)*** *Representative flow cytometry analysis showing the different distribution of CD45.1$^+$ WT and CD45.2$^+$ Bcl3$^{KO/KO}$ cells among all living cells (left) and pTregs isolated from small intestine lamina propria.* ***(M)*** *Quantification of the percentage of CD45.1$^+$ WT cells out of all CD45$^+$ cells, pre-gated on the indicated cell populations isolated from small intestine lamina propria and spleen. Each dot represents the respective cell compartment within an individual mouse. Mean ± SD from at least two independent experiments is shown. Rag1$^{KO/KO}$ mixed bone marrow recipients n≥11. Statistical analysis was performed using either a two-tailed student t-test and corrected for multiple comparisons using the Holm-Sidak method (B-G), one-way ANOVA corrected via Sidak (I), or two-way ANOVA corrected via Sidak (K). P value of <0.05 was considered statistically significant with * p <0.05, ** p < 0.01, *** p < 0.001, **** p < 0.0001, ns = not significant.*

In summary, these results indicate that Bcl3 regulates certain parts of Treg biology particularly the induction of RORyt$^+$ Tregs in a cell-intrinsic manner and not via affecting the local microenvironment or other immune cells.

3.2.7 Overlapping DEGs show signature of altered Bcl3 expression in Tregs

The previously presented bulkRNAseq data has emphasized the impact of different cellular subsets on the informative value of DEG and GSEA evaluation. As the emergence of tTreg signature genes within sorted RORyt$^+$ Tregs was presumably originating from DPTregs, it was decided to analyse the transcriptional profile at the single cell level. Hence, single cell RNA sequencing (scRNAseq) of CD4$^+$ T cells from small intestine lamina propria derived from the mixed bone marrow chimeras was performed (**Figure 14A, left**). Because the focus of this thesis was the changes within Tregs, the data was filtered for clusters with high *Foxp3* expression (Clusters 5, 6, 11 and 12) and the positive cells were then reclustered (**Figure 14A, right**). This resulted in seven new clusters representing distinct Treg subpopulations (**Figure 14B**). The transcriptional signatures of pTreg, tTreg and resting Tregs, previously acquired from steady state scRNAseq (**Figure 1F**), were utilized to calculate scores of each cell for the individual signatures (**Figure 14C**). Additionally, a heatmap showing the cluster defining genes was created to determine the

nature of the relevant cell clusters (**Figure 14D**). Thereby, Cluster0 and Cluster1 were labelled as pTregs (based on *Ccr2*, *Zfp36*, *Asb2*, *Ccr9,* and *Jun* expression) and Cluster2 and Cluster4 as tTregs (based on *Ikzf2*, *Cd83*, *Tnfrsf9,* and *Fam46a* expression). Cluster5 and Cluster6 were deemed to encompass an assortment of different cells experiencing stress (based on *Hsp90ab1, Hspa8,* and *Hspd1*) or clustering together because of an altered activation status (based on *Tnfsf8*, *Ccr7*, *Evl*, *S100a4* and *Tcf7* expression), respectively.

Further investigation of the impact Bcl3 deficiency has on the distribution of Treg subpopulations in scRNAseq data recreated the phenotype observed after *ex vivo* flow cytometry analysis of mixed bone marrow recipients (**Figure 13**) in the sequencing results: Loss of Bcl3 in Tregs produced more cells in pTreg clusters (Cluster0 and Cluster1) and fewer cells in tTreg clusters (Cluster2 and Cluster4) (**Figure 14E**). Moreover, Cluster3 occurred to be almost solely consisting of Tregs induced from Bcl3 deficient bone marrow. Considering the gene expression profile of this cluster (**Figure 14D**), it may be concluded that Cluster3 corresponds to DPTregs that exclusively appear in Bcl3 deficient Tregs. Notably, the Cluster3 defining genes contain genes involved in T cell activation (*Fosb* and *Furin*) and secretion of typical Th1 or Th17 cytokines (*Ifng*, *Il17a* and *Il22*) indicating an overall activated phenotype for DPTregs.

To additionally investigate the transcriptional signature of altered Bcl3 expression in Treg subclusters at the single cell level, the DEGs of Bcl3 deficient compared to Bcl3 sufficient Tregs were calculated within each of the tTreg and pTreg clusters. Thus, the influence of microenvironment and cellular composition on the calculated gene signature could be minimised. Afterwards, the DEGs from all four clusters were overlapped to discover 26 consistently upregulated and seven consistently downregulated genes encompassing the basic Bcl3-dependent genes across all tTreg and pTreg clusters (**Figure 14F**). Lastly, these overlapping DEGs were compared to the previously described bulkRNAseq DEGs by once more determining the overlap of DEGs. This comparison resulted in nine universally upregulated genes such as *Cd83*, *Bcl2l1,* and *Furin* and two genes that were downregulated in Bcl3 deficient Tregs throughout all assays (*Ctse* and *Nfkbid*) (**Figure 14G**).

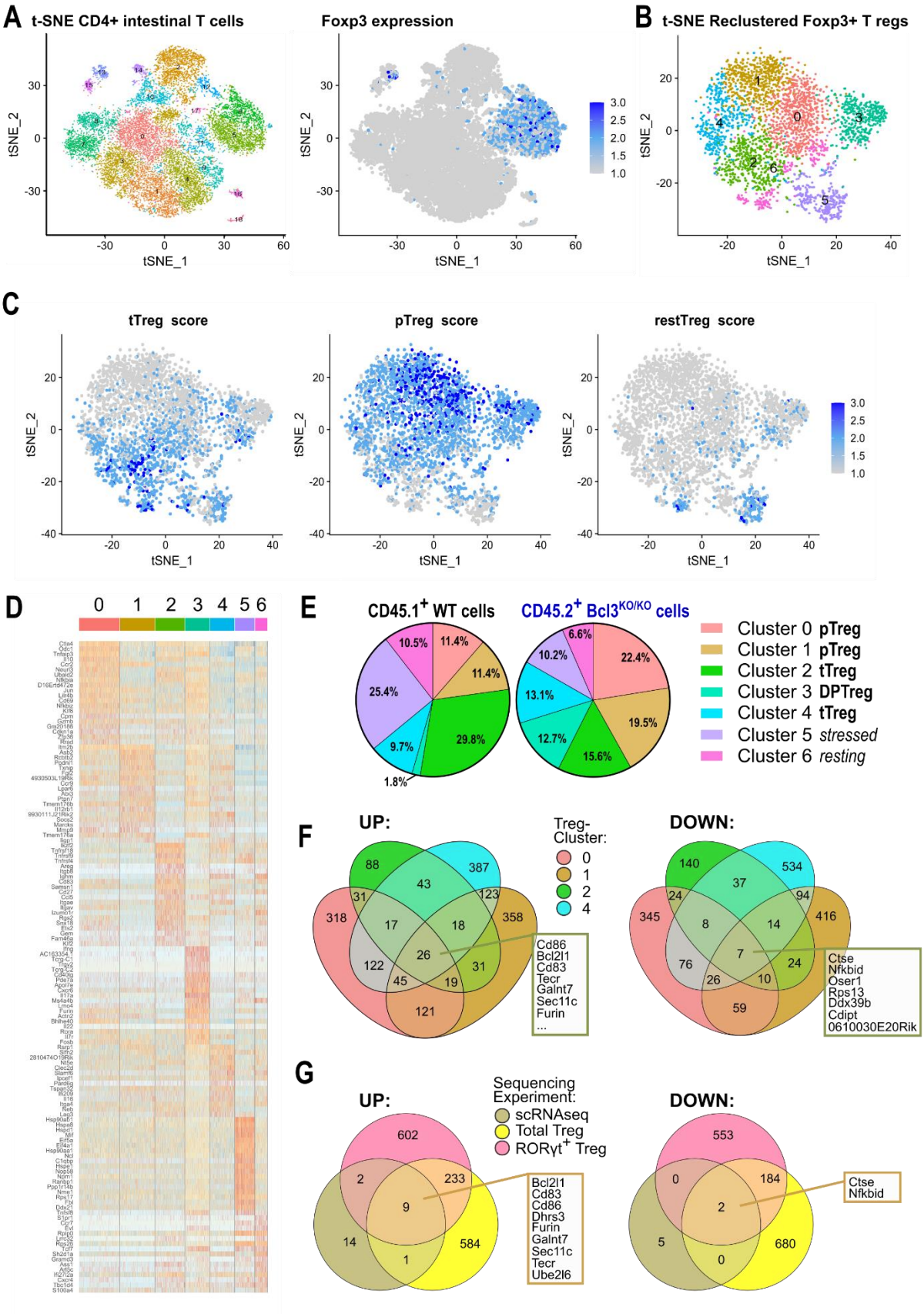

Figure 14: ***scRNAseq analysis reveals Bcl3 dependent signatures in Treg subsets.*** *scRNAseq of CD4⁺ T cells isolated from small intestine lamina propria of Rag1$^{KO/KO}$ mixed bone marrow chimeras shown in Fig.3.* ***(A)*** *tSNE dimensionality reduction of scRNAseq data from CD4⁺ T cells of three mixed bone marrow chimeras showing*

clustering (left) and Foxp3 expression (right). ***(B)*** *tSNE dimensionality reduction of reclustered cells from Foxp3 expressing clusters 5, 6, 11 and 12.* ***(C)*** *Treg subset definition according to predefined scores. tTreg (left) showing average expression of Nrp1, Ikzf2, Cd83, Il1rl1, Calca, Ccr8, Tnfrsf9, Ipmk, Nfkb1, Fam46a, Rel and Dusp10. pTreg score (middle) showing average expression of Rorc, Ltb4r1, Ccr2, Cxcr6, Zfp36, Asb2, Ccr9, Jun and Gimap1. restingTreg score (right) showing average expression of Ccr7, Satb1, Lef1, Tcf7, Evl, Klf2, Tnfsf11, Tnfsf8 and Xcl1.* ***(D)*** *Heatmap of the top 20 DEGs of each cluster shown in (B).* ***(E)*** *Distribution of Treg subclusters depending on all reclustered Foxp3^{+} cells separated by the origin of cells in mixed chimeras (CD45.1^{+} WT – left and CD45.2^{+} Bcl3$^{KO/KO}$ – right).* ***(F)*** *Overlapping DEGs comparing cells of WT and Bcl3$^{KO/KO}$ origin from the Treg subclusters 0, 1, 2 and 4.* ***(G)*** *Overlapping DEGs from different RNA sequencing experiments: bulk RNA sequencing analysis of total Tregs (yellow), bulk RNA sequencing analysis of RORyt expressing Tregs (pink) and shared DEGs from single cell clusters shown in (F) (brown). Shared upregulated genes – left, downregulated genes – right. Each column represents an individual cell use or average over all selected cells and n=3 mice. Statistical analysis was performed using the R package Seurat.*

Altogether, scRNAseq transcriptional analysis validated the impact of Bcl3 deficiency seen in the previous phenotypic description of individual Treg subsets and indicated an activated phenotype for the unusual RORyt^{+}Helios^{+} DPTregs together with multiple target gene candidates for the Bcl3 dependent regulation of Treg development.

3.2.8 Bcl3 dependent inhibition of CD83 is insufficient for the increase in RORyt^{+} Tregs

Included in the persistently upregulated genes in Bcl3 deficient Tregs was the immunoglobulin superfamily member *Cd83.* Although CD83 is most stably expressed on DCs, it has been shown to be expressed on various activated immune cells and play an important role in Treg stability and differentiation [182], [183]. Hence, the first aim was to confirm the Bcl3 dependent regulation of CD83 expression on the protein level. Isolated lymphocytes from the spleen, mesenteric lymph nodes, and small intestine lamina propria were therefore stained with an antibody specific for CD83 in addition to Treg subpopulation markers. Concomitant with the bulk and scRNAseq data, increased frequencies, and mean fluorescence intensity (MFI) of CD83 expression was measured on pTregs, tTregs, and DPTregs in all analysed organs of Bcl3 deficient animals (**Figure 15A - C**). Besides, the expression of CD83 was increased in tTregs as compared to pTregs irrespective of genotype (**Figure 15D** and **E**), approving the previously described tTreg signature gene list (**Figure 1F**). To further reinforce the claim of Bcl3 dependent regulation of CD83, the enhanced expression of CD83 in Tregs was approved in mice with a Treg specific loss of Bcl3 in comparison with littermate controls (**Figure 15F** and **G**).

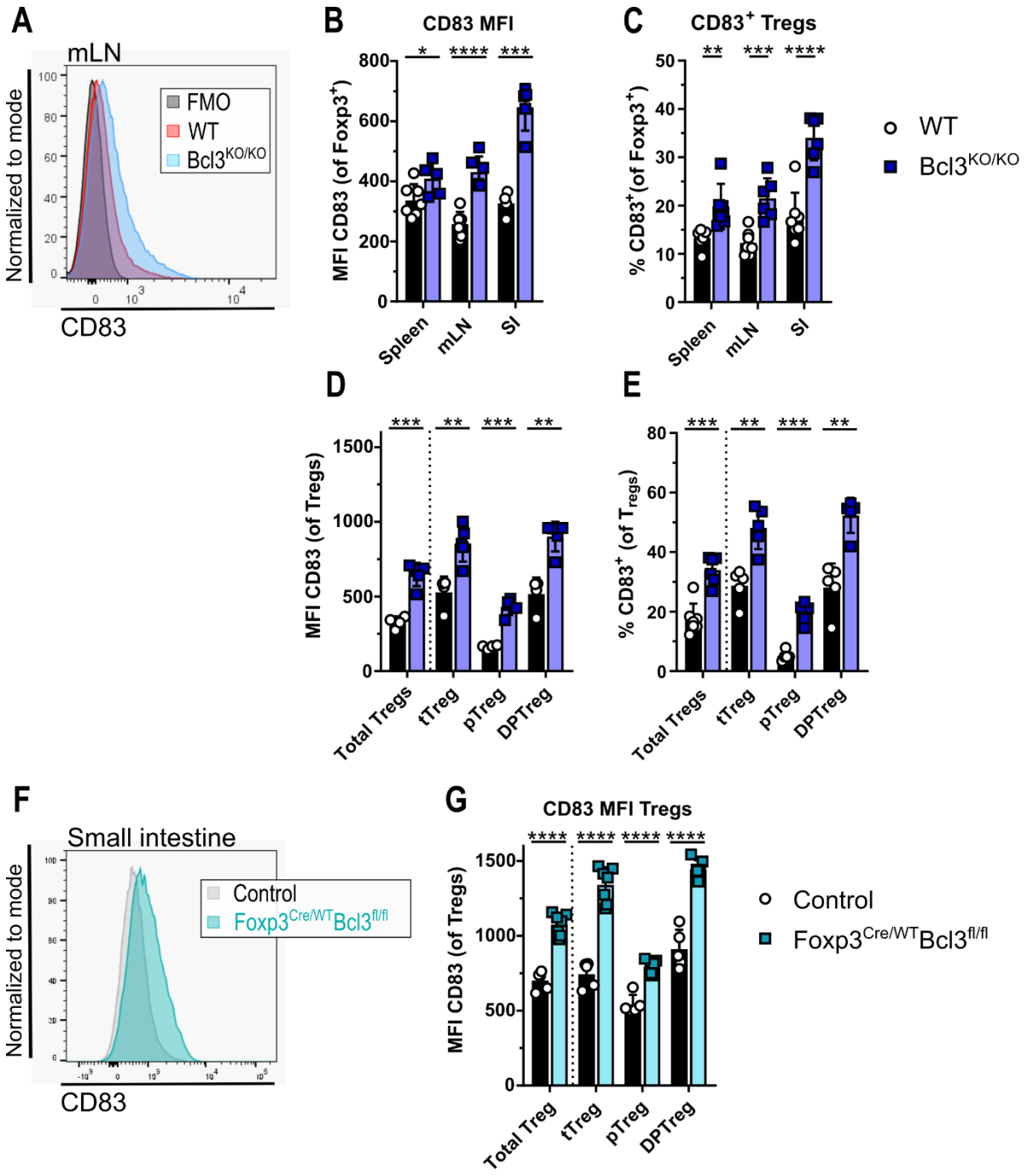

Figure 15: ***Bcl3 dependent suppression of CD83 expression can be confirmed on protein level. (A)*** *Representative flow cytometry histogram illustrating CD83 staining intensity on WT or Bcl3$^{KO/KO}$ regulatory T cells (CD4$^+$Foxp3$^+$) from mesenteric lymph nodes (mLN) and fluorescence minus one (FMO) control lacking the CD83 stain.* ***(B)*** *Quantification of the analysis presented in (A) showing mean fluorescence intensity (MFI) of CD83 staining on Tregs from the spleen, mLN and lamina propria of the small intestine (SI).* ***(C)*** *Percentage of CD83$^+$ cells among Foxp3$^+$ Tregs from spleen, mLN and SI of WT and Bcl3$^{KO/KO}$ mice. (D) MFI of CD83 staining on all Foxp3$^+$CD4$^+$ Tregs (total Tregs), RORγt$^-$Helios$^+$ tTregs, RORγt$^+$Helios$^-$ pTregs and RORγt$^+$Helios$^+$ DPTregs isolated from the lamina propria of the small intestine of WT or Bcl3$^{KO/KO}$ mice.* ***(E)*** *Percentage of CD83$^+$ cells among all Foxp3$^+$CD4$^+$ Tregs (total Tregs), tTregs, pTregs and DPTregs isolated from the SI of WT or Bcl3$^{KO/KO}$ mice.* ***(F)*** *Representative flow cytometry histogram depicting CD83 staining intensity on regulatory T cells from SI of Foxp3$^{Cre/WT}$Bcl3$^{fl/fl}$ conditional knockout and control mice.* ***(G)*** *Summary of data shown in (F). Each dot represents an individual mouse. Mean ± SD from at least two*

*independent experiments is shown. (A-E) WT n =7 mice and Bcl3$^{KO/KO}$ n=6 mice; (G) Control n=7 mice and Foxp3$^{Cre/WT}$Bcl3$^{fl/fl}$ n=7 mice. Statistical analysis was performed using a two-tailed student t-test corrected for multiple comparisons using the Holm-Sidak method. P value of <0.05 was considered statistically significant with * p <0.05, ** p < 0.01, *** p < 0.001, **** p < 0.0001, ns = not significant.*

Finally, the aim was to examine the potential impact of increased CD83 expression on the development of RORγt^{+} Treg populations. Bcl3 deficiency led to an increase in CD83 on transcription and protein level and inflated RORγt^{+} Treg populations. Therefore, loss of CD83 in Tregs was hypothesized to have an adverse influence on pTreg induction and hence cause diminished frequencies of RORγt^{+} Tregs. Thus, the abundance of Treg subsets was analysed in the spleen, mesenteric lymph nodes, and small intestine lamina propria of mice with a T cell specific deficiency of CD83 (CD4$^{Cre/WT}$CD83$^{fl/fl}$) and control animals. However, although Tregs of CD4$^{Cre/WT}$CD83$^{fl/fl}$ mice were, in fact, devoid of CD83 expression (**Figure 16A**), no decrease in overall Treg frequencies was measured (**Figure 16B** and **C**). Furthermore, there were no significant differences in pTreg and tTreg abundances or cell counts (**Figure 16D** - **F**).

In summary, these results indicate that Bcl3 indeed regulates the expression of CD83; yet the exclusive alteration of CD83 expression in CD4^{+} cells is inadequate to reproduce the drastic impact of Bcl3 on RORγt^{+} Treg induction.

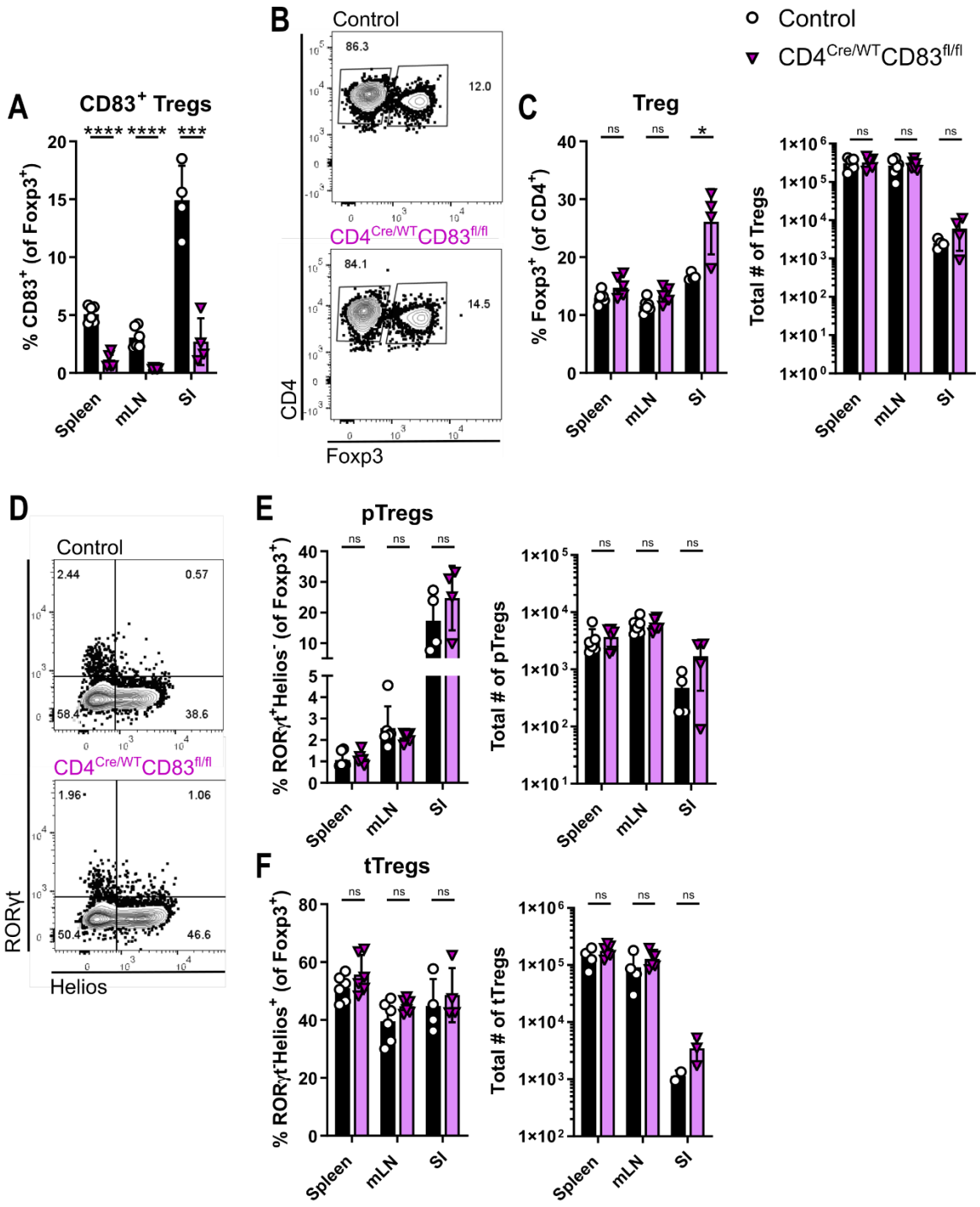

Figure 16: ***Bcl3 dependent suppression of CD83 expression is insufficient to account for the Treg intrinsic increase of RORγt expressing Tregs.*** *(A) Percentage of CD83⁺ cells among Foxp3⁺ Tregs from spleen, mLN and SI of CD4$^{Cre/WT}$CD83$^{fl/fl}$ and control mice. (B) Representative flow cytometry plots of Foxp3 expression among CD4⁺ T cells from mLN of CD4 specific conditional CD83 knockout (CD4$^{Cre/WT}$CD83$^{fl/fl}$) and control animals. (C) Percentages and total cell numbers of Tregs in indicated organs as shown in (B). (D) Representative flow cytometry plots for Helios and RORγt expression in pre-gated Foxp3⁺ T cells from mLN of CD4$^{Cre/WT}$CD83$^{fl/fl}$ and control animal. (E) Percentage (left) and total cell number (right) of RORγt⁺Helios⁻ pTregs from spleen, mLN and SI as shown in (D). (F) Percentage (left) and total cell number (right) of RORγt⁻Helios⁺ tTregs of Foxp3⁺ Tregs from spleen, mLN and SI as shown in (D). Each dot represents an individual mouse. Mean ± SD is shown. Control n=6 mice and CD4$^{Cre/WT}$CD83$^{fl/fl}$ n=6 mice. Statistical analysis was performed using a two-tailed student t-test and corrected for multiple comparisons using the Holm-Sidak method. P value of <0.05 was considered statistically significant with * p <0.05, ** p < 0.01, *** p < 0.001, **** p < 0.0001, ns = not significant.*

3.2.9 Summary

In short, it was demonstrated that loss of Bcl3 induces an expansion of pTregs and the development of an atypical RORγt^{+}Helios^{+} double positive (DPTreg) subset in a cell intrinsic manner. In a competitive setting of WT and KO bone marrow, Bcl3 deficient cells were biased towards the induction of intestinal pTregs and filled this niche almost exclusively, ousting WT cells. Furthermore, these inflated Tregs were superior in their potential to produce anti-inflammatory cytokines and at least as effective in an *in vivo* suppression assay as their Bcl3 competent counterpart. Although the data on Bcl3 dependent regulation of CD83 is convincing, it is not sufficient to cause the expansion of RORγt^{+} Tregs. Instead, altered responsiveness to IL-2 and IL-6 signalling in Bcl3 deficient Tregs, shown by GSEA of bulkRNAseq data poses as a promising mechanistic hypothesis.

4 DISCUSSION

The aim of this study was to gain further insight into the complex relations between commensal microbiota and the intestinal immune system, in particular RORγt$^+$ Tregs. The first step of this process was to analyse the impact of delayed or impaired colonisation with commensal microbes on the TCR repertoire of intestinal T cells and the severity of sensitisation towards dietary antigens. To that end, mice maturing with a disrupted microbiome, either under germfree conditions or receiving broad antibiotics, were utilized to expose the effect of impaired early colonisation on intestinal diversity and oral tolerance. In the second part of this study, the impact of the atypical IκB member Bcl3 on the development and functionality of intestinal Tregs was investigated to further unveil molecular mechanisms of intestinal tolerance.

4.1 DELAYED MICROBIAL COLONISATION IMPACTS INTESTINAL HOMEOSTASIS

RORγt expressing cells contribute to homeostasis and tolerance in the intestinal tract. While Th17 cells fight bacterial infections, Helios$^-$RORγt$^+$ pTregs establish active immune tolerance towards commensal microbes by controlling the activation of effector T cells [70], [71], [79]. As previously described, the scRNAseq data shown in this thesis demonstrate the importance of the NFκB pathway for the differentiation and maintenance of Tregs [133], [135]. T cell or Treg specific loss of the NFκB genes c-Rel (*Rel*) or RelA (*Rela*) diminishes the development of thymic Tregs and their functionality in the periphery [131]–[134]. However, the expression of an NFκB signature is drastically decreased in pTreg associated clusters. This finding poses as an important analytic tool, as the expression of NFκB related genes can be utilized in order to distinguish between pTregs and tTregs in the intestine on a transcriptional level. It can be furthermore concluded that negative regulation of the NFκB pathway may be involved in pTreg development, proposing the investigation of NFκB inhibitors as players in pTreg induction.

Concomitant with their differentiation in the periphery as a response to commensals, GF mice and ABX treated animals harbour reduced abundances of pTregs in their gut [71], [72]. Despite the fact that the capacity of intestinal Treg induction has been indicated to be maternally transmitted via IgA levels, inhibiting proper colonisation at the weaning stage three weeks after birth leads to dysregulated Treg populations and thereby predestines for inflammatory diseases [77], [94]. This discrepancy highlights that although pTregs can be induced in GF mice by microbial transplants, a critical window of opportunity exists to achieve a homeostatic setpoint [77].

4.1.1 Treg TCR diversity is decreased upon impaired microbial diversity early in life

Tregs generated in the thymus are selected based on their TCR affinity to self-antigens, whereas peripherally induced Tregs exit negative selection in the thymus as naive T cells due to differing TCR specificity. Consequently, pTregs and tTregs possess contrasting TCR repertoires [73]. Recolonised animals were used to evaluate the influence of manipulated microbiome early in life on TCR diversity in adults by co-housing ABX treated or GF mice with SPF control animals. As mice were colonised by cagemate microbiota at the age of six weeks, the critical window of opportunity was already closed [77]. Nevertheless, two weeks of co-housing were sufficient to amply colonise ex-ABX and ex-GF mice, measured by an increase in 16S rRNA alpha diversity. Similar frequencies of Th17 cells and pTregs were induced by the microbes, confirming the fact that distinct bacteria possess distinct RORγt$^+$ cell induction potential [71], [72]. Overshooting of Th17 cell abundance, especially in ex-ABX mice could be explained by excessive proliferation upon bacterial recognition. This is supported by a decrease in naïve CD4$^+$ T cell population size, as they differentiate upon cognate antigen detection.

Surprisingly, cellular distribution in ex-GF intestines differed drastically from ABX treated and undisturbed SPF specimens. Approximately 47% of all intestinal CD4$^+$ T cells in those mice produce granzyme A, granzyme B and granzyme K which are usually associated with CD8$^+$ cytotoxic T lymphocytes (CTL) [184]. Consistent with the scRNAseq data shown, CD4$^+$ granzyme secreting cells, also known as CD4$^+$ CTL, are transcriptionally closest to Th1 cells [185]. In correspondence to Th1 cells, CD4$^+$ CTL are essential for antiviral immunity by

killing virus infected cells [186]. A healthy microbiome consists not only of bacteria but also of non-bacterial microorganisms such as fungi and viruses [187]. This $CD4^+$ CTL population is greatly reduced in ex-ABX mice, where only bacteria were eradicated by the antibiotic cocktail but the virome should stay intact in contrast to ex GF mice where no viral strains are expected. It can, thus, be assumed that this population arises from viral colonisation upon co-housing. This hypothesis is supported by the routine detection of norovirus strains in the animal facility used for these experiments. Furthermore, these cells pose as a possible explanation for the accelerated inflammation in late-colonised animals, as $CD4^+$ CTL have been demonstrated to promote colitis [77], [188]. However, the exact impact of viral strains on intestinal homeostasis is yet to be analysed in depth.

To evaluate if population sizes change due to differentiation or proliferation, TCR diversity can be assessed, as the pure multiplication of a few clones drastically decreases the variety of TCRs. The presented data generally confirms the vastly superior TCR diversity of naïve T cells and resting Tregs presumably due to their inactive state and therefore low proliferative activity. Although Treg populations were equally represented in abundance among the three groups, a decreased Shannon index of Treg TCRs was observed in ex-ABX and ex-GF mice. This could be caused by newly induced Tregs proliferating and thereby more cells expressing the same TCR, decreasing the overall diversity. In Treg subpopulations this effect is only visible in tendency among pTregs and resting Tregs, supporting the claim that late induction of pTregs decreases their TCR diversity. In the literature decreased TCR diversity is most frequently associated with old age, chronic viral infections or poor prognosis in cancer [189], [190]. However, *Hong et al* demonstrated, that TCR diversity is also reduced in IBD patients supporting the importance of a diverse TCR repertoire for intestinal homeostasis [191]. A recent study of the connection between the TCR repertoire and the intestinal microbiome proposed that colonisation of germfree mice increases the TCR overlap of effector T cells and pTregs, and clonal expansion of T cells with a specificity for conserved structures, confirming the data presented in this thesis [192].

Hence, it can be concluded from this study that late intestinal colonisation outside of the aforementioned window of opportunity during weaning indeed influences intestinal

cellular composition and Treg TCR diversity. However, due to the high variance in the data and the limited number of analysed animals, further investigations need to be performed to pinpoint a significant effect on TCR diversity or confirm TCR overlap in Tregs and effector T cells as published for colitis patients [103]. Furthermore, it would be interesting to analyse intraepithelial lymphocyte (IEL) populations after late colonisation to determine if the relation between pTregs towards CD4-IELs is impacted by impaired early colonisation [193].

4.1.2 Early colonisation in food allergy

The intestinal frequency of pTregs is decreased in mice with diminished microbial complexity but can be rescued upon colonisation. However, these late-colonised animals possess an altered composition of intestinal $CD4^+$ cells and reduced Treg TCR diversity. To determine if primary colonisation at an early age influences oral tolerance persistently, mice were first co-housed for two weeks to enable equal colonisation and then sensitised against OVA via oral gavage for several weeks. Finally, they were challenged with OVA *i.v.* to induce a food allergic reaction. The severity of anaphylaxis was measured by a drop in body temperature. Although the reaction towards food allergy induction varied greatly, the data showed that the initial colonisation significantly influenced the outcome of food allergy. The hygiene hypothesis postulates that children encountering a higher bacterial load in their environment while growing up develop fewer cases of atopic diseases [111]. However, in this study SPF mice from in-house breeding, harbouring the least controlled microbiome, developed the most severe anaphylaxis while ex-GF mice developed notably milder allergic reactions.

Overall, the effect of food allergen sensitisation in GF mice is not consistent in the literature. While *Stefka et al.* indicated that GF mice develop a more severe allergy towards peanut allergen, *Schwarzer et al*. published that GF mice cannot be sensitised towards OVA in a food allergen model [175], [176]. A more recent study showed that GF mice equalled SPF mice in their anaphylactic reaction towards OVA but minimal colonisation with seven bacterial ASF strains decreased the loss in body temperature. The more complex the microbiome of analysed animals, the more acute the allergic reaction [75]. Interestingly, concurring with the data presented in this thesis, all studies reported

increased serum IgE levels in sensitised GF mice independent of challenge outcome, deeming its validity as a prognosis marker uncertain [75], [175], [176].

It remains questionable if this altered oral tolerance is implemented by an underdeveloped immune system incapable of a proper immune reaction in GF mice or other yet to be defined protective mechanisms.

It was repeatedly published that proper induction of pTregs is essential for intestinal tolerance towards dietary antigen [79], [118], [121]. The data presented in this study demonstrate that even though pTreg abundances were comparable among all groups after colonisation, the severity of food allergy varied significantly. Therefore, further studies are needed to determine which bacterial strains provide protection against food allergy in microbial transplantation studies, as pTreg induction by microbial diversity alone unduly simplifies this complex relationship. It must also be considered that these models are artificial and imperfect. Since a very strong immune response is triggered, the effects of the microbiome maybe masked. With further research, it may be possible to pinpoint a certain timepoint to admit specific beneficial bacterial cultures to provide protection from severe dietary allergies.

4.2 THE ROLE OF THE ATYPICAL IκB MEMBER BCL3 IN PTREG DEVELOPMENT

In this study, scRNAseq data of intestinal Tregs confirmed the importance of the NFκB pathway in controlling intestinal Treg survival and development by demonstrating distinctly lower expression of NFκB signature genes in pTregs compared to tTregs [135]. Despite their greatly beneficial potential in IBD therapy [106]–[108], only a few transcriptional regulators for the differentiation of this microbiota-induced Treg subset have been discovered: deletion of c-MAF has been shown to be detrimental to the development of RORγt^{+}Helios^{-} Tregs [70], [194] as was the NFκB member RelA [134]. However, it remains unclear if and how Treg intrinsic mechanisms control the expansion of intestinal pTregs. Surprisingly, global knockout and conditional knockout of the nuclear NFκB co-factor Bcl3 in Tregs result in an expansion of the well-known microbiome

induced RORγt^{+}Helios^{-} Treg subset, contrasting many other knockouts decreasing Treg functionality or survival [195].

In this thesis, direct evidence is provided to state that the atypical IκB protein Bcl3 plays a major role in determining Treg intrinsic regulation for the development of Foxp3^{+} Tregs and especially for RORγt^{+} Treg subsets.

4.2.1 Increased RORγt^{+} Treg frequencies upon loss of Bcl3

In contrast to other NFκB proteins such as RelA, Bcl3 lacks a Rel homology domain to directly bind DNA to affect transcription, like all other IκB family members. Bcl3 exerts its effect on RORγt^{+} Treg subsets via interfering or supporting the binding of p50 or p52 dimers to consensus κB binding sequences in the DNA or via yet-to-be-discovered interactions with other pathways [138], [196], [197]. Increased abundances of pTregs could be confirmed in both total and Treg-specific knockout of Bcl3 and additionally in mixed bone marrow chimeras. Surprisingly, a RORγt^{+}Helios^{+} Treg subset occurred in the absence of Bcl3 in all analysed models. This unusual double positive subset of Tregs is normally absent in healthy mice on the C57BL/6 background. Presumably due to the distinct differentiation of pTregs in the periphery, RORγt is usually exclusively expressed on Helios^{-} Tregs.

In addition to total Bcl3 knockout animals, expanded populations of both RORγt^{+} Treg subsets were also found in Treg specific Bcl3 deficient mice and mixed bone marrow chimeras. Therefore, this data indicates a Treg intrinsic effect of Bcl3 on pTreg and DPTreg development, excluding possible bystander effects of Bcl3 deficiency e.g., in dendritic cells for the described Treg phenotype [157]. This data is especially interesting, as there are only very few reports of inflated instead of decreased Treg populations. But it remains to be determined if Bcl3 also affects other specialised Treg populations such as muscle Tregs involved in injury repair [61].

4.2.2 RORγt^{+}Helios^{+} Tregs stem from thymically derived Tregs

The nature of the newly induced atypical RORγt^{+}Helios^{+} Treg subset (DPTreg) remained to be further characterised. Although this Treg subset has previously been noted under conditions of immune dysregulation, it was never analysed in depth. For example, similar

upregulation of RORγt expression in Helios$^+$ Tregs was found in IL-2 deficient animals developing an autoimmune syndrome (unpublished results) or in mice with a dendritic cell deficiency displaying an autoimmune myeloproliferative disorder [198] suggesting a role for this Treg subset in autoimmunity. Additionally, deficiency of STAT3 specifically in Tregs increased the abundance of RORγt$^+$Helios$^+$ Tregs [71] indicating that improper STAT3 signalling or a highly inflamed environment are favourable circumstances for the initiation of RORγt expression in Helios$^+$ tTregs. Previously, STAT3 signalling was reported to be associated with Bcl3 expression in cancer patients [199], [200] and a STAT3 dependent Bcl3 upregulation in a virus infection could be demonstrated [153], reinforcing the assumption that this interaction is also essential for proper Treg homeostasis.

Concomitant with the involvement of STAT3 in IL-6 signalling, the differentiation of pTregs is supported in the presence of IL-6 [71] and tTregs were published to be capable of RORγt expression under highly inflammatory conditions created by elevated IL-6 levels [201]. These previously published data suggest a role of RORγt$^+$Helios$^+$ Tregs in inflammatory conditions. As the colonisation of germfree and ABX treated mice induced large abundances of pTregs but not DPTregs it can be assumed that their differentiation is independent of the intestinal microbiota.

A great extent of DPTregs was generated upon co-transfer of splenic Tregs devoid of Bcl3 in a T cell transfer colitis model, as a model for an *in vivo* Treg suppression assay. However, as mice receiving Bcl3 deficient Tregs and thereby developing large amounts of DPTregs were completely protected from harsh colitis symptoms, it can be concluded that DPTregs do not possess a purely inflammatory nature. Furthermore, as splenic Tregs were used in the transfer, the vast majority of transplanted cells initially expressed Helios but were negative for RORγt expression. Although Helios expression was retained in all transferred Tregs after protecting from colitis, only Bcl3 deficient Tregs initiated RORγt expression. This data on the one hand suggests that DPTregs originate from Helios expressing tTregs upregulating RORγt and not from pTregs. On the other hand, the results indicate that Bcl3 suppresses this differentiation at steady state.

Transcriptional data derived from scRNAseq analysis of DPTregs revealed signatures associated with IFNγ and IL-17 production, corresponding to elevated IL-17 production in

these Tregs after *in vitro* restimulation. However, Bcl3 deficient Tregs were at least as efficient in protecting from colitis as their WT counterparts. Hence, the increased abundance of RORγt^{+}Helios^{+} Tregs in the periphery may be interpreted as a consequence of a pro-inflammatory environment that is normally suppressed by Bcl3 and possibly by IL-6/STAT3 signalling.

4.2.3 Decreased stability of Tregs upon Bcl3 deficiency

Strong pro-inflammatory conditions have been demonstrated to promote a trans-differentiation of Tregs favouring a Th17-like phenotype that might even contribute to disease pathology under certain circumstances [43]. During this study, it was noted that although more Bcl3 deficient Tregs produced the anti-inflammatory cytokines IL-10 and TGFβ while also displaying unimpaired suppressive capacity in a T cell transfer colitis model, a considerable percentage of Bcl3 deficient Tregs lost the expression of the lineage defining transcription factor Foxp3 after co-transfer. Instead, those ex-Tregs upregulated RORγt expression and thereby adopted a Th17-like phenotype. This bias of Bcl3$^{KO/KO}$ Tregs towards the Th17 cell fate was in fact previously reported [179] and was also observed by increased Th17 cell abundances in intestinal lamina propria of Bcl3 deficient mice in this thesis.

Surprisingly, this bias was additionally found in Treg transplant recipients and mice with a Treg specific knockout of Bcl3, indicating that these inflated Th17 cell populations might be originating from ex-Tregs undergoing trans-differentiation.

One possible hypothesis for this phenotype could be a Bcl3 dependent upregulation of RORγt in all CD4^{+} T cell subsets, theoretically resulting in more pTregs, Th17 cells and DPTregs. However, as mice with a Treg specific Bcl3 deficiency and Treg transfer recipients, also displayed increased frequencies of Th17 cells, this hypothesis can be disputed. It can therefore be assumed that Bcl3 likely poses as a regulator to inhibit trans-differentiation of Tregs in favour of Th17-like cells. It would be interesting to explore the methylation of the conserved TSDR (Treg-specific demethylated region) in Bcl3 deficient Tregs at steady state or during inflammation. Thereby, one could determine if the decreased stability of Foxp3 expression is a result of a less demethylated TSDR [44].

4.2.4 Bcl3 regulates cytokine sensitivity

Nonetheless, the mechanism behind the effect of Bcl3 on the differentiation of T helper cells remained undetermined. As previously stated, Bcl3 does not possess a DNA binding domain and therefore can only regulate the transcriptional response to external signals by aiding or inhibiting other members of the NFκB family. RNA sequencing data from Bcl3 deficient and control Tregs was compared in order to address this mechanism. To narrow down potential pathways and create a target gene list with minimal bias, overlapping Bcl3-dependent DEGs were calculated from three independent experiments, incorporating transcriptomic data from bulk and single cell RNA sequencing.

On the one hand, the resulting gene list includes several genes that play a role in signal peptide processing (*Sec11c*) and metabolic pathway regulation (*Dhrs3*, *Galnt7, Tecr,* and *Ubel6*). On the other hand, several of the Bcl3 regulated signature genes have been implicated to be involved in Treg functionality and differentiation. The DEGs *Bcl2l1* and *Furin* have been published to aid in Treg survival and function and to be upregulated upon Treg activation [202]–[205]. Concomitant with these results and the expansion and overall activated phenotype, both *Furin* and *Bcl2l1* were upregulated in Bcl3 deficient Tregs. Although *Nfkbid* (IκBNS) and *Ctse* (Cathepsin E) are suggested to play a role in Treg precursor development [206] and IL-10/IL-35 independent suppression mechanisms of Tregs [207], they were downregulated upon Bcl3 deficiency in Tregs. Additionally, it was shown that IκBNS supports *de novo* development of Th17 cells [208], [209], indicating that inflated Th17 cell populations documented in mice with Bcl3 deficient Tregs indeed originated from transdifferentiated Tregs rather than *de novo* differentiated Th17 cells or uncontrolled Th17 cell proliferation due to Bcl3 deficient dysfunctional Tregs. However, it remains to be determined if reduced IκBNS expression may result in the decreased stability observed in Bcl3 deficient Tregs.

Furthermore, CCR9 the chemokine receptor responsible for gut-homing is upregulated in Bcl3 deficient Tregs [210]. Regarding the fact that CCR9 deficient mice were shown to develop inflated Treg populations, contradicting the effect seen in Bcl3 deficient mice it is unlikely to contribute to the elevated Treg populations [211]. Although $CCR9^{KO/KO}$ mice are more susceptible to induced colitis [212] and CCR9 expression is elevated in small

bowel Crohn's patients, CCR9-blockers were so far trialled unsuccessfully for the therapy of IBD [213], indicating a more complex involvement of CCR9 in colitis. However, increased expression of CCR9 poses a possible explanation for the altered distribution of bone marrow cells lacking Bcl3 in a mixed chimeric environment, as those cells were drastically biased towards engraftment in the peripheral intestinal organs. Therefore, it can be assumed that altered CCR9 expression explains that the strongest effect of Bcl3 deficiency is seen in the intestines, but it is unlikely to directly influence pTreg development.

Since loss of CD83 expression in Tregs impairs their stability and differentiation and leads to a more pro-inflammatory phenotype [182], it can be hypothesised that Bcl3 dependent suppression of CD83 contributes to increased Treg frequencies in Bcl3 deficient mice. Although enhanced CD83 expression in $Bcl3^{KO/KO}$ cells could be confirmed on RNA and protein level, $CD4^{+}$ T cell specific CD83 deficiency surprisingly did not impair the development of pTregs. Therefore, increased CD83 expression is presumably not the sole source of the extensive impact Bcl3 deficiency exerts on Tregs.

Nevertheless, next to *Cd83* several other genes known to be involved in IL-2 signalling (*Bcl2l1*, *Cd86*, *Dhrs3*, and *Furin*) were found to be universally upregulated in Bcl3 deficient Tregs. Consistent with a suspected altered cytokine responsiveness, gene set enrichment analysis approved the increased implementation of IL-6/STAT3 and IL2/STAT5 signalling in Bcl3 deficient pTregs and decreased TNFα signalling. Considering that TNFα signalling is reportedly necessary to prohibit methylation of the Foxp3 region and thereby retain the phenotypic stability of Tregs [214], these results are consistent with the previously mentioned reduced Treg stability upon loss of Bcl3. In addition to that, decreased IL6/STAT3 signalling has been published to impair Foxp3 expression stability in tTregs [215]. IL-2/STAT5 and IL-6/STAT3 are furthermore crucial for an undisturbed differentiation of tTregs [45], [216] and the development of pTregs [71], again indicating that Bcl3 deficiency in Tregs destabilizes Foxp3 expression and creates a developmental bias towards pTreg differentiation via altered cytokine sensitivity.

Given the governing role STAT3 signalling can play in IBD [217], it remains to be determined whether Bcl3 as a target of small molecule inhibitors [218] could be suitable for the therapy of IBD patients.

4.3 Conclusion

In summary, the data presented in this thesis underline the importance of an undisturbed early intestinal microbiome for the development of healthy and diverse Treg populations. Disturbance of the microbial diversity early in life decreases the intestinal TCR diversity and acutely impacts the outcome of food allergy as summarised in **Figure 17**. The exact timing and microbial strains of providing protection from oral sensitisation require further investigation.

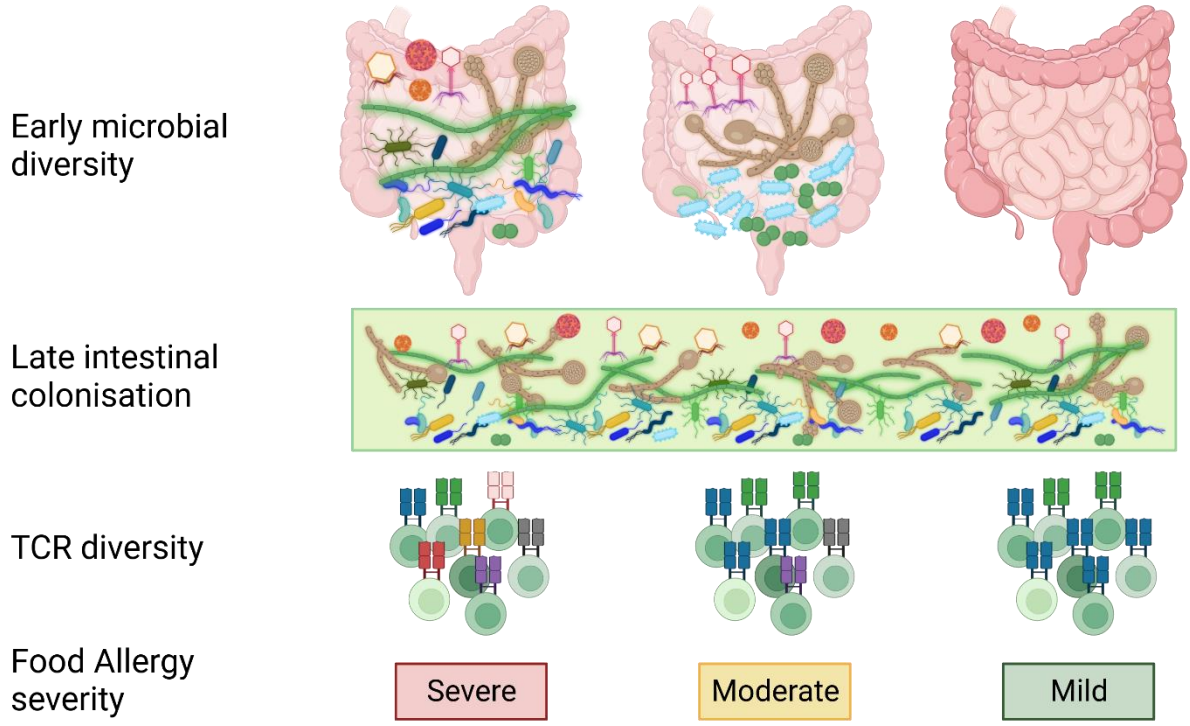

*Figure 17: **The impact of reduced microbial complexity early in life.** If intestinal colonisation is disturbed at a young age, the TCR diversity of intestinal T cells is impaired even after late colonisation with a fully diverse microbiome. The impact on the outcome of food allergen sensitisation is not directly proportionate to early microbial complexity. Created with BioRender.com*

Furthermore, evidence was provided that Bcl3 inhibits the differentiation of pTregs in a T cell-intrinsic manner. Bcl3 deficiency enabled the development of an uncommon intestinal Treg population co-expressing the usually exclusive transcription factors Helios and RORγt. Upon loss of Bcl3, inflated RORγt^{+} Treg populations produced high levels of the anti-inflammatory cytokines IL-10 and TGFβ and presented an overall activated

phenotype. Regardless of an internal bias to trans-differentiate towards Th17-like cells, Bcl3 deficient Tregs were perfectly efficient in suppressing effector T cells in a transfer colitis model. Sequencing data of pTregs revealed a Bcl3-dependent gene signature exposing altered cytokine responsiveness towards IL-2, IL-6 and TNFα. Therefore, it can be concluded that Bcl3 acts as a molecular regulator dampening the development of intestinal Treg subsets as presented in **Figure 18.** Bcl3 may thereby be investigated as a therapeutic target candidate to regain intestinal immune tolerance in IBD patients.

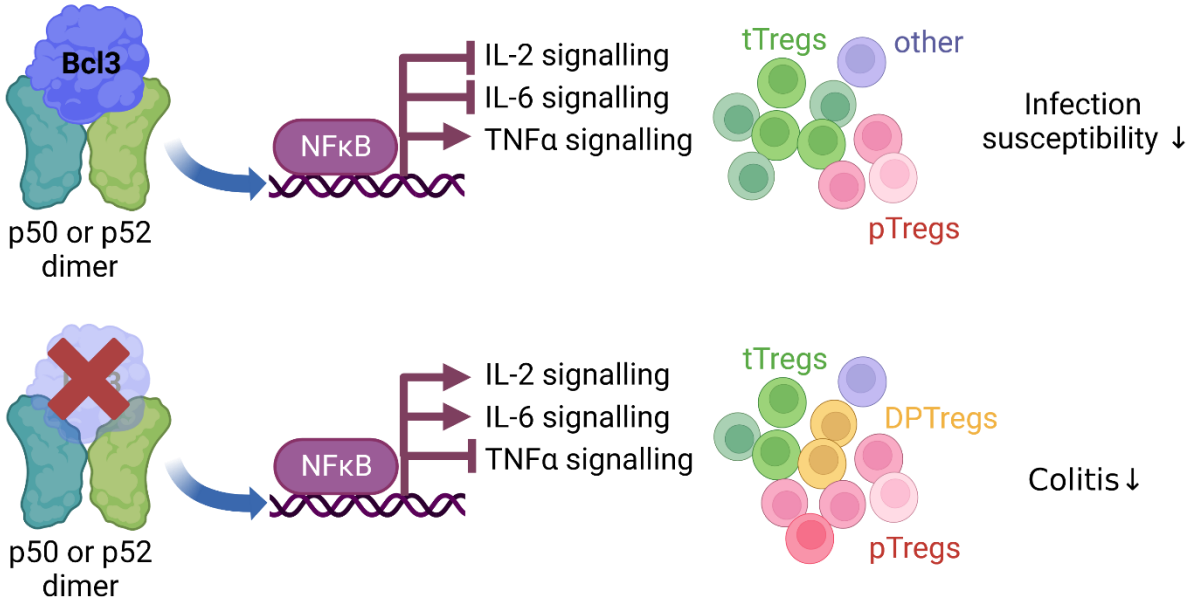

Figure 18: ***Scheme depicting the mechanistic hypothesis for Bcl3 regulated intestinal Treg induction****. Bcl3 is proposed to be involved in NFκB dependent expression of genes, leading to elevated TNFα signalling and homeostatic development of pTregs and tTregs. In Bcl3 deficient cells, TNFα signalling is reduced in favour of IL-6 and IL-2 signalling leading to inflated pTreg populations and the differentiation of DPTregs. This shifted equilibrium leads to a decreased risk of colitis but elevated infection susceptibility. Created with BioRender.com*

As NFκB related genes were significantly higher expressed in tTregs ad compared to pTregs, it remains to be determined how other IκB members influence the differentiation of Tregs. Especially *Nfkbid* is a promising candidate, as it is continuously downregulated upon loss of Bcl3.

ACKNOWLEDGEMENTS

Caspar Ohnmacht

Thank you for your supervision and for giving me this opportunity. For allowing me to develop my own approaches and for trusting me in my decisions, but still always having an open door. Thank you for giving me guidance or freedom depending on what I needed at the time. This work and I have both benefited greatly from your input.

Michael Schloter / Dirk Busch

Thank you for your mentoring, support and professional advice as active members of my thesis committee.

Nadine Hövelmeyer and her whole group

Thank you for your scientific input, for lively discussions and your excellent experimental expertise.

Daphne del Carmen Kolland / Anna-Lena Geiselhöringer

I am forever grateful for your experimental assistance and your incredible scientific expertise. Thank you for letting me borrow a brain if needed and for always having an open ear during the toughest times. I could not have done this without your help.

Ann-Marie Maier, Anela Arifovic, Luisa Kreft, Maria Szente-Pasztoi, Karsten Huth, Wenjing Chen, Cristina Körber and all other companions within the AG Ohnmacht

Thank you so much for helping me with my experiments, for great scientific discussions, and most importantly for your mental support. Thank you for being amazing colleagues.

Carsten Schmidt-Weber, Benjamin Schnautz, Johanna Grosch, Johannes Grosch, Sonja Heine and all other IAF/ZAUM members.

Thank you for your laboratory and organizational assistance, for your scientific expertise, and for your time.

My friends and family: Marilena Uhl, Nina Fischer, Gerlinde Köhler and Lisa Köhler

Thank you for your support and understanding, and for providing distraction whenever necessary.

Maximilian Wurzer

Thank you so much for always giving me backup, be it on a professional or non-professional level. Thank you for your infinite patience, for supporting me so fiercely, and for literally picking me up off the floor.

LIST OF FIGURES

LIST OF TABLES

LITERATURE

[1] A. Köhler *et al.*, "The atypical IκB family member Bcl3 determines differentiation and fate of intestinal RORγt+ regulatory T cell subsets.," *Mucosal Immunol.*, 2024.

[2] K. Murphy and C. Weaver, *Janeway Immunologie*, 9th editio. Berlin, Heidelberg: Springer Berlin Heidelberg, 2018.

[3] B. Beutler, "Innate immunity: An overview," *Mol. Immunol.*, vol. 40, no. 12, pp. 845–859, 2004, doi: 10.1016/j.molimm.2003.10.005.

[4] P. J. Murray and T. A. Wynn, "Protective and pathogenic functions of macrophage subsets," *Nat. Rev. Immunol.*, vol. 11, no. 11, pp. 723–737, Nov. 2011, doi: 10.1038/nri3073.

[5] Y. Xing, S. C. Jameson, and K. A. Hogquist, "Thymoproteasome subunit-β5T generates peptide-MHC complexes specialized for positive selection," *Proc. Natl. Acad. Sci. U. S. A.*, vol. 110, no. 17, pp. 6979–6984, 2013, doi: 10.1073/pnas.1222244110.

[6] M. S. Anderson *et al.*, "Projection of an immunological self shadow within the thymus by the aire protein," *Science (80-.).*, vol. 298, no. 5597, pp. 1395–1401, 2002, doi: 10.1126/science.1075958.

[7] J. Derbinski, A. Schulte, B. Kyewski, and L. Klein, "Promiscuous gene expression in medullary thymic epithelial cells mirrors the peripheral self," *J. Immunol.*, vol. 196, no. 7, pp. 2915–2922, 2016, doi: 10.1038/ni723.

[8] J. Aaltonen *et al.*, "An autoimmune disease, APECED, caused by mutations in a novel gene featuring two PHD-type zinc-finger domains," *Nat. Genet.*, vol. 17, no. 4, pp. 399–403, Dec. 1997, doi: 10.1038/ng1297-399.

[9] F. A. Harding, J. G. McArthur, J. A. Gross, D. H. Raulet, and J. P. Allison, "CD28-mediated signalling co-stimulates murine T cells and prevents induction of anergy in T-cell clones," *Nature*, vol. 356, no. 6370, pp. 607–609, Apr. 1992, doi: 10.1038/356607a0.

[10] J. Zhu, H. Yamane, and W. E. Paul, "Differentiation of effector CD4+ T cell populations," *Annu. Rev. Immunol.*, vol. 28, no. 1, pp. 445–489, 2010, doi: 10.1146/annurev-immunol-030409-101212.

[11] R. L. Coffman and J. Carty, "A T cell activity that enhances polyclonal IgE production and its inhibition by interferon-gamma.," *J. Immunol.*, vol. 136, no. 3, pp. 949–54, Feb. 1986, [Online]. Available: http://www.ncbi.nlm.nih.gov/pubmed/2934482.

[12] T. R. Mosmann, H. Cherwinski, M. W. Bond, M. A. Giedlin, and R. L. Coffman, "Two types of murine helper T cell clone. I. Definition according to profiles of lymphokine activities and secreted proteins.," *J. Immunol.*, vol. 136, no. 7, pp. 2348–57, Apr. 1986, [Online]. Available: http://www.ncbi.nlm.nih.gov/pubmed/2419430.

[13] S. J. Szabo, S. T. Kim, G. L. Costa, X. Zhang, C. G. Fathman, and L. H. Glimcher, "A

novel transcription factor, T-bet, directs Th1 lineage commitment," *Cell*, vol. 100, no. 6, pp. 655–669, 2000, doi: 10.1016/S0092-8674(00)80702-3.

[14] S. E. Macatonia *et al.*, "Dendritic cells produce IL-12 and direct the development of Th1 cells from naive CD4+ T cells.," *J. Immunol.*, vol. 154, no. 10, pp. 5071–9, May 1995, [Online]. Available: http://www.ncbi.nlm.nih.gov/pubmed/7730613.

[15] F. Powrie, M. W. Leach, S. Mauze, S. Menon, L. B. Caddle, and R. L. Coffman, "Inhibition of Th1 responses prevents inflammatory bowel disease in scid mice reconstituted with CD45RBhi CD4+ T cells.," *Immunity*, vol. 1, no. 7, pp. 553–62, Oct. 1994, doi: 10.1016/1074-7613(94)90045-0.

[16] Y. Cong *et al.*, "CD4+ T cells reactive to enteric bacterial antigens in spontaneously colitic C3H/HeJBir mice: increased T helper cell type 1 response and ability to transfer disease.," *J. Exp. Med.*, vol. 187, no. 6, pp. 855–64, Mar. 1998, doi: 10.1084/jem.187.6.855.

[17] C. Ohnmacht, C. Schwartz, M. Panzer, I. Schiedewitz, R. Naumann, and D. Voehringer, "Basophils Orchestrate Chronic Allergic Dermatitis and Protective Immunity against Helminths," *Immunity*, vol. 33, no. 3, pp. 364–374, 2010, doi: 10.1016/j.immuni.2010.08.011.

[18] W. E. Paul and J. Zhu, "How are T(H)2-type immune responses initiated and amplified?," *Nat. Rev. Immunol.*, vol. 10, no. 4, pp. 225–35, Apr. 2010, doi: 10.1038/nri2735.

[19] W. Zheng and R. A. Flavell, "The transcription factor GATA-3 is necessary and sufficient for Th2 cytokine gene expression in CD4 T cells.," *Cell*, vol. 89, no. 4, pp. 587–96, May 1997, doi: 10.1016/s0092-8674(00)80240-8.

[20] J. Zhu *et al.*, "Conditional deletion of Gata3 shows its essential function in TH1-TH2 responses," *Nat. Immunol.*, vol. 5, no. 11, pp. 1157–1165, 2004, doi: 10.1038/ni1128.

[21] N. Murakami-Satsutani *et al.*, "IL-33 promotes the induction and maintenance of Th2 immune responses by Enhancing the function of OX40 ligand," *Allergol. Int.*, vol. 63, no. 3, pp. 443–455, 2014, doi: 10.2332/allergolint.13-OA-0672.

[22] M. Michelet, B. Balbino, L. Guilleminault, and L. L. Reber, "IgE in the pathophysiology and therapy of food allergy," *Eur. J. Immunol.*, vol. 51, no. 3, pp. 531–543, 2021, doi: 10.1002/eji.202048833.

[23] L. E. Harrington *et al.*, "Interleukin 17-producing CD4+ effector T cells develop via a lineage distinct from the T helper type 1 and 2 lineages.," *Nat. Immunol.*, vol. 6, no. 11, pp. 1123–32, Nov. 2005, doi: 10.1038/ni1254.

[24] H. Park *et al.*, "A distinct lineage of CD4 T cells regulates tissue inflammation by producing interleukin 17.," *Nat. Immunol.*, vol. 6, no. 11, pp. 1133–41, Nov. 2005, doi: 10.1038/ni1261.

[25] I. I. Ivanov *et al.*, "The Orphan Nuclear Receptor RORγt Directs the Differentiation Program of Proinflammatory IL-17+ T Helper Cells," *Cell*, vol. 126, no. 6, pp. 1121–1133, 2006, doi: 10.1016/j.cell.2006.07.035.

[26] F. Y. Yue, A. Merchant, C. M. Kovacs, M. Loutfy, D. Persad, and M. A. Ostrowski, "Virus-Specific Interleukin-17-Producing CD4 + T Cells Are Detectable in Early Human Immunodeficiency Virus Type 1 Infection," *J. Virol.*, vol. 82, no. 13, pp. 6767–6771, 2008, doi: 10.1128/jvi.02550-07.

[27] K. I. Happel *et al.*, "Divergent roles of IL-23 and IL-12 in host defense against Klebsiella pneumoniae.," *J. Exp. Med.*, vol. 202, no. 6, pp. 761–9, Sep. 2005, doi: 10.1084/jem.20050193.

[28] H. R. Conti *et al.*, "Th17 cells and IL-17 receptor signaling are essential for mucosal host defense against oral candidiasis," *J. Exp. Med.*, vol. 206, no. 2, pp. 299–311, 2009, doi: 10.1084/jem.20081463.

[29] I. I. Ivanov *et al.*, "Induction of intestinal Th17 cells by segmented filamentous bacteria.," *Cell*, vol. 139, no. 3, pp. 485–98, Oct. 2009, doi: 10.1016/j.cell.2009.09.033.

[30] S. Crotty, "Follicular helper CD4 T cells (TFH).," *Annu. Rev. Immunol.*, vol. 29, pp. 621–63, 2011, doi: 10.1146/annurev-immunol-031210-101400.

[31] R. I. Nurieva *et al.*, "Generation of T follicular helper cells is mediated by interleukin-21 but independent of T helper 1, 2, or 17 cell lineages.," *Immunity*, vol. 29, no. 1, pp. 138–49, Jul. 2008, doi: 10.1016/j.immuni.2008.05.009.

[32] R. J. Johnston *et al.*, "Bcl6 and Blimp-1 are reciprocal and antagonistic regulators of T follicular helper cell differentiation.," *Science*, vol. 325, no. 5943, pp. 1006–10, Aug. 2009, doi: 10.1126/science.1175870.

[33] R. I. Nurieva *et al.*, "Bcl6 mediates the development of T follicular helper cells.," *Science*, vol. 325, no. 5943, pp. 1001–5, Aug. 2009, doi: 10.1126/science.1176676.

[34] G. Martins and K. Calame, "Regulation and functions of Blimp-1 in T and B lymphocytes.," *Annu. Rev. Immunol.*, vol. 26, pp. 133–69, 2008, doi: 10.1146/annurev.immunol.26.021607.090241.

[35] S. Sakaguchi, N. Mikami, J. B. Wing, A. Tanaka, K. Ichiyama, and N. Ohkura, "Regulatory T Cells and Human Disease," *Annu. Rev. Immunol.*, vol. 38, pp. 541–566, 2020, doi: 10.1146/annurev-immunol-042718-041717.

[36] G. L. Stritesky *et al.*, "Murine thymic selection quantified using a unique method to capture deleted T cells," *Proc. Natl. Acad. Sci. U. S. A.*, vol. 110, no. 12, pp. 4679–4684, 2013, doi: 10.1073/pnas.1217532110.

[37] C. S. Hsieh, H. M. Lee, and C. W. J. Lio, "Selection of regulatory T cells in the thymus," *Nat. Rev. Immunol.*, vol. 12, no. 3, pp. 157–167, 2012, doi: 10.1038/nri3155.

[38] J. D. Fontenot, M. A. Gavin, and A. Y. Rudensky, "Foxp3 programs the development and function of CD4+CD25+ regulatory T cells.," *Nat. Immunol.*, vol. 4, no. 4, pp. 330–6, Apr. 2003, doi: 10.1038/ni904.

[39] S. Hori, T. Nomura, and S. Sakaguchi, "Control of regulatory T cell development by the transcription factor Foxp3," *J. Immunol.*, vol. 198, no. 3, pp. 981–985, 2017, doi: 10.1126/science.1079490.

[40] M. E. Brunkow *et al.*, “Disruption of a new forkhead/winged-helix protein, scurfin, results in the fatal lymphoproliferative disorder of the scurfy mouse,” *Nat. Genet.*, vol. 27, no. 1, pp. 68–73, 2001, doi: 10.1038/83784.

[41] C. L. Bennett *et al.*, “The immune dysregulation, polyendocrinopathy, enteropathy, X-linked syndrome (IPEX) is caused by mutations of FOXP3,” *Nat. Genet.*, vol. 27, no. 1, pp. 20–21, 2001, doi: 10.1038/83713.

[42] C. L. Bennett *et al.*, “A rare polyadenylation signal mutation of the FOXP3 gene (AAUAAA-->AAUGAA) leads to the IPEX syndrome.,” *Immunogenetics*, vol. 53, no. 6, pp. 435–9, Aug. 2001, doi: 10.1007/s002510100358.

[43] N. Komatsu *et al.*, “Pathogenic conversion of Foxp3+ T cells into TH17 cells in autoimmune arthritis.,” *Nat. Med.*, vol. 20, no. 1, pp. 62–8, Jan. 2014, doi: 10.1038/nm.3432.

[44] S. Floess *et al.*, “Epigenetic control of the foxp3 locus in regulatory T cells,” *PLoS Biol.*, vol. 5, no. 2, pp. 0169–0178, 2007, doi: 10.1371/journal.pbio.0050038.

[45] C.-W. J. Lio and C.-S. Hsieh, “A two-step process for thymic regulatory T cell development.,” *Immunity*, vol. 28, no. 1, pp. 100–11, Jan. 2008, doi: 10.1016/j.immuni.2007.11.021.

[46] K. B. Vang, J. Yang, S. A. Mahmud, M. A. Burchill, A. L. Vegoe, and M. A. Farrar, “IL-2, -7, and -15, but Not Thymic Stromal Lymphopoeitin, Redundantly Govern CD4+Foxp3+ Regulatory T Cell Development,” *J. Immunol.*, vol. 181, no. 5, pp. 3285–3290, 2008, doi: 10.4049/jimmunol.181.5.3285.

[47] X. Tai *et al.*, “Foxp3 transcription factor is proapoptotic and lethal to developing regulatory T cells unless counterbalanced by cytokine survival signals.,” *Immunity*, vol. 38, no. 6, pp. 1116–28, Jun. 2013, doi: 10.1016/j.immuni.2013.02.022.

[48] J. D. Fontenot, J. P. Rasmussen, M. A. Gavin, and A. Y. Rudensky, “A function for interleukin 2 in Foxp3-expressing regulatory T cells,” *Nat. Immunol.*, vol. 6, no. 11, pp. 1142–1151, 2005, doi: 10.1038/ni1263.

[49] R. Setoguchi, S. Hori, T. Takahashi, and S. Sakaguchi, “Homeostatic maintenance of natural Foxp3+ CD25+ CD4+ regulatory T cells by interleukin (IL)-2 and induction of autoimmune disease by IL-2 neutralization,” *J. Exp. Med.*, vol. 201, no. 5, pp. 723–735, 2005, doi: 10.1084/jem.20041982.

[50] P. Pandiyan, L. Zheng, S. Ishihara, J. Reed, and M. J. Lenardo, “CD4+CD25+Foxp3+ regulatory T cells induce cytokine deprivation-mediated apoptosis of effector CD4+ T cells,” *Nat. Immunol.*, vol. 8, no. 12, pp. 1353–1362, 2007, doi: 10.1038/ni1536.

[51] T. Chinen *et al.*, “An essential role for the IL-2 receptor in T reg cell function,” *Nat. Immunol.*, vol. 17, no. 11, pp. 1322–1333, 2016, doi: 10.1038/ni.3540.

[52] Kajsa Wing *et al.*, “CTLA-4 Control over Foxp3+Regulatory T Cell Function,” *Science (80-.).*, vol. 322, no. 5899, pp. 271–275, 2008.

[53] M. Tekguc, J. B. Wing, M. Osaki, J. Long, and S. Sakaguchi, “Treg-expressed CTLA-4

depletes CD80/CD86 by trogocytosis, releasing free PD-L1 on antigen-presenting cells," *Proc. Natl. Acad. Sci. U. S. A.*, vol. 118, no. 30, 2021, doi: 10.1073/pnas.2023739118.

[54] M. O. Li and R. A. Flavell, "Contextual Regulation of Inflammation: A Duet by Transforming Growth Factor-β and Interleukin-10," *Immunity*, vol. 28, no. 4, pp. 468–476, 2008, doi: 10.1016/j.immuni.2008.03.003.

[55] S. G. Zheng, J. D. Gray, K. Ohtsuka, S. Yamagiwa, and D. A. Horwitz, "Generation Ex Vivo of TGF-β-Producing Regulatory T Cells from CD4+CD25− Precursors," *J. Immunol.*, vol. 169, no. 8, pp. 4183–4189, Oct. 2002, doi: 10.4049/jimmunol.169.8.4183.

[56] S. G. Zheng, J. Wang, P. Wang, J. D. Gray, and D. a Horwitz, "IL-2 Is Essential for TGF-β to Convert Naive CD4+CD25− Cells to CD25+Foxp3+ Regulatory T Cells and for Expansion of These Cells," *J. Immunol.*, vol. 178, no. 4, pp. 2018–2027, Feb. 2007, doi: 10.4049/jimmunol.178.4.2018.

[57] E. M. Shevach and A. M. Thornton, "tTregs, pTregs, and iTregs: similarities and differences.," *Immunol. Rev.*, vol. 259, no. 1, pp. 88–102, May 2014, doi: 10.1111/imr.12160.

[58] A. M. Thornton *et al.*, "Expression of Helios, an Ikaros transcription factor family member, differentiates thymic-derived from peripherally induced Foxp3+ T regulatory cells.," *J. Immunol.*, vol. 184, no. 7, pp. 3433–41, Apr. 2010, doi: 10.4049/jimmunol.0904028.

[59] D. Kolodin *et al.*, "Antigen- and cytokine-driven accumulation of regulatory T cells in visceral adipose tissue of lean mice.," *Cell Metab.*, vol. 21, no. 4, pp. 543–57, Apr. 2015, doi: 10.1016/j.cmet.2015.03.005.

[60] C. Li *et al.*, "TCR Transgenic Mice Reveal Stepwise, Multi-site Acquisition of the Distinctive Fat-Treg Phenotype.," *Cell*, vol. 174, no. 2, pp. 285-299.e12, Jul. 2018, doi: 10.1016/j.cell.2018.05.004.

[61] D. Burzyn *et al.*, "A special population of regulatory T cells potentiates muscle repair.," *Cell*, vol. 155, no. 6, pp. 1282–95, Dec. 2013, doi: 10.1016/j.cell.2013.10.054.

[62] C. Schiering *et al.*, "The alarmin IL-33 promotes regulatory T-cell function in the intestine," *Nature*, vol. 513, no. 7519, pp. 564–568, 2014, doi: 10.1038/nature13577.

[63] R. J. Miragaia *et al.*, "Single-Cell Transcriptomics of Regulatory T Cells Reveals Trajectories of Tissue Adaptation," *Immunity*, vol. 0, no. 0, pp. 1–12, 2019, doi: 10.1016/J.IMMUNI.2019.01.001.

[64] E. A. Wohlfert *et al.*, "GATA3 controls Foxp3$^+$ regulatory T cell fate during inflammation in mice.," *J. Clin. Invest.*, vol. 121, no. 11, pp. 4503–15, Nov. 2011, doi: 10.1172/JCI57456.

[65] M. Delacher *et al.*, "Genome-wide DNA-methylation landscape defines specialization of regulatory T cells in tissues," *Nat. Immunol.*, vol. 18, no. 10, pp. 1160–1172, 2017, doi: 10.1038/ni.3799.

[66] M. Pichery *et al.*, “Endogenous IL-33 Is Highly Expressed in Mouse Epithelial Barrier Tissues, Lymphoid Organs, Brain, Embryos, and Inflamed Tissues: In Situ Analysis Using a Novel Il-33–LacZ Gene Trap Reporter Strain,” *J. Immunol.*, vol. 188, no. 7, pp. 3488–3495, Apr. 2012, doi: 10.4049/jimmunol.1101977.

[67] B. M. Matta *et al.*, “IL-33 is an unconventional Alarmin that stimulates IL-2 secretion by dendritic cells to selectively expand IL-33R/ST2+ regulatory T cells.,” *J. Immunol.*, vol. 193, no. 8, pp. 4010–20, Oct. 2014, doi: 10.4049/jimmunol.1400481.

[68] A. Vasanthakumar *et al.*, “The transcriptional regulators IRF4, BATF and IL-33 orchestrate development and maintenance of adipose tissue-resident regulatory T cells,” *Nat. Immunol.*, vol. 16, no. 3, pp. 276–285, 2015, doi: 10.1038/ni.3085.

[69] W. Kuswanto *et al.*, “Poor Repair of Skeletal Muscle in Aging Mice Reflects a Defect in Local, Interleukin-33-Dependent Accumulation of Regulatory T Cells.,” *Immunity*, vol. 44, no. 2, pp. 355–67, Feb. 2016, doi: 10.1016/j.immuni.2016.01.009.

[70] M. Xu *et al.*, “C-MAF-dependent regulatory T cells mediate immunological tolerance to a gut pathobiont,” *Nature*, vol. 554, no. 7692, pp. 373–377, 2018, doi: 10.1038/nature25500.

[71] C. Ohnmacht *et al.*, “The microbiota regulates type 2 immunity through ROR t+ T cells,” *Science (80-.).*, vol. 349, no. 6251, pp. 989–993, 2015, doi: 10.1126/science.aac4263.

[72] E. Sefik *et al.*, “Individual intestinal symbionts induce a distinct population of RORγ+ regulatory T cells,” *Science (80-.).*, vol. 349, no. 6251, pp. 993–997, 2015, doi: 10.1126/science.aaa9420.Individual.

[73] A. M. Thornton *et al.*, “Helios + and Helios − Treg subpopulations are phenotypically and functionally distinct and express dissimilar TCR repertoires,” *Eur. J. Immunol.*, pp. 1–50, 2019, doi: 10.1002/eji.201847935.

[74] K. S. Kim *et al.*, “Dietary antigens limit mucosal immunity by inducing regulatory T cells in the small intestine,” *Science (80-.).*, vol. 351, no. 6275, pp. 858–863, 2016, doi: 10.1126/science.aac5560.

[75] L. Kreft, “Regulation of immune tolerance and allergic predisposition by the intestinal microbiome,” Technische Universität München (TUM), 2023.

[76] S. Yamazaki, A. J. Bonito, R. Spisek, M. Dhodapkar, K. Inaba, and R. M. Steinman, “Dendritic cells are specialized accessory cells along with TGF-β for the differentiation of Foxp3+ CD4+ regulatory T cells from peripheral Foxp3- precursors,” *Blood*, vol. 110, no. 13, pp. 4293–4302, 2007, doi: 10.1182/blood-2007-05-088831.

[77] Z. Al Nabhani *et al.*, “A Weaning Reaction to Microbiota Is Required for Resistance to Immunopathologies in the Adult,” *Immunity*, vol. 50, no. 5, pp. 1276-1288.e5, 2019, doi: 10.1016/j.immuni.2019.02.014.

[78] L. Dethlefsen, M. McFall-Ngai, and D. A. Relman, “An ecological and evolutionary perspective on human-microbe mutualism and disease.,” *Nature*, vol. 449, no. 7164,

pp. 811–8, Oct. 2007, doi: 10.1038/nature06245.

[79] C. Ohnmacht, "Tolerance to the Intestinal Microbiota Mediated by ROR(γt) + Cells," *Trends Immunol.*, vol. 37, no. 7, pp. 477–486, Jul. 2016, doi: 10.1016/j.it.2016.05.002.

[80] E. Mazzini, L. Massimiliano, G. Penna, and M. Rescigno, "Oral Tolerance Can Be Established via Gap Junction Transfer of Fed Antigens from CX3CR1+ Macrophages to CD103+ Dendritic Cells," *Immunity*, vol. 40, no. 2, pp. 248–261, 2014, doi: 10.1016/j.immuni.2013.12.012.

[81] J. H. Niess *et al.*, "CX3CR1-mediated dendritic cell access to the intestinal lumen and bacterial clearance," *Science (80-.).*, vol. 307, no. 5707, pp. 254–258, 2005, doi: 10.1126/science.1102901.

[82] U. Hadis *et al.*, "Intestinal Tolerance Requires Gut Homing and Expansion of FoxP3+ Regulatory T Cells in the Lamina Propria," *Immunity*, vol. 34, no. 2, pp. 237–246, 2011, doi: 10.1016/j.immuni.2011.01.016.

[83] T. Worbs *et al.*, "Oral tolerance originates in the intestinal immune system and relies on antigen carriage by dendritic cells," *J. Exp. Med.*, vol. 203, no. 3, pp. 519–527, 2006, doi: 10.1084/jem.20052016.

[84] J. Pezoldt *et al.*, "Neonatally imprinted stromal cell subsets induce tolerogenic dendritic cells in mesenteric lymph nodes," *Nat. Commun.*, vol. 9, no. 1, 2018, doi: 10.1038/s41467-018-06423-7.

[85] M. Pasztoi *et al.*, "Mesenteric lymph node stromal cell-derived extracellular vesicles contribute to peripheral de novo induction of Foxp3+ regulatory T cells," *Eur. J. Immunol.*, vol. 47, no. 12, pp. 2142–2152, 2017, doi: 10.1002/eji.201746960.

[86] R. Verma *et al.*, "Cell surface polysaccharides of *Bifidobacterium bifidum* induce the generation of Foxp3 $^{+}$ regulatory T cells," *Sci. Immunol.*, vol. 3, no. 28, p. eaat6975, 2018, doi: 10.1126/sciimmunol.aat6975.

[87] P. M. Smith *et al.*, "The microbial metabolites, short-chain fatty acids, regulate colonic Treg cell homeostasis.," *Science*, vol. 341, no. 6145, pp. 569–73, Aug. 2013, doi: 10.1126/science.1241165.

[88] S. Hang *et al.*, "Bile acid metabolites control TH17 and Treg cell differentiation.," *Nature*, vol. 576, no. 7785, pp. 143–148, Dec. 2019, doi: 10.1038/s41586-019-1785-z.

[89] C. Campbell *et al.*, "Bacterial metabolism of bile acids promotes generation of peripheral regulatory T cells," *Nature*, vol. 581, no. 7809, pp. 475–479, 2020, doi: 10.1038/s41586-020-2193-0.

[90] S. Rakoff-Nahoum, J. Paglino, F. Eslami-Varzaneh, S. Edberg, and R. Medzhitov, "Recognition of Commensal Microflora by Toll-Like Receptors Is Required for Intestinal Homeostasis," *Cell*, vol. 118, no. 2, pp. 229–241, Jul. 2004, doi: 10.1016/j.cell.2004.07.002.

[91] S. Wang *et al.*, "MyD88 Adaptor-Dependent Microbial Sensing by Regulatory T Cells

Promotes Mucosal Tolerance and Enforces Commensalism.," *Immunity*, vol. 43, no. 2, pp. 289–303, Aug. 2015, doi: 10.1016/j.immuni.2015.06.014.

[92] J. J. Bunker and A. Bendelac, "IgA Responses to Microbiota," *Immunity*, vol. 49, no. 2, pp. 211–224, 2018, doi: 10.1016/j.immuni.2018.08.011.

[93] J. J. Bunker *et al.*, "Innate and Adaptive Humoral Responses Coat Distinct Commensal Bacteria with Immunoglobulin A.," *Immunity*, vol. 43, no. 3, pp. 541–53, Sep. 2015, doi: 10.1016/j.immuni.2015.08.007.

[94] D. Ramanan *et al.*, "An Immunologic Mode of Multigenerational Transmission Governs a Gut Treg Setpoint," *Cell*, May 2020, doi: 10.1016/j.cell.2020.04.030.

[95] K. Suzuki *et al.*, "Aberrant expansion of segmented filamentous bacteria in IgA-deficient gut," *Proc. Natl. Acad. Sci. U. S. A.*, vol. 101, no. 7, pp. 1981–1986, 2004, doi: 10.1073/pnas.0307317101.

[96] J. Ochoa-Repáraz *et al.*, "Role of Gut Commensal Microflora in the Development of Experimental Autoimmune Encephalomyelitis," *J. Immunol.*, vol. 183, no. 10, pp. 6041–6050, 2009, doi: 10.4049/jimmunol.0900747.

[97] C. D. Packey and R. B. Sartor, "Interplay of commensal and pathogenic bacteria, genetic mutations, and immunoregulatory defects in the pathogenesis of inflammatory bowel diseases," *J. Intern. Med.*, vol. 263, no. 6, pp. 597–606, 2008, doi: 10.1111/j.1365-2796.2008.01962.x.

[98] R. Duchmann, I. Kaiser, E. Hermann, W. Mayet, K. Ewe, and K. H. Meyer Zum Buschenfelde, "Tolerance exists towards resident intestinal flora but is broken in active inflammatory bowel disease (IBD)," *Clin. Exp. Immunol.*, vol. 102, no. 3, pp. 448–455, 1995, doi: 10.1111/j.1365-2249.1995.tb03836.x.

[99] B. Khor, A. Gardet, and R. J. Xavier, "Genetics and pathogenesis of inflammatory bowel disease.," *Nature*, vol. 474, no. 7351, pp. 307–17, Jun. 2011, doi: 10.1038/nature10209.

[100] S. Fujino *et al.*, "Increased expression of interleukin 17 in inflammatory bowel disease.," *Gut*, vol. 52, no. 1, pp. 65–70, Jan. 2003, doi: 10.1136/gut.52.1.65.

[101] N. Eastaff-Leung, N. Mabarrack, A. Barbour, A. Cummins, and S. Barry, "Foxp3+regulatory T cells, Th17 effector cells, and cytokine environment in inflammatory bowel disease," *J. Clin. Immunol.*, vol. 30, no. 1, pp. 80–89, 2010, doi: 10.1007/s10875-009-9345-1.

[102] M. Pawlak, D. Detomaso, A. Schnell, R. J. Xavier, N. Yosef, and V. K. Kuchroo, "Induction of a colitogenic phenotype in Th1-like cells depends on interleukin-23 receptor signaling Article Induction of a colitogenic phenotype in Th1-like cells depends on interleukin-23 receptor signaling," *Immunity*, pp. 1–17, 2022, doi: 10.1016/j.immuni.2022.08.007.

[103] S. Chanpimol, B. Seamon, H. Hernandez, M. Harris-love, and M. R. Blackman, "T-cell receptor sequencing reveals the clonal diversity and overlap of colonic effector and FOXP3+ T cells in ulcerative colitis.," *Inflamm. Bowel Dis.*, vol. 21, no. 1, pp. 19–30,

2015, doi: 10.1186/s40945-017-0033-9.Using.

[104] G. J. Britton *et al.*, "Microbiotas from Humans with Inflammatory Bowel Disease Alter the Balance of Gut Th17 and RORγt+ Regulatory T Cells and Exacerbate Colitis in Mice," *Immunity*, vol. 50, no. 1, pp. 212-224.e4, 2019, doi: 10.1016/j.immuni.2018.12.015.

[105] S. Ma *et al.*, "RNA binding protein DDX5 restricts RORγt + T reg suppressor function to promote intestine inflammation," *Sci. Adv.*, vol. 9, no. 5, Feb. 2023, doi: 10.1126/sciadv.add6165.

[106] J. L. Riley, C. H. June, and B. R. Blazar, "Human T Regulatory Cells as Therapeutic Agents: Take a Billion or So of These and Call Me in the Morning," *Immunity*, vol. 30, no. 5, pp. 656–665, 2010, doi: 10.1016/j.immuni.2009.04.006.Human.

[107] M. E. Himmel, Y. Yao, P. C. Orban, T. S. Steiner, and M. K. Levings, "Regulatory T-cell therapy for inflammatory bowel disease: More questions than answers," *Immunology*, vol. 136, no. 2, pp. 115–122, 2012, doi: 10.1111/j.1365-2567.2012.03572.x.

[108] M. C. Fantini and G. Monteleone, "Update on the Therapeutic Efficacy of Tregs in IBD: Thumbs up or Thumbs down?," *Inflamm. Bowel Dis.*, vol. 23, no. 10, pp. 1682–1688, 2017, doi: 10.1097/MIB.0000000000001272.

[109] S. E. Edwards-Salmon, S. L. Padmanabhan, M. Kuruvilla, and J. M. Levy, "Increasing Prevalence of Allergic Disease and Its Impact on Current Practice," *Curr. Otorhinolaryngol. Rep.*, vol. 10, no. 3, pp. 278–284, 2022, doi: 10.1007/s40136-022-00406-5.

[110] G. D'Amato *et al.*, "Climate change and air pollution: Effects on respiratory allergy," *Allergy, Asthma Immunol. Res.*, vol. 8, no. 5, pp. 391–395, 2016, doi: 10.4168/aair.2016.8.5.391.

[111] T. Feehley, A. T. Stefka, S. Cao, and C. R. Nagler, "Microbial regulation of allergic responses to food," *Semin. Immunopathol.*, vol. 34, no. 5, pp. 671–688, 2012, doi: 10.1007/s00281-012-0337-5.

[112] J. Kattan, "The Prevalence and Natural History of Food Allergy," *Curr. Allergy Asthma Rep.*, vol. 16, no. 7, p. 47, Jul. 2016, doi: 10.1007/s11882-016-0627-4.

[113] A. S. Y. Leung, G. W. K. Wong, and M. L. K. Tang, "Food allergy in the developing world," *J. Allergy Clin. Immunol.*, vol. 141, no. 1, pp. 76-78.e1, 2018, doi: 10.1016/j.jaci.2017.11.008.

[114] M. Cecilia Berin, "Targeting type 2 immunity and the future of food allergy treatment," *J. Exp. Med.*, vol. 220, no. 4, pp. 1–10, 2023, doi: 10.1084/jem.20221104.

[115] M. Kubo, "Innate and adaptive type 2 immunity in lung allergic inflammation," *Immunol. Rev.*, vol. 278, no. 1, pp. 162–172, 2017, doi: 10.1111/imr.12557.

[116] U. Gowthaman *et al.*, "Identification of a T follicular helper cell subset that drives anaphylactic IgE," *Sci. Robot.*, vol. 4, no. 34, pp. 1–23, 2019, doi:

10.1126/scirobotics.aax4316.

[117] E. R. Conner and S. S. Saini, “The immunoglobulin E receptor: Expression and regulation,” *Curr. Allergy Asthma Rep.*, vol. 5, no. 3, pp. 191–196, 2005, doi: 10.1007/s11882-005-0037-5.

[118] D. A. Hill *et al.*, “Commensal bacteria-derived signals regulate basophil hematopoiesis and allergic inflammation.,” *Nat. Med.*, vol. 18, no. 4, pp. 538–46, Mar. 2012, doi: 10.1038/nm.2657.

[119] S. W. Hong *et al.*, “Food antigens drive spontaneous IgE elevation in the absence of commensal microbiota,” *Sci. Adv.*, vol. 5, no. 5, 2019, doi: 10.1126/sciadv.aaw1507.

[120] T. Feehley *et al.*, “Healthy infants harbor intestinal bacteria that protect against food allergy.,” *Nat. Med.*, vol. 25, no. 3, pp. 448–453, Mar. 2019, doi: 10.1038/s41591-018-0324-z.

[121] A. Abdel-Gadir *et al.*, “Microbiota therapy acts via a regulatory T cell MyD88/RORγt pathway to suppress food allergy.,” *Nat. Med.*, vol. 25, no. 7, pp. 1164–1174, Jul. 2019, doi: 10.1038/s41591-019-0461-z.

[122] T. Kawai and S. Akira, “Signaling to NF-κB by Toll-like receptors,” *Trends Mol. Med.*, vol. 13, no. 11, pp. 460–469, 2007, doi: 10.1016/j.molmed.2007.09.002.

[123] M. S. Hayden and S. Ghosh, “Shared Principles in NF-κB Signaling,” *Cell*, vol. 132, no. 3, pp. 344–362, 2008, doi: 10.1016/j.cell.2008.01.020.

[124] P. A. Baeuerle and D. Baltimore, “A 65-kappaD subunit of active NF-kappaB is required for inhibition of NF-kappaB by I kappaB.,” *Genes Dev.*, vol. 3, no. 11, pp. 1689–1698, 1989, doi: 10.1101/gad.3.11.1689.

[125] M. S. Hayden and S. Ghosh, “NF-κB, the first quarter-century: Remarkable progress and outstanding questions,” *Genes Dev.*, vol. 26, no. 3, pp. 203–234, 2012, doi: 10.1101/gad.183434.111.

[126] N. J. Solan, H. Miyoshi, E. M. Carmona, G. D. Bren, and C. V. Paya, “RelB cellular regulation and transcriptional activity are regulated by p100,” *J. Biol. Chem.*, vol. 277, no. 2, pp. 1405–1418, 2002, doi: 10.1074/jbc.M109619200.

[127] N. R. Rice, M. L. MacKichan, and A. Israël, “The precursor of NF-κB p50 has IκB-like functions,” *Cell*, vol. 71, no. 2, pp. 243–253, 1992, doi: 10.1016/0092-8674(92)90353-E.

[128] M. Schuster, M. Annemann, C. Plaza-Sirvent, and I. Schmitz, “Atypical IκB proteins - Nuclear modulators of NF-κB signaling,” *Cell Commun. Signal.*, vol. 11, no. 1, pp. 1–11, 2013, doi: 10.1186/1478-811X-11-23.

[129] S. Vallabhapurapu and M. Karin, “Regulation and function of NF-κB transcription factors in the immune system,” *Annu. Rev. Immunol.*, vol. 27, pp. 693–733, 2009, doi: 10.1146/annurev.immunol.021908.132641.

[130] Shao-Cong Sun, “The non-canonical NF-κB pathway in immunity and inflammation,” *Nat. Rev. Immunol.*, vol. 17, no. 9, pp. 545–558, 2017, doi:

10.1038/nri.2017.52.The.

[131] I. Isomura *et al.*, "c-Rel is required for the development of thymic Foxp3+ CD4 regulatory T cells," *J. Exp. Med.*, vol. 206, no. 13, pp. 3001–3014, 2009, doi: 10.1084/jem.20091411.

[132] N. Messina *et al.*, "The NF-κB transcription factor RelA is required for the tolerogenic function of Foxp3+ regulatory T cells," *J. Autoimmun.*, vol. 70, pp. 52–62, 2016, doi: 10.1016/j.jaut.2016.03.017.

[133] H. Oh *et al.*, "An NF-κB Transcription-Factor-Dependent Lineage-Specific Transcriptional Program Promotes Regulatory T Cell Identity and Function.," *Immunity*, vol. 47, no. 3, pp. 450-465.e5, Sep. 2017, doi: 10.1016/j.immuni.2017.08.010.

[134] A. Vasanthakumar *et al.*, "The TNF Receptor Superfamily-NF-κB Axis Is Critical to Maintain Effector Regulatory T Cells in Lymphoid and Non-lymphoid Tissues," *Cell Rep.*, vol. 20, no. 12, pp. 2906–2920, 2017, doi: 10.1016/j.celrep.2017.08.068.

[135] N. Hövelmeyer, M. Schmidt-Supprian, and C. Ohnmacht, "NF-κB in control of regulatory T cell development, identity, and function," *J. Mol. Med.*, vol. 100, no. 7, pp. 985–995, 2022, doi: 10.1007/s00109-022-02215-1.

[136] G. Courtois and T. D. Gilmore, "Mutations in the NF-κB signaling pathway: Implications for human disease," *Oncogene*, vol. 25, no. 51, pp. 6831–6843, 2006, doi: 10.1038/sj.onc.1209939.

[137] H. Ohno, G. Takimoto, and T. W. McKeithan, "The candidate proto-oncogene bcl-3 is related to genes implicated in cell lineage determination and cell cycle control.," *Cell*, vol. 60, no. 6, pp. 991–7, Mar. 1990, doi: 10.1016/0092-8674(90)90347-h.

[138] M. Naumann, F. G. Wulczyn, and C. Scheidereit, "The NF-κB precursor p105 and the proto-oncogene product Bcl-3 are IκB molecules and control nuclear translocation of NF-κB," *EMBO J.*, vol. 12, no. 1, pp. 213–222, 1993, doi: 10.1002/j.1460-2075.1993.tb05647.x.

[139] T. W. McKeithan *et al.*, "BCL3 rearrangements and t(14;19) in chronic lymphocytic leukemia and other B-cell malignancies: A molecular and cytogenetic study," *Genes Chromosom. Cancer*, vol. 20, no. 1, pp. 64–72, 1997, doi: 10.1002/(SICI)1098-2264(199709)20:1<64::AID-GCC10>3.0.CO;2-F.

[140] G. Franzoso *et al.*, "Critical roles for the Bcl-3 oncoprotein in T cell-mediated immunity, splenic microarchitecture, and germinal center reactions.," *Immunity*, vol. 6, no. 4, pp. 479–90, Apr. 1997, doi: 10.1016/s1074-7613(00)80291-5.

[141] E. M. Schwarz, P. Krimpenfort, A. Berns, and I. M. Verma, "Immunological defects in mice with a targeted disruption in Bcl-3," *Genes Dev.*, vol. 11, no. 2, pp. 187–197, 1997, doi: 10.1101/gad.11.2.187.

[142] L. D. Kerr *et al.*, "The proto-oncogene bcl-3 encodes an I kappa B protein.," *Genes Dev.*, vol. 6, no. 12A, pp. 2352–63, Dec. 1992, doi: 10.1101/gad.6.12a.2352.

[143] M. Naumann, F. G. Wulczyn, and C. Scheidereit, “The NF-kappa B precursor p105 and the proto-oncogene product Bcl-3 are I kappa B molecules and control nuclear translocation of NF-kappa B.,” *EMBO J.*, vol. 12, no. 1, pp. 213–22, Jan. 1993, doi: 10.1002/j.1460-2075.1993.tb05647.x.

[144] H. Liu, L. Zeng, Y. Yang, C. Guo, and H. Wang, “Bcl-3: A Double-Edged Sword in Immune Cells and Inflammation,” *Front. Immunol.*, vol. 13, no. March, pp. 1–11, 2022, doi: 10.3389/fimmu.2022.847699.

[145] G. P. Nolan *et al.*, “The bcl-3 proto-oncogene encodes a nuclear I kappa B-like molecule that preferentially interacts with NF-kappa B p50 and p52 in a phosphorylation-dependent manner.,” *Mol. Cell. Biol.*, vol. 13, no. 6, pp. 3557–3566, 1993, doi: 10.1128/mcb.13.6.3557.

[146] V. Bours *et al.*, “The oncoprotein Bcl-3 directly transactivates through kappa B motifs via association with DNA-binding p50B homodimers.,” *Cell*, vol. 72, no. 5, pp. 729–39, Mar. 1993, doi: 10.1016/0092-8674(93)90401-b.

[147] G. Franzoso *et al.*, “The oncoprotein Bcl-3 can facilitate NF-κB-mediated transactivation by removing inhibiting p50 homodimers from select κB sites,” *EMBO J.*, vol. 12, no. 10, pp. 3893–3901, 1993, doi: 10.1002/j.1460-2075.1993.tb06067.x.

[148] N. Watanabe, T. Iwamura, T. Shinoda, and T. Fujita, “Regulation of NFKB1 proteins by the candidate oncoprotein BCL-3: Generation of NF-κB homodimers from the cytoplasmic pool of p50-p105 and nuclear translocation,” *EMBO J.*, vol. 16, no. 12, pp. 3609–3620, 1997, doi: 10.1093/emboj/16.12.3609.

[149] P. E. Collins, P. A. Kiely, and R. J. Carmody, “Inhibition of transcription by B cell leukemia 3 (Bcl-3) protein requires interaction with nuclear factor κB (NF-κB) p50,” *J. Biol. Chem.*, vol. 289, no. 10, pp. 7059–7067, 2014, doi: 10.1074/jbc.M114.551986.

[150] R. J. Carmody, Q. Ruan, S. Palmer, B. Hilliard, and Y. H. Chen, “Negative regulation of toll-like receptor signaling by NF-κB p50 ubiquitination blockade,” *Science (80-.).*, vol. 317, no. 5838, pp. 675–678, 2007, doi: 10.1126/science.1142953.

[151] W. Pan, L. Deng, H. Wang, and V. Y. F. Wang, “Atypical IκB Bcl3 enhances the generation of the NF-κB p52 homodimer,” *Front. Cell Dev. Biol.*, vol. 10, no. August, pp. 1–16, 2022, doi: 10.3389/fcell.2022.930619.

[152] A. Rebollo, L. Dumoutier, J.-C. Renauld, A. Zaballos, V. Ayllón, and M.-A. Carlos, “Bcl-3 Expression Promotes Cell Survival following Interleukin-4 Deprivation and Is Controlled by AP1 and AP1-Like Transcription Factors,” *Mol. Cell. Biol.*, vol. 20, no. 10, pp. 3407–3416, 2000, doi: 10.1128/mcb.20.10.3407-3416.2000.

[153] C.-P. Kung and N. Raab-Traub, “Epstein-Barr Virus Latent Membrane Protein 1 Induces Expression of the Epidermal Growth Factor Receptor through Effects on Bcl-3 and STAT3,” *J. Virol.*, vol. 82, no. 11, pp. 5486–5493, 2008, doi: 10.1128/jvi.00125-08.

[154] M. F. J. Bassetti, J. White, J. W. Kappler, and P. Marrack, “Transgenic Bcl-3 slows T cell proliferation,” *Int. Immunol.*, vol. 21, no. 4, pp. 339–348, 2009, doi:

10.1093/intimm/dxp002.

[155] W. Tang *et al.*, “Bcl-3 inhibits lupus-like phenotypes in BL6/lpr mice,” *Eur. J. Immunol.*, vol. 51, no. 1, pp. 197–205, 2021, doi: 10.1002/eji.202048584.

[156] R. A. Corn, C. Hunter, H.-C. Liou, U. Siebenlist, and M. R. Boothby, “Opposing Roles for RelB and Bcl-3 in Regulation of T-Box Expressed in T Cells, GATA-3, and Th Effector Differentiation,” *J. Immunol.*, vol. 175, no. 4, pp. 2102–2110, 2005, doi: 10.4049/jimmunol.175.4.2102.

[157] I. Tassi *et al.*, “The NF-κB regulator Bcl-3 governs dendritic cell antigen presentation functions in adaptive immunity.,” *J. Immunol.*, vol. 193, no. 9, pp. 4303–11, Nov. 2014, doi: 10.4049/jimmunol.1401505.

[158] S. Reißig *et al.*, “Elevated levels of Bcl-3 inhibits Treg development and function resulting in spontaneous colitis,” *Nat. Commun.*, vol. 8, 2017, doi: 10.1038/ncomms15069.

[159] P. Ewels *et al.*, “nf-core : Community curated bioinformatics pipelines,” *bioRxiv*, no. April, p. 610741, 2019, doi: 10.5281/zenodo.1400710.

[160] S. Durinck, P. T. Spellman, E. Birney, and W. Huber, “Mapping identifiers for the integration of genomic datasets with the R/Bioconductor package biomaRt.,” *Nat. Protoc.*, vol. 4, no. 8, pp. 1184–91, 2009, doi: 10.1038/nprot.2009.97.

[161] M. I. Love, W. Huber, and S. Anders, “Moderated estimation of fold change and dispersion for RNA-seq data with DESeq2,” *Genome Biol.*, vol. 15, no. 12, p. 550, Dec. 2014, doi: 10.1186/s13059-014-0550-8.

[162] B. Kevin, R. Sharmila, and L. Myles, “EnhancedVolcano: Publication-ready volcano plots with enhanced colouring and labeling.” 2021, doi: 10.18129/B9.bioc.EnhancedVolcano.

[163] J. Larsson and P. Gustafsson, “A case study in fitting area-proportional euler diagrams with ellipses using eulerr.,” in *CEUR Workshop Proceedings*, 2018, pp. 84–91.

[164] K. Gennady, S. Vladimir, B. Nikolay, S. Boris, A. Maxim N., and S. Alexey, “Fast gene set enrichment analysis.,” *bioRxiv*. 2019, doi: https://doi.org/10.1101/060012.

[165] W. Hadley, *ggplot2: Elegant Graphics for Data Analysis.* Springer-Verlag New York, 2016.

[166] I. Lagkouvardos, S. Fischer, N. Kumar, and T. Clavel, “Rhea: a transparent and modular R pipeline for microbial profiling based on 16S rRNA gene amplicons.,” *PeerJ*, vol. 5, p. e2836, 2017, doi: 10.7717/peerj.2836.

[167] Y. Hao *et al.*, “Integrated analysis of multimodal single-cell data.,” *Cell*, vol. 184, no. 13, pp. 3573-3587.e29, Jun. 2021, doi: 10.1016/j.cell.2021.04.048.

[168] C. Soneson, M. I. Love, and M. D. Robinson, “Differential analyses for RNA-seq: transcript-level estimates improve gene-level inferences.,” *F1000Research*, vol. 4, p. 1521, 2015, doi: 10.12688/f1000research.7563.2.

[169] K. Liedtke *et al.*, "Endogenous CD83 Expression in CD4 + Conventional T Cells Controls Inflammatory Immune Responses," *J. Immunol.*, vol. 204, no. 12, pp. 3217–3226, 2020, doi: 10.4049/jimmunol.2000042.

[170] F. W. Shen *et al.*, "Cloning of Ly-5 cDNA.," *Proc. Natl. Acad. Sci. U. S. A.*, vol. 82, no. 21, pp. 7360–3, Nov. 1985, doi: 10.1073/pnas.82.21.7360.

[171] X. Zhou *et al.*, "Selective miRNA disruption in T reg cells leads to uncontrolled autoimmunity.," *J. Exp. Med.*, vol. 205, no. 9, pp. 1983–91, Sep. 2008, doi: 10.1084/jem.20080707.

[172] P. Mombaerts, J. Iacomini, R. S. Johnson, K. Herrup, S. Tonegawa, and V. E. Papaioannou, "RAG-1-deficient mice have no mature B and T lymphocytes.," *Cell*, vol. 68, no. 5, pp. 869–77, Mar. 1992, doi: 10.1016/0092-8674(92)90030-g.

[173] R. P. Orcutt, F. J. Gianni, and R. J. Judge, "Development of an 'altered Schaedler flora' for NCI gnotobiotoc rodents," *Microecol. Ther.*, vol. 17, no. 59, 1987.

[174] A. Liberzon, C. Birger, H. Thorvaldsdóttir, M. Ghandi, J. P. Mesirov, and P. Tamayo, "The Molecular Signatures Database (MSigDB) hallmark gene set collection.," *Cell Syst.*, vol. 1, no. 6, pp. 417–425, Dec. 2015, doi: 10.1016/j.cels.2015.12.004.

[175] M. Schwarzer *et al.*, "Germ-free mice exhibit mast cells with impaired functionality and gut homing and do not develop food allergy," *Front. Immunol.*, vol. 10, no. FEB, pp. 1–12, 2019, doi: 10.3389/fimmu.2019.00205.

[176] A. T. Stefka *et al.*, "Commensal bacteria protect against food allergen sensitization.," *Proc. Natl. Acad. Sci. U. S. A.*, vol. 111, no. 36, pp. 13145–50, Sep. 2014, doi: 10.1073/pnas.1412008111.

[177] M. A. Curotto de Lafaille and J. J. Lafaille, "Natural and adaptive foxp3+ regulatory T cells: more of the same or a division of labor?," *Immunity*, vol. 30, no. 5, pp. 626–35, May 2009, doi: 10.1016/j.immuni.2009.05.002.

[178] M. B. Azad *et al.*, "Infant gut microbiota and food sensitization: associations in the first year of life.," *Clin. Exp. Allergy*, vol. 45, no. 3, pp. 632–43, Mar. 2015, doi: 10.1111/cea.12487.

[179] W. Tang *et al.*, "The oncoprotein and transcriptional regulator Bcl-3 governs plasticity and pathogenicity of autoimmune T cells.," *Immunity*, vol. 41, no. 4, pp. 555–66, Oct. 2014, doi: 10.1016/j.immuni.2014.09.017.

[180] B. H. Yang *et al.*, "Foxp3+ T cells expressing RORγt represent a stable regulatory T-cell effector lineage with enhanced suppressive capacity during intestinal inflammation," *Mucosal Immunol.*, vol. 9, no. 2, pp. 444–457, 2016, doi: 10.1038/mi.2015.74.

[181] N. Hövelmeyer *et al.*, "Overexpression of Bcl-3 inhibits the development of marginal zone B cells," *Eur. J. Immunol.*, vol. 44, no. 2, pp. 545–552, 2014, doi: 10.1002/eji.201343655.

[182] M. Doebbeler *et al.*, "CD83 expression is essential for Treg cell differentiation and

stability," *JCI insight*, vol. 3, no. 11, pp. 1–16, 2018, doi: 10.1172/jci.insight.99712.

[183] Z. Li *et al.*, "CD83: Activation marker for antigen presenting cells and its therapeutic potential," *Front. Immunol.*, vol. 10, no. JUN, pp. 1–9, 2019, doi: 10.3389/fimmu.2019.01312.

[184] D. E. Jenne and J. Tschopp, "Granzymes, a Family of Serine Proteases Released from Granules of Cytolytic T Lymphocytes upon T Cell Receptor Stimulation," *Immunol. Rev.*, vol. 103, no. 1, pp. 53–71, 1988, doi: 10.1111/j.1600-065X.1988.tb00749.x.

[185] A. Takeuchi and T. Saito, "CD4 CTL, a cytotoxic subset of CD4+ T cells, their differentiation and function," *Front. Immunol.*, vol. 8, no. FEB, pp. 1–7, 2017, doi: 10.3389/fimmu.2017.00194.

[186] N. B. Marshall and S. L. Swain, "Cytotoxic CD4 T cells in antiviral immunity," *J. Biomed. Biotechnol.*, vol. 2011, pp. 2–9, 2011, doi: 10.1155/2011/954602.

[187] M. Matijašić, T. Meštrović, H. Č. Paljetak, M. Perić, A. Barešić, and D. Verbanac, "Gut microbiota beyond bacteria-mycobiome, virome, archaeome, and eukaryotic parasites in IBD," *Int. J. Mol. Sci.*, vol. 21, no. 8, pp. 1–21, 2020, doi: 10.3390/ijms21082668.

[188] A. Takeuchi *et al.*, "CRT AM determines the CD4+ cytotoxic T lymphocyte lineage," *J. Exp. Med.*, vol. 213, no. 1, pp. 123–138, 2016, doi: 10.1084/jem.20150519.

[189] Q. Qi *et al.*, "Diversity and clonal selection in the human T-cell repertoire," *Proc. Natl. Acad. Sci. U. S. A.*, vol. 111, no. 36, pp. 13139–13144, 2014, doi: 10.1073/pnas.1409155111.

[190] A. Aran, L. Garrigós, G. Curigliano, J. Cortés, and M. Martí, "Evaluation of the TCR Repertoire as a Predictive and Prognostic Biomarker in Cancer: Diversity or Clonality?," *Cancers (Basel).*, vol. 14, no. 7, 2022, doi: 10.3390/cancers14071771.

[191] S. N. Hong, J. Y. Park, S. Y. Yang, C. Lee, Y. H. Kim, and J. G. Joung, "Reduced diversity of intestinal T-cell receptor repertoire in patients with Crohn's disease," *Front. Cell. Infect. Microbiol.*, vol. 12, no. August, pp. 1–12, 2022, doi: 10.3389/fcimb.2022.932373.

[192] K. Nagashima *et al.*, "Mapping the T cell repertoire to a complex gut bacterial community," *Nature*, vol. 621, no. 7977, pp. 162–170, 2023, doi: 10.1038/s41586-023-06431-8.

[193] T. Sujino *et al.*, "Tissue adaptation of regulatory and intraepithelial CD4+ T cells controls gut inflammation," *Science (80-.).*, vol. 352, no. 6293, pp. 1581–1586, Jun. 2016, doi: 10.1126/science.aaf3892.

[194] C. Neumann *et al.*, "c-Maf-dependent Treg cell control of intestinal TH17 cells and IgA establishes host–microbiota homeostasis," *Nat. Immunol.*, vol. 20, no. 4, pp. 471–481, 2019, doi: 10.1038/s41590-019-0316-2.

[195] W. Tang *et al.*, "Bcl-3 suppresses differentiation of RORγt+ regulatory T cells," *Immunology and Cell Biology*, vol. 99, no. 6. pp. 586–595, 2021, doi:

10.1111/imcb.12441.

[196] E. N. Hatada *et al.*, "The ankyrin repeat domains of the NF-κB precursor p105 and the protooncogene bcl-3 act as specific inhibitors of NF-κB DNA binding," *Proc. Natl. Acad. Sci. U. S. A.*, vol. 89, no. 6, pp. 2489–2493, 1992, doi: 10.1073/pnas.89.6.2489.

[197] D. L. Bundy and T. W. McKeithan, "Diverse effects of BCL3 phosphorylation on its modulation of NF-κB p52 homodimer binding to DNA," *J. Biol. Chem.*, vol. 272, no. 52, pp. 33132–33139, 1997, doi: 10.1074/jbc.272.52.33132.

[198] C. Ohnmacht *et al.*, "Constitutive ablation of dendritic cells breaks self-tolerance of CD4 T cells and results in spontaneous fatal autoimmunity," *J. Exp. Med.*, vol. 206, no. 3, pp. 549–559, 2009, doi: 10.1084/jem.20082394.

[199] K. Brocke-Heidrich *et al.*, "BCL3 is induced by IL-6 via Stat3 binding to intronic enhancer HS4 and represses its own transcription," *Oncogene*, vol. 25, no. 55, pp. 7297–7304, 2006, doi: 10.1038/sj.onc.1209711.

[200] H. Zhao, W. Wang, Q. Zhao, G. Hu, K. Deng, and Y. Liu, "BCL3 exerts an oncogenic function by regulating STAT3 in human cervical cancer.," *Onco. Targets. Ther.*, vol. 9, pp. 6619–6629, 2016, doi: 10.2147/OTT.S118184.

[201] J. Yang, M. Zou, J. Pezoldt, X. Zhou, and J. Huehn, "Thymus-derived Foxp3+ regulatory T cells upregulate RORγt expression under inflammatory conditions," *J. Mol. Med.*, vol. 96, no. 12, pp. 1387–1394, 2018, doi: 10.1007/s00109-018-1706-x.

[202] R. Haque, F. Lei, X. Xiong, Y. Wu, and J. Song, "FoxP3 and Bcl-xL cooperatively promote regulatory T cell persistence and prevention of arthritis development," *Arthritis Res. Ther.*, vol. 12, no. 2, 2010, doi: 10.1186/ar2983.

[203] F. Issa, K. Milward, R. Goto, G. Betts, K. J. Wood, and J. Hester, "Transiently activated human regulatory T cells upregulate BCL-XL expression and acquire a functional advantage in vivo," *Front. Immunol.*, vol. 10, no. APR, pp. 1–13, 2019, doi: 10.3389/fimmu.2019.00889.

[204] M. Pesu, L. Muul, Y. Kanno, and J. J. O'Shea, "Proprotein convertase furin is preferentially expressed in T helper 1 cells and regulates interferon gamma," *Blood*, vol. 108, no. 3, pp. 983–985, 2006, doi: 10.1182/blood-2005-09-3824.

[205] M. Pesu *et al.*, "T-cell-expressed proprotein convertase furin is essential for maintenance of peripheral immune tolerance," *Nature*, vol. 455, no. 7210, pp. 246–250, 2008, doi: 10.1038/nature07210.

[206] M. Schuster *et al.*, "IκBNS Protein Mediates Regulatory T Cell Development via Induction of the Foxp3 Transcription Factor," *Immunity*, vol. 37, no. 6, pp. 998–1008, 2012, doi: 10.1016/j.immuni.2012.08.023.

[207] M. R. Pillai *et al.*, "The plasticity of regulatory T cell function.," *J. Immunol.*, vol. 187, no. 10, pp. 4987–97, Nov. 2011, doi: 10.4049/jimmunol.1102173.

[208] M. Annemann *et al.*, "IκBNS Regulates Murine Th17 Differentiation during Gut Inflammation and Infection," *J. Immunol.*, vol. 194, no. 6, pp. 2888–2898, 2015, doi:

10.4049/jimmunol.1401964.

[209] K. M. Jeltsch *et al.*, "Cleavage of roquin and regnase-1 by the paracaspase MALT1 releases their cooperatively repressed targets to promote TH17 differentiation," *Nat. Immunol.*, vol. 15, no. 11, pp. 1079–1089, 2014, doi: 10.1038/ni.3008.

[210] S. Uehara, A. Grinberg, J. M. Farber, and P. E. Love, "A Role for CCR9 in T Lymphocyte Development and Migration," *J. Immunol.*, vol. 168, no. 6, pp. 2811–2819, 2002, doi: 10.4049/jimmunol.168.6.2811.

[211] H. L. Evans-Marin *et al.*, "Unexpected regulatory role of CCR9 in regulatory T cell development," *PLoS One*, vol. 10, no. 7, pp. 1–16, 2015, doi: 10.1371/journal.pone.0134100.

[212] M. A. Wurbel, M. G. McIntire, P. Dwyer, and E. Fiebiger, "CCL25/CCR9 interactions regulate large intestinal inflammation in a murine model of acute colitis," *PLoS One*, vol. 6, no. 1, 2011, doi: 10.1371/journal.pone.0016442.

[213] J. Zhang *et al.*, "Biarylsulfonamide CCR9 inhibitors for inflammatory bowel disease," *Bioorganic Med. Chem. Lett.*, vol. 25, no. 17, pp. 3661–3664, 2015, doi: 10.1016/j.bmcl.2015.06.046.

[214] W. Y. Tseng *et al.*, "TNF receptor 2 signaling prevents DNA methylation at the Foxp3 promoter and prevents pathogenic conversion of regulatory T cells," *Proc. Natl. Acad. Sci. U. S. A.*, vol. 116, no. 43, pp. 21666–21672, 2019, doi: 10.1073/pnas.1909687116.

[215] L. Kastner, D. Dwyer, and F. X.-F. Qin, "Synergistic Effect of IL-6 and IL-4 in Driving Fate Revision of Natural Foxp3+ Regulatory T Cells," *J. Immunol.*, vol. 185, no. 10, pp. 5778–5786, 2010, doi: 10.4049/jimmunol.0901948.

[216] M. A. Burchill *et al.*, "Linked T cell receptor and cytokine signaling govern the development of the regulatory T cell repertoire.," *Immunity*, vol. 28, no. 1, pp. 112–21, Jan. 2008, doi: 10.1016/j.immuni.2007.11.022.

[217] K. Sugimoto, "Role of STAT3 in inflammatory bowel disease," *World J. Gastroenterol.*, vol. 14, no. 33, pp. 5110–5114, 2008, doi: 10.3748/wjg.14.5110.

[218] J. Soukupová *et al.*, "The Discovery of a Novel Antimetastatic Bcl3 Inhibitor.," *Mol. Cancer Ther.*, vol. 20, no. 5, pp. 775–786, May 2021, doi: 10.1158/1535-7163.MCT-20-0283.